Monthly Notices
of the
ROYAL ASTRONOMICAL SOCIETY

MNRAS **488,** 4690–4731 (2019)
Advance Access publication 2019 August 7

doi:10.1093/mnras/stz1642

Probing quasar winds using intrinsic narrow absorption lines

Chris Culliton [1]★ Jane Charlton,[1] Mike Eracleous,[1] Rajib Ganguly[2] and Toru Misawa[3]

[1]*Department of Astronomy and Astrophysics, The Pennsylvania State University, 525 Davey Lab, University Park, PA 16802, USA*
[2]*Department of Computer Science, Engineering, and Physics, University of Michigan-Flint, Murchie Science Building, 303 Kearsley Street, Flint, MI 48502, USA*
[3]*School of General Education, Shinshu University, 3-1-1 Asahi, Matsumoto, Nagano 390-8621, Japan*

Accepted 2019 May 22. Received 2019 February 28; in original form 2019 February 28

ABSTRACT

We use the spectra of 73 quasars ($1.5 \lesssim z \lesssim 5$) from the VLT UVES archive to catalogue and study narrow absorption lines (NALs) that are physically associated with (intrinsic to) the quasars. We identify 410 NAL systems containing C IV, N V, and/or Si IV doublets. Based on the assumption that only systems intrinsic to the quasar can exhibit partial coverage of the background source(s), we identify 34 reliably intrinsic NAL systems and 11 systems that are potentially intrinsic, as well as 4 mini-broad absorption lines (BALs) and 1 BAL. The minimum fraction of quasars with at least one intrinsic system is shown to be 38 per cent. We identify intrinsic NALs with a wide range of properties, including apparent ejection velocity, coverage fraction, and ionization level. There is a continuous distribution of properties, rather than discrete families, ranging from partially covered C IV systems with black Ly α and with a separate low-ionization gas phase to partially covered N V systems with partially covered Ly α and without detected low-ionization gas. Even more highly ionized associated and intrinsic absorption systems (O VI, Ne VIII, and Mg X doublets) have been presented in separate studies; these may represent an extension of the above sequence. We also use the properties of the NALs in conjunction with recent models of accretion disc winds that predict the origins of the absorbing gas in order to determine the model that best characterizes our sample. Additionally, we construct a model describing the spatial distributions, geometries, and varied ionization structures of intrinsic NALs.

Key words: accretion, accretion discs – galaxies: active – (*galaxies*:) quasars: absorption lines – (*galaxies*:) quasars: general.

1 INTRODUCTION

Quasars and other active galactic nuclei (AGNs) are commonly believed to be powered through accretion of material from an accretion disc on to a supermassive black hole (SMBH). Within the optical/UV spectra of quasars are broad permitted emission lines from the Balmer series of hydrogen, Ly α, and various abundant ions (i.e. Mg II λ2798, and C IV $\lambda\lambda$1548, 1551, etc.). These broad emission lines have very large widths, implying bulk speeds of the order of 10^3–10^4 km s^{-1} within the broad-line region and SMBH masses of $10^6 \lesssim M_{\rm BH} \lesssim 10^{10}$ M$_\odot$ (e.g. Kormendy & Richstone 1995; Gebhardt & Thomas 2009). The disc itself provides mechanisms of transporting angular momentum. The magnetorotational instability has been shown to be one such mechanism, as it is very robust in producing turbulence and the transport of angular momentum in discs (Velikov 1959; Chandrasekhar 1960; Balbus & Hawley 1991). Outflows are an alternate mechanism for carrying angular momentum away from the disc, and appear to be an essential part of an AGN. The outflows may be accelerated by magnetocentrifugal forces, radiation pressure in lines and continuum, momentum driving, and/or radiation pressure acting on dust (Blandford & Payne 1982; Begelman, de Kool & Sikora 1991; Emmering, Blandford & Shlosman 1992; Arav, Li & Begelman 1994; Konigl & Kartje 1994; de Kool & Begelman 1995; Proga, Stone & Kallman 2000; Proga 2003; Proga & Kallman 2004; Everett 2005; Ostriker et al. 2010; Baskin & Laor 2012; Roth et al. 2012).

Outflows from an AGN accretion disc are also thought to be important for galaxy evolution because they can deliver energy and momentum feedback to the surrounding galaxy and intergalactic medium (IGM). Feedback from an AGN can heat the gas of both the interstellar medium (ISM) and IGM, inhibiting star formation (e.g. Silk & Rees 1998; Granato et al. 2004; Di Matteo, Springel & Hernquist 2005; Springel, Di Matteo & Hernquist 2005; Ciotti & Ostriker 2007). These feedback mechanisms are critical for determining the properties of present-day galaxies. One such example is that the quasar host galaxy will become redder more rapidly through passive evolution of its stars. Outflows also serve to enrich the IGM with heavy elements (Scannapieco & Oh 2004).

★ E-mail: cculliton848@hotmail.com

According to many models (i.e. Begelman et al. 1991; Arav et al. 1994; Murray & Chiang 1998; Proga et al. 2000; Proga & Kallman 2004; Everett 2005), the outflows of quasars start deep within the potential well of the black hole and are launched above the disc. The models suggest that at high latitudes, a low-density, highly ionized wind prevails. Most of the material, however, remains at a low latitude, 'hugging' the disc. The low-latitude material is predominately warm, with low-ionization conditions and a wide range of velocities, in which broad absorption lines (BALs; $\Delta v > 2000$ km s^{-1}) could potentially form. At the interface between the low-density/high-latitude and high-density/low-latitude material are believed to be dense filaments of gas (see, for example, the simulations by Proga & Kallman 2004). These filaments can form mini-BALs ($500 < \Delta v < 2000$ km s^{-1}) or narrow intrinsic absorption lines (intrinsic NALs; $\Delta v < 500$ km s^{-1}).

BALs and mini-BALs are easily identified as being intrinsic to the quasar as it is very unlikely that intervening objects or the host galaxy's ISM would produce absorption lines as broad as BALs or mini-BALs. BALs are detected in roughly 10–25 per cent of optically selected quasars (e.g. Foltz et al. 1989; Weymann et al. 1991; Tolea, Krolik & Tsvetanov 2002; Hewett & Foltz 2003; Reichard et al. 2003a,b). Although this fraction is not easy to determine due to differential selection effects between BAL quasars and non-BAL quasars, it is usually assumed to be the fraction of the solid angle subtended by the medium creating such lines.

NAL systems are much harder to classify as intrinsic. Observed narrow absorption lines can originate from the disc winds associated with the quasar itself, from gas from the quasar host galaxy's ISM that gets swept-up in the wind, or they can originate in foreground objects such as galaxies, the IGM, or the ISM of the Milky Way (see Ganguly & Brotherton 2008, for a review). The most common ways to identify an absorption system as intrinsic are: (1) measuring a coverage fraction $C_f < 1$, which results from dilution of absorption troughs by unocculted light from the background source(s) or (2) determining that the absorption system's profile or equivalent width (EW) is variable with time (e.g. Barlow & Sargent 1997; Hamann et al. 1997a; Ganguly et al. 1999, 2003; Misawa et al. 2003; Narayanan et al. 2004; Wise et al. 2004; Misawa et al. 2007). Since NALs are less variable than mini-BALs or BALs (Misawa, Charlton & Eracleous 2014; Chen et al. 2015), in this paper, we use the former method. Additional, less commonly used means of identifying intrinsic absorption lines are described in Barlow & Sargent (1997). The coverage fraction determination utilizes the residual flux ratios between the two members of the doublet, with deviations from the 2:1 optical depth ratio dictated by atomic physics assumed to originate from a partial occultation of the quasar central engine by the absorption system. A coverage fraction of unity means that the background source is completely covered, while a small value of the coverage fraction implies that the absorption system covers only a small portion of the background source. The coverage fraction is used to identify intrinsic absorption lines since only systems physically associated with the quasar are likely to exhibit partial coverage.

Mini-BALs can be determined to be intrinsic using the methods for both BALs and NALs; they exhibit partial coverage like NALs, while their time variability and their widths imply that they are intrinsic to the quasar like a BAL. Mini-BALs, though less studied than NALs or BALs, are as common as BALs (Rodríguez Hidalgo 2009). The difference between BALs, mini-BALs, and NALs may simply be that they are viewed along different lines of sight to the central engine.

A census of intrinsic NALs and their observed characteristics would allow us to probe important properties of quasar outflows. Once specific intrinsic NALs are identified, we can carry out detailed studies of their properties, deriving the physical conditions and range of ionization parameters in the absorber, and creating a model of the absorbers themselves. This would also allow us to derive physical constraints for modelling. Currently, there is an ambiguity about which model best describes the observed properties of intrinsic NALs. Depending on which model we choose, the energy and momentum imparted by the outflow on to the ISM of the host galaxy are different. In the most commonly invoked model (e.g. Proga et al. 2000; Proga 2003; Proga & Kallman 2004), the intrinsic NALs arise in filaments that are formed by instabilities in the wind at distances of the order of 10^{15}–10^{16} cm ($\sim 10^{-2}$ pc) from the central engine. More recent models (Kurosawa & Proga 2009; Faucher-Giguère 2012; Faucher-Giguère & Quataert 2012) suggest that such filaments originate at larger distances from the SMBH, of the order of 1 pc or more, consisting of the ISM gas swept-up by the wind, and propagate away from the quasar. This is supported by several studies that suggest that absorbers can be located at much larger distances, such as 100–1000 pc scales (i.e. Arav et al. 2013; Borguet et al. 2013; Leighly et al. 2014; Chamberlain & Arav 2015). It should be noted, however, that models invoking a more distant origin for the absorber allow for only low velocity offsets from the host quasar. The high velocity offsets of some NALs argue for an origin in a fast outflow and favour an origin in an accretion disc wind.

The rate of occurrence and properties of absorbers along a quasar sightline may be related to the radio properties of the quasar. Strong associated C IV absorption lines, or strong C IV absorption lines that fall within 5000 km s^{-1} of the quasar emission redshift, were found to have a higher rate of occurrence in radio-loud quasars than radio-quiet ones, though they are seen in both the types of quasars (Foltz et al. 1986; Anderson et al. 1987; Sargent, Boksenberg & Steidel 1988; Barthel, Tytler & Vestergaard 1997). A small excess of high-velocity C IV absorbers is seen in radio-quiet quasars compared to radio-loud quasars (Richards et al. 1999; Richards 2001). Additionally, the type of radio-loud quasar is important, as lobe-dominated radio-loud quasars have been found to display stronger associated C IV absorption than core-dominated objects (Barthel et al. 1997), and an excess of C IV absorbers in flat-spectrum radio-loud quasars has been found as compared to steep-spectrum radio-loud quasars (Richards et al. 1999; Richards 2001). Becker et al. (2000) found that a quasar's radio loudness parameter, $\mathcal{R} = f_\nu(5\ \mathrm{GHz})/f_\nu(4400\ \text{Å})$ (Kellermann et al. 1989, 1994), determines the likelihood that a quasar hosts a BAL, and provided a maximum $\mathcal{R}$ for BALQSOs. At low redshifts, associated absorption lines do not occur in radio-loud, flat-spectrum quasars (Ganguly et al. 2001; Culliton et al., in preparation), though they are present in high-redshift sources (Vestergaard 2003; Misawa et al. 2007; Ganguly et al. 2013). It is therefore important to consider whether the radio properties are related to the incidence of intrinsic NAL absorption. Vestergaard (2003) did not find differences between radio-loud and radio-quiet quasars, but had intervening systems diluting any trends and only considered $\mathrm{EW_{obs}} > 0.5$ Å C IV absorbers. Misawa et al. (2007) also did not find any differences between radio-loud and quiet quasars in their sample of 37. We have doubled the sample and will therefore revisit this issue.

With the above considerations in mind, this paper attempts to identify intrinsic NALs for further study in the high-resolution spectra of 73 quasars with $z \approx 1.5$–5 through the use of a partial coverage analysis. This work also motivates to create our own simple models of both the absorbers themselves and their distance from the

host quasar, based on the properties of the NALs. This work is an extension of the work of Misawa et al. (2007), who studied intrinsic NALs in quasars at $z = 2$–4. The observations used in Misawa et al. (2007) were performed with Keck/HIRES to study high-redshift quasars, with an initial objective of studying D I abundance ratios in the Ly α forest (e.g. O'Meara et al. 2001). In the Misawa et al. (2007) survey, intrinsic NALs were identified through the partial coverage method, regardless of velocity shift from the quasar. Our goals are to extend that sample to both higher and lower redshifts, using the same methods of that survey. We use the results to create a catalogue of intrinsic absorbers, based on both kinematic and ionization properties, to consider if there are relationships between ionization state, coverage fraction, and the distance from the host quasar, to differentiate between quasar outflow models, and model the absorbers themselves.

2 BASIC OBSERVED PROPERTIES OF THE QUASARS IN OUR SAMPLE

In this paper, we use the high-resolution ($R \sim 45\,000$) spectra of 73 quasars from the VLT UVES archive, with a redshift range $1.4 < z < 4.7$. These are a subset of the 81 quasars found in the archive before 2006 June that were used for the Narayanan et al. (2007) survey of weak Mg II absorbers, excluding the 8 quasars at $z < 1.4$ for which the N V emission line would not be covered. Our sample also excluded known BAL quasars, though one BAL was found, and exhibits a preference for optically bright quasars that allow high-resolution observations. As the presence of BALs gives an enhanced probability of finding C IV associated absorption lines (Ganguly et al. 2001), the exclusion of BAL quasars may bias our sample against intrinsic NALs. However, the properties of the intrinsic NALs in our sample of quasars are unlikely to be significantly different from the NALs found towards BAL quasars.

Since we aim to determine whether the intrinsic NAL incidence rate and physical properties depend on quasar properties, we present relevant quasar properties in Table 1. The observational details were given in table 1 of Narayanan et al. (2007). Our Table 1 lists the emission redshift, $z_{\rm em}$ in column 2, and the optical luminosity, L_ν(4400 Å), at 4400 Å in the quasar rest frame in column 3. The radio luminosity, L_ν(radio), is listed in column 4 of Table 1, where 'radio' is the observed frequency of the available observation, given in column 5. The value of L_ν(5 GHz) was obtained from L_ν(radio), assuming a radio spectral index of $\alpha_{\rm r} = 0.7$. The $z_{\rm em}$, L_ν(4400 Å), and L_ν(5 GHz) distributions are presented as histograms in Fig. 1, where the grey-shaded regions represent quasars with limits on L_ν(5 GHz). The luminosities were derived from the optical flux f_ν(opt) and the radio flux f_ν(5 GHz) using the luminosity distance formula given in equation (24) of Hogg (1999). In a few cases where the 1.4 GHz luminosity was unavailable, we note the alternative frequency that was used as a proxy. In this paper, we use the WMAP cosmological parameters of $H_0 = 71$ km s^{-1} Mpc^{-1}, $\Omega_{\rm M} = 0.27$, $\Omega_{\rm k} = 0$, and $\Omega_\Lambda = 0.73$.

To determine which quasars are radio loud, we use the radio-loudness parameter, $\mathcal{R}$, which is defined as the ratio of the rest-frame radio and optical fluxes (see the previous section). The criterion for radio loudness adopted by Kellermann et al. (1989, 1994) is $\mathcal{R} \geq 10$, while Misawa et al. (2007) adopt $\mathcal{R} \geq 23$. Table 1 also lists $\mathcal{R}$ for each quasar and an indication of whether the quasar is radio loud (L) or radio quiet (Q). Our data show a clear distinction between radio-loud quasars ($\mathcal{R} > 250$) and radio-quiet quasars ($\mathcal{R} \leq 30$), so we select $\mathcal{R} = 30$ as the radio-loud/quiet boundary. Fig. 1 shows these distinct groupings, with only upper limits on $\mathcal{R}$ in grey, and cases with $\mathcal{R}$ measurements below the radio-loudness threshold in black (in all the panels). One quasar of note is Q0141–3932. It is at the centre of the cluster of radio-loud quasars in Fig. 1 with a radio-loudness parameter of $\mathcal{R} \leq 1874$, but we only have an upper limit on its radio luminosity. Therefore, this quasar may still be radio quiet, and is therefore unconstrained.

Out of the 73 quasars in our sample, 21 quasars, or 29 per cent, are confirmed to be radio loud. This is close to the fraction of radio-loud quasars in the Misawa et al. (2007) sample (32 per cent) but significantly higher than the fraction of radio-loud quasars in the general quasar population. Studies based on much larger samples of quasars (Ivezić et al. 2002; Cirasuolo et al. 2003) differ in their conclusions about the shape of the distribution of $\mathcal{R}$, but both find a small fraction of radio-loud quasars (∼5–8 per cent).

3 DATA REDUCTION AND ANALYSIS

3.1 Data reduction and identification of NALs

The spectra of the 73 quasars, retrieved from the ESO archive, were reduced with the ESO-MIDAS ECHELLE/UVES package, as described in Narayanan et al. (2007). After wavelength calibration, we applied heliocentric velocity corrections and rebinned the spectra to 0.03 Å. We then normalized the spectra by applying a continuum fit, determined using the IRAF SFIT procedure.[1]

We catalogued all absorption lines detected to at least the 5σ confidence level, then identified all the N V, C IV, and Si IV doublets up to $+10\,000$ km s^{-1} to the red of the rest wavelength of the emission redshift[2] if possible. Doublets were also catalogued down to the blueward limits for N V, C IV, and Si IV of -5000, $-70\,000$, and $-40\,000$ km s^{-1}, respectively, where each limit is set by the velocity offset required to avoid contamination by the Ly α forest. In most quasars, the contamination of N V lines by the Ly α forest blueward of the -5000 km s^{-1} limit does not allow reliable identification of the doublet. However, four N V systems were detected at higher blueshifted velocities in gaps in the Ly α forest. Doublets were confirmed if the profiles of the two members had shapes consistent with each other, and if Ly α, if covered and expected, was detected.

It is common for the profiles of the doublets to be complex, with multiple components and lines. A line is defined as a contiguous absorbed region in a normalized spectrum without a return to unity. A line can have multiple kinematic components, but absorption troughs, even those close to each other, are considered to be separate lines if they are separated by unabsorbed regions. Multicomponent lines were deblended into individual kinematic components using the software package MINFIT (Churchill & Vogt 2001) as in Misawa et al. (2007). Individual components were represented as Voigt profiles using the coverage fraction ($C_{\rm f}$), redshift, column density (N in cm^{-2}), and Doppler parameter (b in km s^{-1}) as free parameters, and the model was convolved with the instrumental profile before comparison with the data. Models with fewer kinematic components were preferentially chosen over those with a

[1] IRAF is distributed by the National Optical Astronomy Observatories, which are operated by AURA, Inc., under cooperative agreement with the National Science Foundation.

[2] The velocity offset, $v_{\rm shift}$, is defined as positive for NALs that are redshifted relative to the quasar emission redshift, and negative for NALs that are blueshifted.

Table 1. Sample quasars and their properties.

QSO[a] (1)	z_{em} (2)	$\log(L_\nu(4400\,\text{Å}))$[b] (erg s^{-1} Hz^{-1}) (3)	$\log[L_\nu(\text{radio})]$[c] erg s^{-1} Hz^{-1} (4)	ν[d] (GHz) (5)	$\log[L_\nu(5\,\text{GHz})]$[e] erg s^{-1} Hz^{-1} (6)	$\log \mathcal{R}$ [f] (7)	L/Q[g] (8)
Q0001–2340	2.28	31.778	<32.498	1.4	<31.956	<0.18	Q
Q0002–422	2.76	31.556	<32.642	1.4	<32.083	<0.53	Q
Q0010–0012	2.145	30.66	<32.451	1.4	<31.915	<1.25	Q
Q0011+0055	2.31	30.685	<32.508	1.4	<31.965	<1.28	Q
Q0013–0029	2.087	30.919	<32.43	1.4	<31.896	<0.98	Q
Q0042–2930	2.388	31.21	<32.534	1.4	<31.988	<0.78	Q
Q0048–2545	2.082	30.795	<32.428	1.4	<31.894	<1.10	Q
Q0049–2820	2.256	30.972	33.925	1.4	33.384	2.41	L
Q0055–269	3.66	31.688	33.004	1.4	32.416	0.728	Q
Q0058–2914	3.093	30.428	33.58	1.4	33.01	2.58	L
Q0100+130	2.681	31.795	<32.621	1.4	<32.064	<0.27	Q
Q0102–1902	3.04	31.173	<32.713	1.4	<32.144	<0.97	Q
Q0105+061	1.96	31.374	<32.381	1.4	<31.852	<0.48	Q
Q0109–3518	2.405	31.601	<32.539	1.4	<31.992	<0.39	Q
Q0112+0300	2.819	31.012	<32.658	1.4	<32.096	<1.08	Q
Q0122–380	2.2	31.467	<32.471	1.4	<31.932	<0.47	Q
Q0128–2150	1.9	31.989	<32.356	1.4	<31.83	<–0.16	Q
Q0130–4021	3.023	31.682	<32.709	1.4	<32.14	<0.46	Q
Q0136–231	1.893	30.606	34.665	1.4	34.139	3.53	L
Q0141–3932	1.807	28.52	<32.316	1.4	<31.795	<3.27	?
Q0151–4326	2.74	31.593	<32.637	1.4	<32.078	<0.49	Q
Q0237–23	2.223	31.662	35.877	1.4	35.338	3.68	L
Q0328–272	1.816	30.341	34.454	1.4	33.932	3.59	L
Q0329–255	2.685	31.42	34.729	1.4	34.172	2.75	L
Q0329–385	2.435	31.6	33.625	1.4	33.077	1.48	Q
Q0401–1711	4.23	31.06	<32.946	1.4	<32.343	<1.28	Q
Q0420–388	3.117	31.738	34.628	1.4	34.057	2.32	L
Q0421–2624	2.277	31.581	<32.497	1.4	<31.956	<0.37	Q
Q0425–5214	2.25	31.414	<32.488	1.4	<31.948	<0.53	Q
Q0429–4901	1.94	31.839	<32.373	1.4	<31.845	<0.00	Q
Q0549–213	2.245	30.481	34.899	1.4	34.359	3.88	L
Q0551–3637	2.318	31.311	<32.511	1.4	<31.968	<0.66	Q
Q0810+2554	1.5	31.582	<32.165	1.4	<31.659	<0.08	Q
Q0926–0201	1.661	31.554	<32.248	1.4	<31.734	<0.18	Q
Q0951–0450	4.369	30.996	<32.968	1.4	<32.362	<1.37	Q
Q0952+179	1.472	31.157	34.816	1.4	34.311	3.15	L
Q1101–264	2.145	31.884	33.232	1.4	32.696	0.812	Q
Q1108–0747	3.922	31.263	<32.894	1.4	<32.299	<1.04	Q
Q1114–0822	4.495	31.393	<32.987	1.4	<32.378	<0.98	Q
Q1114–220	2.282	30.25	34.986	1.4	34.444	4.19	L
Q1122–1648	2.405	31.758	<32.539	1.4	<31.992	<0.24	Q
Q1140+2711	2.63	31.609	<32.606	1.4	<32.051	<0.44	Q
Q1151+068	2.762	31.16	<32.643	1.4	<32.083	<0.92	Q
Q1157+014[h]	1.9997	31.233	34.439	1.4	33.909	2.68	L
Q1158–1843	2.448	31.599	<32.552	1.4	<32.004	<0.40	Q
Q1159+1337	3.984	31.106	<32.904	1.4	<32.306	<1.20	Q
Q1202–0725	4.694	31.77	<33.016	1.4	<32.402	<0.63	Q
Q1209+0919	3.3	30.869	<32.772	1.4	<32.195	<1.33	Q
Q1246–0217	2.106	31.061	<32.437	1.4	<31.902	<0.84	Q
Q1331+170	2.084	31.59	34.881	4.85	34.725	3.13	L
Q1337+113	2.919	30.991	<32.683	1.4	<32.118	<1.13	Q
Q1341–1020	2.135	31.31	<32.448	1.4	<31.912	<0.60	Q
Q1347–2457	2.534	31.748	<32.578	1.4	<32.027	<0.28	Q
Q1418–064	3.689	31.532	35.051	1.4	34.463	2.93	L
Q1444+014	2.206	30.774	<32.473	1.4	<31.934	<1.16	Q
Q1448–232	2.215	31.528	34.721	1.4	34.181	2.65	L
Q1621–0042	3.7	31.74	<32.853	1.4	<32.264	<0.52	Q
Q1629+120	1.795	30.821	34.902	4.85	34.758	3.94	L
Q2000–330	3.773	31.563	35.118	1.4	34.527	2.96	L
Q2044–168	1.932	31.283	34.844	1.4	34.316	3.03	L
Q2116–358	2.341	31.405	<32.518	1.4	<31.974	<0.57	Q
Q2132–433	2.42	31.333	<32.544	1.4	<31.996	<0.66	Q

Table 1 – *continued*

QSO[a] (1)	z_{em} (2)	$\log(L_\nu(4400\,\text{Å}))$[b] (erg s^{-1} Hz^{-1}) (3)	$\log[L_\nu(\text{radio})]$[c] erg s^{-1} Hz^{-1} (4)	ν[d] (GHz) (5)	$\log[L_\nu(5\,\text{GHz})]$[e] erg s^{-1} Hz^{-1} (6)	$\log \mathcal{R}$[f] (7)	L/Q[g] (8)
Q2059–360	3.092	30.743	<32.725	1.4	<32.155	<1.41	Q
Q2204–408	3.155	31.487	34.134	4.85	33.941	2.45	L
Q2206–199	2.56	31.465	<32.586	1.4	<32.034	<0.57	Q
Q2215–0045	1.475	31.106	<32.151	1.4	<31.646	<0.54	Q
Q2217–2818	2.406	31.798	<32.539	1.4	<31.993	<0.20	Q
Q2222–3939	2.18	31.222	<32.464	1.4	<31.926	<0.70	Q
Q2225–2258	1.891	31.399	<32.352	1.4	<31.827	<0.43	Q
Q2243–6031	3.01	31.451	33.451	0.843	32.729	1.28	Q
Q2314–409	2.448	30.808	34.643	4.85	34.472	3.66	L
Q2344+0342	4.239	31.261	<32.947	1.4	<32.344	<1.08	Q
Q2347–4342	2.88	31.58	<32.673	1.4	<32.11	<0.53	Q

Notes. [a]Quasar coordinate name.
[b]Optical luminosity at 4400 Å in the quasar rest frame.
[c]Observed radio luminosity. If no radio source is detected within 10 arcsec of the optical source, we use the detection limit of the survey as an upper limit to the radio flux.
[d]Radio frequency corresponding to the observed radio luminosity given in column 4.
[e]Radio luminosity at 5 GHz in the quasar rest frame, obtained from the observed luminosity using a spectra index of $\alpha_r = 0.7$.
[f]Radio-loudness parameter, defined in Section 2.
[g]Radio-loud or radio-quiet quasar (see Section 4 for definition).
[h]BAL quasar.

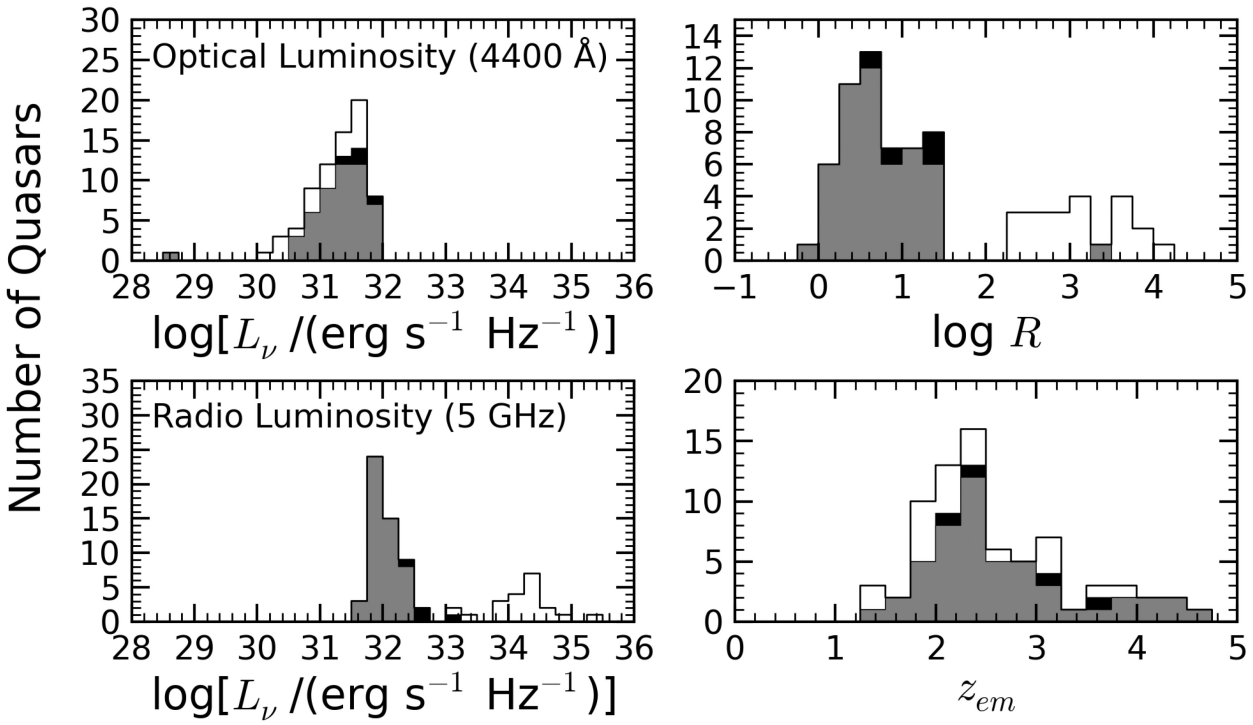

Figure 1. Distribution of optical (4400 Å) and radio (5 GHz) specific luminosities, as well as the radio-loudness parameter and emission redshift of the 73 quasars in our sample. The grey-shaded bins represent those quasars for which only an upper limit was determined for the radio luminosity. The black-shaded bins are those quasars for which a radio luminosity was measured, but the radio-loudness parameter is still small enough for the quasar to be considered radio quiet. The radio-loud objects cluster at 5 GHz luminosities between 10^{34} and 10^{35} erg s^{-1} Hz^{-1}, and show a distinct separation from radio-quiet objects. It is unclear whether the one grey-shaded bin at $\log R \approx 3.3$ belongs to the radio-loud or radio-quiet class of objects. Its R places it among the radio-loud objects, yet no radio flux was detected, leaving it with only an upper limit on its radio-loudness parameter.

larger number of components, provided that the smaller number of components still provided an acceptable fit as determined by the F-test. NALs that lay within 200 km s^{-1} of each other were combined into a single system, because a set of lines with such small velocity offsets is thought not to be physically independent (e.g. Sargent et al. 1988; Misawa et al. 2007). It seems unlikely that components separated by less than 200 km s^{-1} are not related in some way. Within 200 km s^{-1}, components tend to cluster, whereas

at velocities above 200 km s^{-1}, the distribution of components is more random, and seemingly unrelated to each other. Additionally, 200 km s^{-1} corresponds approximately to the rotation speed of a massive galaxy, so systems at speeds separated by less than that speed seem likely to be physically associated with each other in some way.

We identified intrinsic NAL candidates by looking for an incomplete occultation of light from the continuum and/or emission-line sources in C IV, N V, and Si IV doublets. The ratio of optical depths of the doublet members should obey $\tau_b/\tau_r = f_b\lambda_b/f_r\lambda_r$, where τ_b and τ_r are the true optical depths of the blue and red members of the doublets, respectively, f_b and f_r are the oscillator strengths of the doublet, and λ_b and λ_r are the wavelengths of each doublet member (e.g. Savage & Sembach 1991). For the doublet transitions C IV λλ1548, 1551, N V λλ1239, 1243, and Si IV λλ1394, 1403, atomic physics dictates that $f_b\lambda_b/f_r\lambda_r = 2$. We attribute cases where $\tau_b/\tau_r < 2$ to partial coverage of the source of radiation, allowing unocculted light to change the relative strength of the doublet lines (e.g. Wampler, Bergeron & Petitjean 1993; Wampler, Chugai & Petitjean 1995; Barlow & Sargent 1997; Hamann, Barlow & Junkkarinen 1997b; Hamann et al. 1997a; Ganguly et al. 1999). We consider the corresponding NALs to be candidate intrinsic NALs, since partial coverage is not seen for intervening absorbers except in the rare case of cold, very small gas clouds (e.g. Kobayashi et al. 2002; Jones et al. 2007; Chen & Qin 2013). It is important to note that although partial coverage is the more likely cause of deviations of the line ratios from their expected values, deviations can also result from local emission by the absorbers (Wampler et al. 1995), or from the scattering of background photons into our line of sight (e.g. Ganguly et al. 1999).

3.2 Coverage fraction

We follow the methods of Misawa et al. (2007) to determine the values of the coverage fraction both on a pixel-by-pixel basis, and for kinematic components from the Voigt profile fits. The coverage fraction is defined as the fraction of all photons at a given wavelength that are incident on the absorber, with a physical range of $0 < C_f \leq 1$. In order to determine the coverage fraction, we assume a single extended background source (which emits the continuum and the broad emission lines), and use the methods and equations described in detail in Ganguly et al. (1999) and Misawa et al. (2007).

Based on the results of the coverage fraction analysis, each NAL was then classified into one of three classes based on our confidence that it is intrinsic. Class A includes those NALs that were reliably intrinsic, such as mini-BALs or those that MINFIT determined to have a coverage fraction less than unity with high significance [$C_f + 3\sigma(C_f) < 1$ for at least one kinematic component]. Class B NALs are those that are potential candidates, such as line-locked systems or those whose coverage fraction was determined to be within 1σ of unity by both MINFIT and the pixel-by-pixel method at the centre of at least one component. Class C includes lines that did not show partial coverage, or were unacceptable for classification due to problems with the model or continuum fits (especially in the case of weak lines), a critical data defect, or large systematic errors. Examples of cases with large systematic errors are: weak components at the edge of a system, weak components between much stronger components, components in a heavily blended region (except for regions with extremely high S/N), and components for which we obtained unphysical values of C_f in the first fitting trial. For such components, C_f is set to unity, and the fits are repeated for the other components in the system.

We found that for all quasars, a 5σ detection of C IV was possible over at least 95 per cent of the path-length at an observed EW of 0.031 Å or higher (assuming an unresolved line). For an unresolved N V line, a 5σ detection could be made over at least 95 per cent of the path-length for any given quasar at an observed EW of 0.036 Å or higher. Si IV detections can be made at an observed EW of 0.029 Å or higher (assuming an unresolved line). At the minimum wavelength for our survey, those EW limits correspond to rest-frame EWs for the blueward doublet members of 0.016 Å for C IV, 0.015 Å for N V, and 0.013 Å for Si IV. The systems with EWs greater than the minimum rest-frame EW for the given transition define the 'homogeneous' sample. There are four homogeneous samples, one for each of C IV, N V, and Si IV, and one for systems that have at least one transition with a rest-frame EW greater than the minimum rest-frame EW for the given transition. Our ensuing analysis and presentation of figures pertain only to these homogenous samples. Some weaker systems are detected in quasar spectra with higher S/N, but these systems are not in the relevant homogeneous sample.

For systems with a detected doublet that has multiple components within one or more lines, the entire doublet for that system is classified based on its highest reliability intrinsic component. If even one component from that doublet satisfies the criteria for class A, then the entire doublet is class A. If there are no class A components for the doublet, but there is at least one class B component, then the entire doublet is class B. Finally, if multiple doublets are detected for the same system (i.e. C IV, N V, Si IV), then the entire system is classified based on the highest reliability intrinsic component for any of the transitions. Table 2 presents the results of this classification. It gives the total number of systems, lines, and components found in the sample, as well as in the homogeneous sample. The table also presents the total number of systems within the different reliability classes and the number of systems detected in the different doublets (C IV, N V, Si IV). We refer to specific intrinsic systems by the doublet used to determine the system to be intrinsic. For example, if a system was found to be a class A system due to the measured coverage fraction in the C IV transition, that system would be known as a C IV NAL system. Similarly, if the system is intrinsic due to measurements of N V or Si IV, the system would be known as a N V NAL system or a Si IV NAL system. If multiple transitions give coverage fractions that result in the system being considered intrinsic, such as C IV and N V, that system would be both a C IV NAL system and a N V NAL system. Of the 399 systems in our homogeneous sample, we found that 90 per cent were detected in C IV, 6 per cent in N V, and 13 per cent in Si IV. The fraction of C IV systems in the homogeneous sample that are classified as either class A or B is 11 per cent. For Si IV systems, the intrinsic fraction (8 per cent) is consistent with that value, while systems with N V detected are more likely to be intrinsic (38 per cent).

4 RESULTS AND DISCUSSION

In Section 3.2, the rest-frame EW limits for the blueward member of the C IV, N V, and Si IV doublets were found to be 0.016, 0.015, and 0.013 Å, respectively. Using the results from the previous sections, we examine the statistical properties of the NALs and their relationships to the quasars hosting them. We study the distributions of EW, velocity offset, and coverage fraction. We also explore the relationships between the quasar's properties, such as luminosity and radio loudness, and the incidence rates and properties of the intrinsic NALs.

Table 2. Census of systems, lines, and kinematic components.

Ion (1)	Class (2)	Systems[a] (3)	Lines (4)	Components[b] (5)
All	All[c]	414	636	1685
	Homogeneous[d]	398	620	1659
	A	35	57	173
	B	11	25	56
	C	352	538	1430
C IV	All[c]	373	513	1397
	Homogeneous[d]	360	500	1375
	A	29	42	112
	B	9	18	41
	C	322	440	1222
N V	All[c]	25	39	116
	Homogeneous[d]	24	39	116
	A	8	10	49
	B	1	4	8
	C	15	25	59
Si IV	All[c]	56	84	172
	Homogeneous[d]	51	81	168
	A	3	5	12
	B	1	3	7
	C	47	73	149

Notes. [a]Combined multiple NALs that lie within 200 km s^{-1} of each other. See the discussion in Section 3.1.
[b]Narrow kinematic components deblended by Voigt profile fitting with MINFIT.
[c]All lines that are detected at greater than a 5σ confidence level, $W_{obs}/\sigma(W_{obs}) \geq 5$, regardless of their EW.
[d]Doublets with rest-frame EWs of their stronger (bluer) components larger than the minimum EW that corresponds to the 5σ detection limit, W_{min}. These limits are W_{min}(C IV) = 0.016 Å, W_{min}(N V) = 0.015 Å, and W_{min}(Si IV) = 0.014 Å (see Section 3.1).

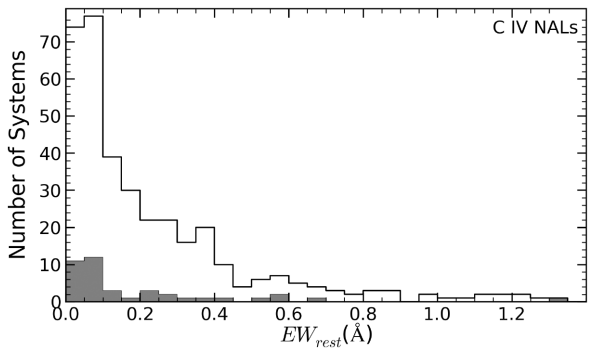

Figure 2. The distribution of EWs of the candidate intrinsic systems (class A+B; shaded) versus all C IV systems (class A+B+C; not shaded).

4.1 EW distribution

As described in Section 3.2, the rest-frame EW limits for the blueward doublet members were 0.016 Å for C IV, 0.015 Å for N V, and 0.013 Å for Si IV. The rest-frame EW distribution of the 1548 Å member of all C IV doublets detected in our sample is shown in Fig. 2. The spectral resolution and S/N of some of the VLT/UVES archival spectra allow us to measure NAL EWs that are considerably weaker than in previous surveys. The shaded histogram in Fig. 2 shows the number of reliably or potentially intrinsic C IV systems (class A+B) with a given rest-frame EW bin. A substantial portion of class A and class B C IV NALs (10 or 26 per cent) and of all C IV NALs (86 or 25 per cent) within the homogenous sample have EWs lower than the detection limit of 0.056 Å of the Misawa et al. (2007) survey. Our EW distribution has the same shape as that of Misawa et al. (2007) at larger values. The main difference comes from filling in more of the EW distribution at small values. Also, with a larger sample than that of Misawa et al. (2007), we have more absorbers at all EWs. The distributions of the following two samples, class A+B and class A+B+C, cannot be distinguished from each other to any significance. A KS test comparing the two samples to see if they are from the same parent population returns a KS statistic of 0.19 and a *P*-value of 0.15, indicating that the test fails to find a difference in the two distributions with significant confidence. An Anderson–Darling test to compare the same finds the same result. It returns an AD statistic of 0.73 and a *P*-value of 0.16. As such, the two distributions are indistinguishable from each other, indicating that one does need high-quality and/or multi-epoch data to find intrinsic systems. It is difficult to determine the coverage fraction for C IV doublets with low EWs, but in some high signal-to-noise spectra this has been possible, leading to a population of very weak intrinsic C IV absorbers. When comparing to the results of Misawa et al. (2007), we should keep in mind the presence of this additional population of weak absorbers.

Early studies of C IV associated absorption lines (Weymann et al. 1979; Young, Sargent & Boksenberg 1982; Foltz et al. 1986; Vestergaard 2003) had much higher rest-frame EW limits (0.3–0.6 Å) than either the present survey or that of Misawa et al. (2007). In our sample, 85 per cent of intrinsic NALs and 75 per cent of all NALs had rest-frame EWs below 0.3 Å. For example, Vestergaard (2003) examined the relationship between radio properties and strong C IV NALs (EW$_{rest}$ > 0.5 Å) in quasars that were previously not known to be BAL quasars. Strong C IV systems were not found to have a preference for either radio-quiet or radio-loud quasars. However, this result applied to NALs with a much higher EW than in our sample, and likely included intervening absorbers that would dilute any trends with radio properties. In our study, we are able to identify intrinsic absorbers instead of making a statistical comparison. If we similarly limit our sample to the strongest C IV systems, those with EW$_{rest}$ > 0.5 Å, we can determine whether our rejection of BAL quasars affects our sample of intrinsic NALs. If we take into account the different method of measuring the EW of C IV [previous studies, including that of Vestergaard (2003), included both members of the C IV doublet in the calculation of the EW], we find that the Vestergaard sample of 114 quasars (66 radio-loud quasars and 48 radio-quiet quasars) includes 32 quasars that contain 39 C IV doublets with EW$_{rest}$ > 0.5 Å. Of those quasars, 19, containing 23 systems, are radio-loud quasars. The remaining 16 systems are found in the spectra of 13 radio-quiet quasars. Using Vestergaard's survey statistics, we can predict the incidence of strong C IV NALs expected in our survey and the fraction of quasars in which those strong C IV NALs should appear. We expect to find 7 C IV NALs in radio-loud quasars, and 16 in radio-quiet quasars. We actually find 1 class A+B C IV NAL, and a total of 9 C IV NALs in our 21 radio-loud quasars, while we find 4 class A+B C IV NALs, and a total of 37 C IV NALs in our 52 radio-quiet quasars. If we instead consider the number of quasars that we expect to have at least one strong C IV NAL, we expect to find them in 6 radio-loud and 14 radio-quiet quasars. We find them in 1 radio-loud quasar for class A+B C IV NALs and 8 for all C IV NALs in radio-loud quasars. We find those systems in 3 radio-quiet quasars for class A+B C IV NALs and 27 radio-quiet quasars for all C IV NALs. The predictions based on Vestergaard (2003) are then bounded by the results of our intrinsic and total samples. This is consistent with some of our class C C IV NALs actually being

Table 3. Statistical properties of systems.

Sample (1)	Number/Density (2)	C IV AAL (3)	C IV Non-AAL (4)	C IV Total (5)	N V AAL (6)	N V Non-AAL (7)	N V Total (8)	Si IV AAL (9)	Si IV Non-AAL (10)	Si IV Total (11)
Path-length[a]	δz	33.9	97.6	131.0	28.5	0	28.5	35.7	51.9	87.6
	$\delta\beta$	9.8	30.8	40.6	8.0	0	8.0	10.0	15.8	26.0
Class A	N[b]	10 (10)	19 (16)	29 (24)	8 (8)	0 (0)	8 (8)	2 (2)	1 (1)	3 (3)
	dN/dz	0.3	0.19	0.22	0.28	...[c]	0.28	0.056	0.019	0.034
	dN/dβ	1.0	0.62	0.71	1.0	...[c]	1.0	0.2	0.063	0.12
Class A+B	N[b]	13 (12)	25 (20)	38 (29)	9 (9)	0 (0)[c]	9 (9)	2 (2)	2 (2)	4 (3)
	dN/dz	0.38	0.26	0.29	0.32	...[c]	0.32	0.056	0.039	0.046
	dN/dβ	1.3	0.81	0.94	1.1	...[c]	1.1	0.2	0.13	0.15
Class C	N[b]	40 (32)	282 (69)	322 (70)	11 (10)	4 (4)[c]	15 (14)	7 (7)	40 (26)	47 (28)
	dN/dz	1.2	2.9	2.4	0.39	...[c]	0.53	0.2	0.77	0.54
	dN/dβ	4.1	9.2	7.9	1.4	...[c]	1.9	0.69	2.5	1.8
Total	N[b]	53 (37)	307 (89)	360 (72)	20 (18)	4 (4)[c]	24 (22)	9 (9)	42 (28)	51 (28)
	dN/dz	1.6	0.26	2.7	0.7	...[c]	0.84	0.25	0.039	0.58
	dN/dβ	5.4	0.81	8.9	2.5	...[c]	3.0	0.89	0.13	2.0
Systems[d]	A/Total	18.9%	6.19%	8.06%	40.0%	0%	33.3%	22.2%	2.38%	5.88%
	A+B/Total	24.5%	8.14%	10.6%	45.0%	0%	37.5%	22.2%	4.76%	7.84%
Quasars[e]	A/Total	13.7%	21.9%	32.9%	11.0%	0%	11.0%	2.74%	1.37%	4.11%
	A+B/Total	16.4%	27.4%	41.1%	12.3%	0%	12.3%	2.74%	2.74%	4.11%

Notes. [a]The total redshift and velocity intervals considered in the determination of dN/dz and dN/dβ. The interval for each ion is from 10 000 km s^{-1} to the red of the quasar redshift up to the beginning of the Ly α forest, which corresponds to about 70 000 km s^{-1} to the blue of the quasar for C IV, 5000 km s^{-1} for N V, and 40 000 km s^{-1} for Si IV.

[b]N denotes the number of systems (see Section 3.1). The number in parentheses gives the number of quasars in which these systems are detected. All systems are homogeneous systems.

[c]Due to blending with the Ly α forest, no path-length was calculated for N V outside of the associated region. However, four class C systems were found in gaps in the Ly α forest, resulting in a non-zero number of N V systems found over a path-length of zero. The calculated density would therefore be unphysical and is not listed.

[d]Percentage of class A and class A+B systems relative to all systems, broken down by transition and by velocity window (associated versus non-associated).

[e]Percentage of quasars hosting class A and class A+B systems relative to all quasars, broken down by transition and by velocity window (associated versus non-associated).

intrinsic, since Vestergaard's statistical approach would include intrinsic systems with unity coverage fraction. Because we find more systems with large EWs than did Vestergaard (2003), it is unlikely that we are biased against finding C IV absorption lines with large EWs. Whether or not our rejection of BAL quasars affects our sample of intrinsic NALs is unclear. Additionally, in agreement with Vestergaard (2003), we find that neither radio-loud nor radio-quiet quasars are more likely to contain systems with these larger EWs.

4.2 Velocity offset

The velocity offset distribution of intrinsic NALs is important because it can tell us about the ionization structure and location of the quasar outflows. However, not all intrinsic NALs show partial coverage, so the distribution that we present provides only a lower limit on the density of intrinsic NALs. Also, because of contamination by the Ly α forest, our survey is limited in velocity, and some high-ejection velocity intrinsic absorbers could fall in the Ly α forest, which would place them outside the velocity range over which we can probe. Despite these limitations, we calculate the density of systems per unit redshift interval (dN/dz) and per unit velocity interval (dN/d$\beta = c$dN/dv) in Table 3. Densities were calculated for the homogeneous samples of each ion, and are broken down into intrinsic systems (class A and class A+B), class C systems, and all systems (class A+B+C). Intrinsic Si IV densities were much lower than those of C IV ions over the entire path-length

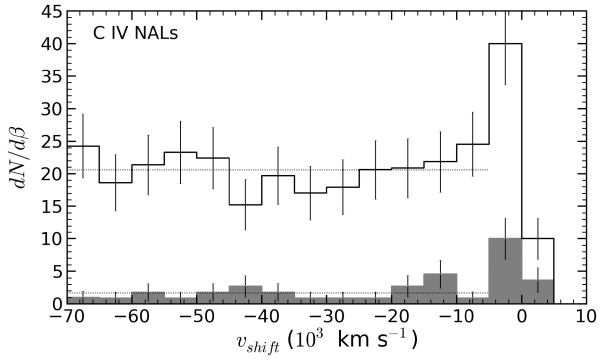

Figure 3. The velocity offset distribution of the class A+B intrinsic NAL systems (shaded) versus all C IV systems (not shaded). The two dotted lines represent the average value of the velocity bins with $v_{\rm shift} < -5000$ km s^{-1}. The upper dotted line is for all C IV systems, while the lower dotted line is for class A+B intrinsic NAL systems.

and in the associated region, and much lower than intrinsic N V densities in the associated region. Intrinsic C IV and N V systems were determined to have about the same density in the associated region. Intrinsic C IV systems, however, were also found beyond 5000 km s^{-1} with densities of half to two thirds the densities within the associated regions. Fig. 3 shows a histogram of C IV densities out to 70 000 km s^{-1}. The two dotted lines represent the average value of the histogram bins at $v_{\rm shift} < -5000$ km s^{-1} for both intrinsic

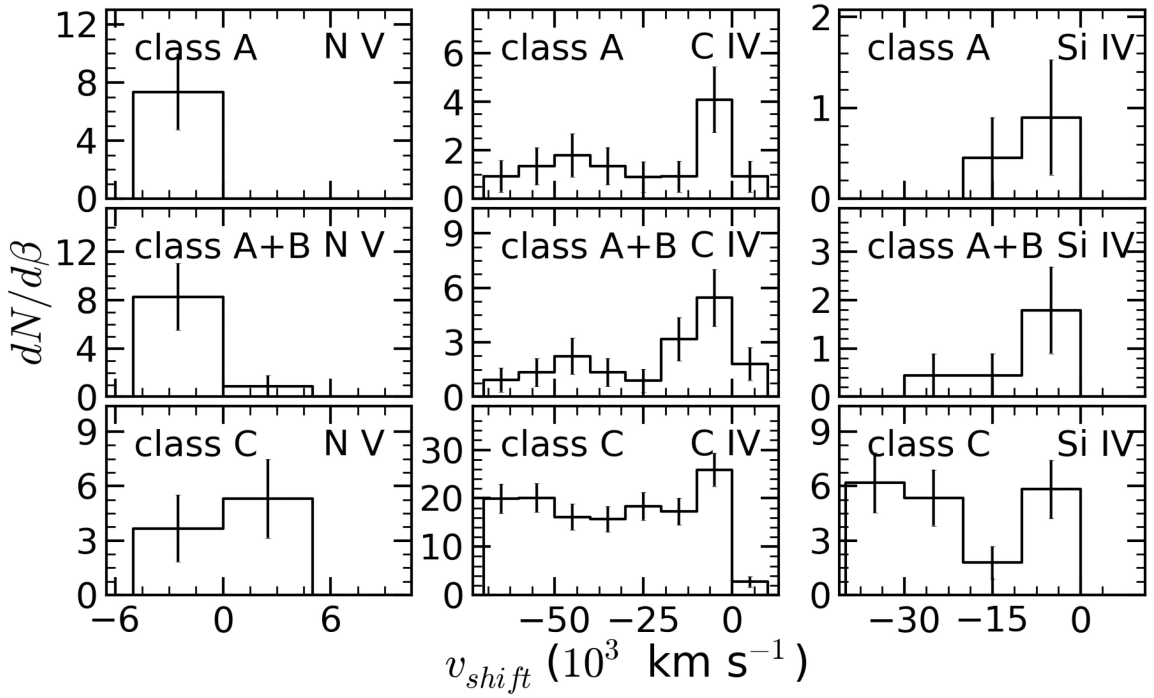

Figure 4. Velocity offset distributions of, from left to right, N V, C IV, and Si IV NALs. For each transition, we plot separately the distribution of class A (top), class A+B (middle), and class C (bottom) systems. Velocity offset distribution is shown for each ion, and separated by class.

and all C IV systems. No high-velocity N V NAL systems were found. It is unclear from this sample whether the Ly α forest makes identifying intrinsic N V NAL systems using the partial coverage method too difficult, or if intrinsic N V NAL systems do not occur at high velocity offsets. Previous studies, however, have found a lack of N V systems outside of the associated region, even at low redshifts (e.g. Fox et al. 2009; Culliton et al., in preparation). Fig. 4 shows plots similar to Fig. 3, with the velocity offset distribution for each ion plotted, and separated by class.

In their statistical sample, Vestergaard (2003) noted a possible correlation between the EW of intrinsic NALs and absorber velocity offset. Many of the absorbers with the largest EWs within our sample do appear to reside within 5000 km s^{-1} of the quasar redshift, as shown in Fig. 5(a). However, the increase of the EW begins around $-15\,000$ km s^{-1}, rather than -5000 km s^{-1}. When comparing the EW distributions of associated intrinsic C IV NALs to non-associated intrinsic C IV NALs, a KS test results in a P-value of 18 per cent. As such, we cannot reject the hypothesis that the two distributions are the same. Using an Anderson–Darling test, however, the P-value is only 4 per cent. If we instead divide the intrinsic C IV NALs at $-15\,000$ km s^{-1}, KS tests show less than a 2 per cent chance of the two samples coming from the same EW distribution, while an Anderson–Darling test results in less than a 1 per cent chance. The trend to have large EW NALs at low velocities is also apparent for both radio-loud and radio-quiet quasar subsamples, if we divide the distributions at $-15\,000$ km s^{-1}, rather than -5000 km s^{-1}.

If we instead consider all C IV NALs of any class that have an observed EW greater than the EW limit of about 0.3 Å used in Vestergaard (2003), we still do not observe increased EWs for C IV NALs within the associated region with any significance. Upon visual inspection, the trend may in fact be reversed, with the largest EWs lying outside the associated region. The Misawa et al. (2007) sample also shows a weak trend in this reversed direction.

4.2.1 *Associated systems*

Associated absorption lines, also known as 'proximate' absorption lines, are generally systems with $z_{\rm abs} \approx z_{\rm QSO}$, regardless of whether they are intrinsic or not. We use a definition for associated absorption lines such that they are specifically those absorption lines that fall within 5000 km s^{-1} of the quasar emission redshift. It has been suggested that many of the associated NALs are physically associated with the quasar itself because the frequency per unit velocity increases with decreasing velocity offset from the quasar (Weymann et al. 1979). Previous surveys (i.e. Weymann et al. 1979; Misawa et al. 2007; Nestor, Hamann & Rodriguez Hidalgo 2008; Tripp et al. 2008; Wild et al. 2008; Ganguly et al. 2013) have shown that the values of dN/dz and dN/dβ for associated NALs are approximately equal to twice the values for non-associated NALs. Fig. 3 compares the velocity offset distribution of all C IV NALs with those that are reliably or potentially intrinsic. The density of all C IV NALs rises near the emission redshift, with dN/dβ for the blue half of the associated region, (-5000)–(0) km s^{-1}, being roughly twice that of higher velocity regions, in agreement with Weymann et al. (1979). The red half of the associated region, 0–5000 km s^{-1}, has a much lower number of total systems, well below the average number of systems for bins with $v_{\rm shift} < -5000$ km s^{-1} (the dotted lines in Fig. 3). However, the fraction of all C IV NALs that are intrinsic is higher from 0 to 5000 km s^{-1} than anywhere else (36 per cent from 0 to 5000 km s^{-1} compared to $\sim$25 per cent from -5000 to 0 km s^{-1}, and $\sim$8 per cent at higher ejection velocities).

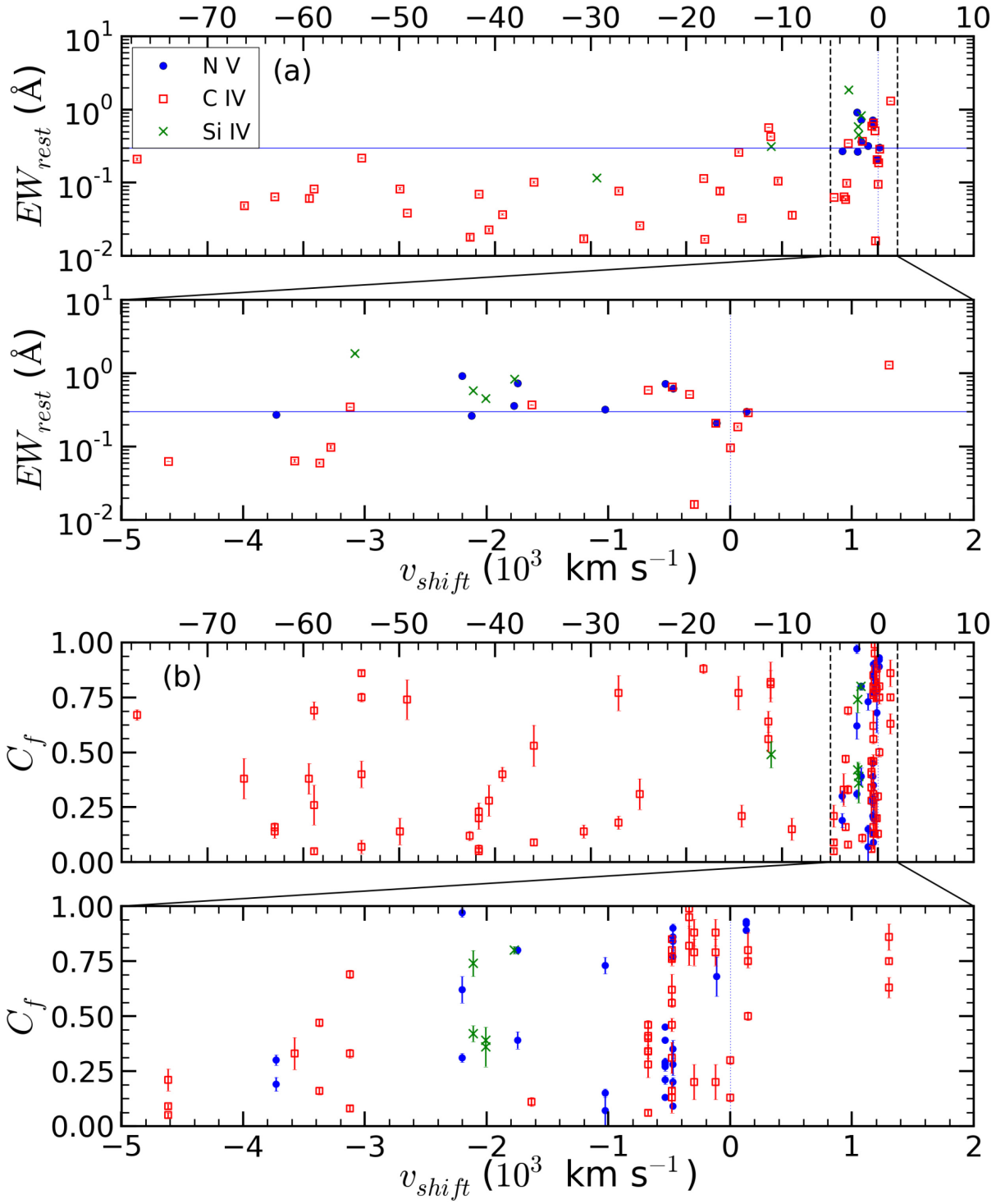

Figure 5. (a) The equivalent width (EW, top pair) and (b) the coverage fraction (C_f, bottom pair) plotted against the velocity offset ($v_{\rm shift}$). The only coverage fractions plotted are those with physical values (i.e. $0 < C_f \leq 1$) and evaluated with high reliability [i.e. $\sigma(C_f) < 0.1$]. The upper panels in each pair display a velocity offset range from −80 000 to 10 000 km s^{-1}, while the lower panels focus on the narrow range between −5000 and 2000 km s^{-1}. The blue circles denote N V NALs, the red squares represent C IV NALs, while the green triangles signify Si IV. The blue horizontal lines in the EW plots are meant to indicate that, while there are no systems at high velocity offset (>12 000 km s^{-1}) with EWs larger than 0.3 Å, roughly half of the systems in the associated region have EWs larger than 0.3 Å.

The fraction of intrinsic C IV systems in our sample is consistent with previous studies of C IV NALs at different redshifts, determined via a variety of different methods. We found that 19 per cent of the associated C IV systems, 22 per cent of the associated Si IV systems, and 40 per cent of the associated N V systems were reliably intrinsic (class A). The sum of reliably and potentially intrinsic (class A +B) associated systems was 25, 22, and 45 per cent of all associated C IV, Si IV, and N V systems, respectively, as seen in Table 3. In

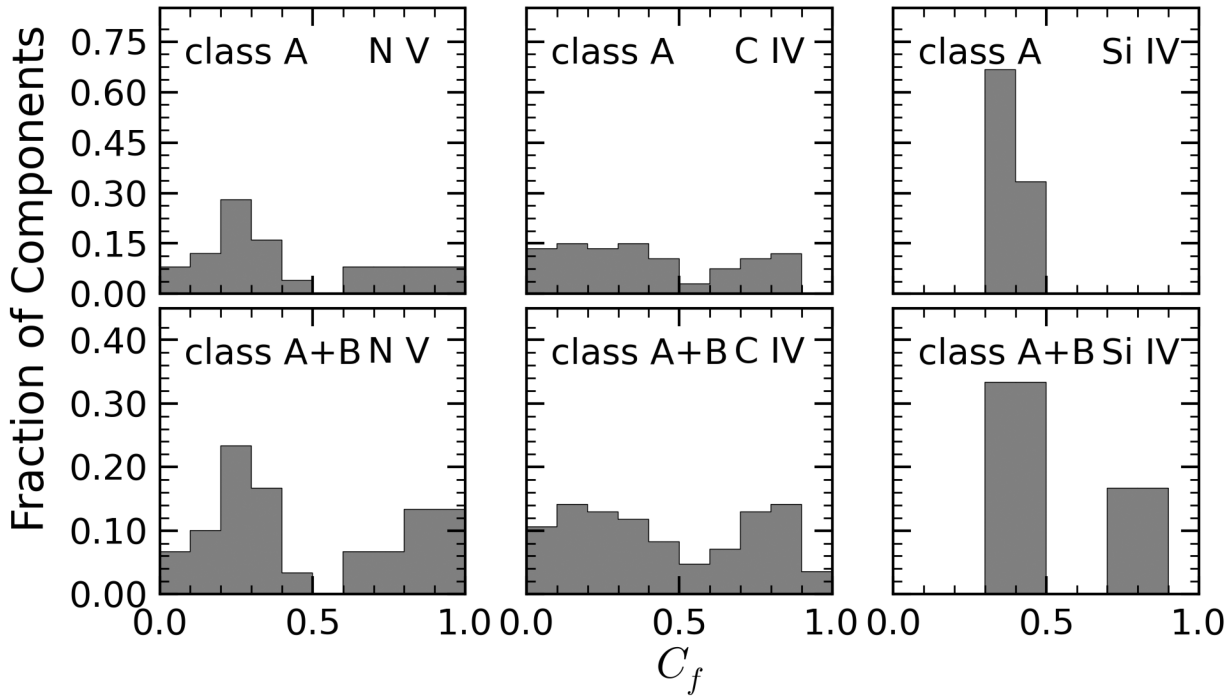

Figure 6. The distribution of coverage fractions of, from left to right, N V, C IV, and Si IV. For each transition, we plot separately the distribution of class A (top) and class A+B (bottom) systems. We only plot those components that have physical values of C_f (i.e. $0 < C_f \leq 1$) and are evaluated with high reliability [i.e. $\sigma(C_f) < 0.1$].

comparison, Misawa et al. (2007) found that 33 per cent of the associated C IV NALs, 0 per cent of the Si IV associated NALs, and 75 per cent of the associated N V NALs were intrinsic (i.e. class A). All of the N V systems found in their sample were associated NALs. Considering all three ions, we found that 19 per cent of associated systems are class A,[3] while 23 per cent are either class A or B, determined through partial coverage in one or more of the ions. However, it must be noted that all of these fractions are actually lower limits to the true fractions. Variability studies yield a similar fraction, as Barlow, Hamann & Sargent (1997), Wise et al. (2004), and Narayanan et al. (2004) found, respectively, that 30, 21, and 23 per cent, of NALs are variable, and therefore intrinsic. We note, however, that partial coverage and variability studies need not yield the same limits on the fraction of intrinsic NALs since systems exhibiting these two behaviours may only partially overlap.

4.2.2 *Intrinsic systems at large velocity offsets*

The non-negligible number and density of intrinsic NALs, even at high velocities, have a direct implication for studies of the cosmological evolution of intervening NALs. Typically, cosmological applications assume any non-associated NALs to be intervening. We find that at $|v_{\rm shift}| > 5000$ km s^{-1}, 6–8 per cent of C IV NALs and 2–5 per cent of Si IV NALs in our sample are intrinsic; the lower bound is set by class A systems, while the upper bound corresponds to class A+B. There are no high-velocity class A or B N V NALs in our sample. N V systems at $|v_{\rm shift}| \gtrsim 5000$ km s^{-1} become blended with the Ly α forest. The only systems that were found in gaps within the Ly α forest were determined to be class C systems. Summing over all ions, 5–6 per cent of all non-associated systems are intrinsic. These numbers are lower limits, based on the fact that not all intrinsic NALs have $C_f < 1$. However, they only apply for the ejection velocity intervals covered by our sample. With some of the systems that were previously believed to be intervening actually being intrinsic, the number density per redshift of intervening systems is slightly reduced.

We can use the results of Richards et al. (1999) and Richards (2001) to try to determine the fraction of intrinsic NALs that can be found at high velocity offsets ($v_{\rm shift} < -5000$ km s^{-1}). Those studies found that the fraction of non-associated NALs that are intrinsic can be as high as 36 per cent at those velocities. Taking that result at face value, Misawa et al. (2007) determined that only 30–50 per cent of intrinsic C IV NALs show the signature of partial coverage. Using our results (as seen in Table 3) and performing the same analysis, we find that only about 15–20 per cent of non-associated intrinsic C IV NALs have coverage fractions less than 1. This is to be expected, as the distribution of coverage fractions in Fig. 5(b) does not appear to prefer lower coverage fractions to higher ones. There is no reason to believe that absorption systems creating NALs cannot be larger than the background source. As long as the absorber is not patchy or allows for scattered light to get around it, preventing deviations from the 2:1 optical depth ratio, then such a system would exhibit a coverage fraction of unity, and appear to be an intervening system.

4.3 Distribution of coverage fractions

Fig. 6 shows the normalized distribution of coverage fractions, broken down by both class and transition. Those components with unphysical values for the coverage fraction are excluded. It appears

[3]This result is not inconsistent with the fraction of systems for each ion in the associated region. Not only are there more C IV systems in the associated region than Si IV or N V systems, but Si IV and N V intrinsic systems commonly also exhibit a C IV component. Thus, their contribution to the fraction of all associated systems that are intrinsic is modest.

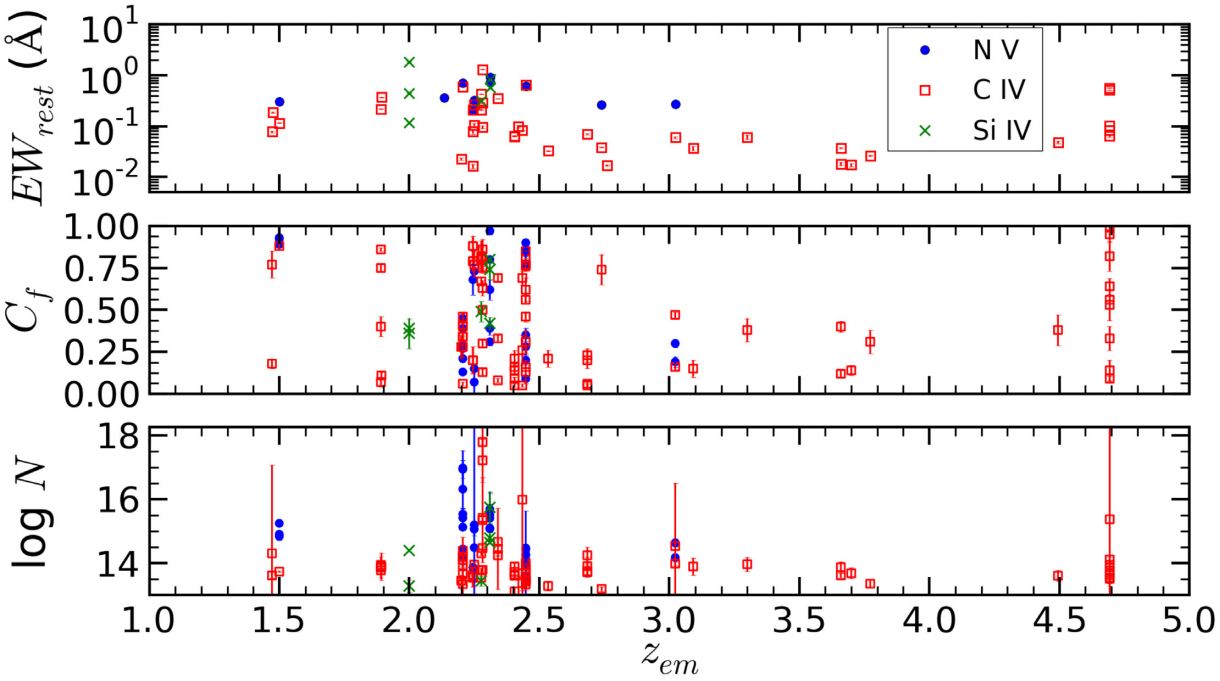

Figure 7. The distribution of the equivalent widths (EW, top) and the coverage fractions (C_f, middle) of each kinematic component within the intrinsic absorber, and the total column density (N, bottom) of the intrinsic absorbers plotted against the host quasar's emission redshift (z). The blue circles denote components or systems found using N V, the red squares represent C IV components or systems, and the green triangles signify Si IV components or systems.

that components in class A and/or class B systems do not prefer a specific coverage fraction, and instead are uniformly distributed between 0 and 1.

Some intrinsic NAL systems allow the measurement of the coverage fraction in multiple transitions (e.g. Yuan et al. 2002; Ganguly et al. 2003). It has been observed that higher ionization transitions tend to have larger coverage fractions than lower ionization transitions (Petitjean & Srianand 1999; Srianand & Petitjean 2000; Muzahid et al. 2013). One possible explanation is that the effective size of either the broad emission-line region (BELR) or the continuum source is not the same for all transitions. The BELR, in particular, appears to have a different size depending on the transition as measurements of the effective BELR size for different emission lines using reverberation show the size to be bigger for ions with smaller ionization potentials (e.g. Onken & Peterson 2002). The BELR comes from the innermost part of the disc, which transitions from producing X-rays to UV radiation as radius increases (e.g. Onken & Peterson 2002). Transitions requiring a higher ionization parameter would then need to cover a smaller region of the disc, as opposed to low-ionization transitions. A second possibility is that different lines form in different regions of the absorber (e.g. Ganguly et al. 2003, 2005, 2006, 2013). For example, an absorbing filament could comprise a tenuous, highly ionized 'atmosphere' surrounding a denser, lower ionization 'core'. This could explain why the coverage fractions measured for different components within the same system are often different, making it nearly impossible to assign a single coverage fraction to the entire system.

The physically meaningful coverage fractions of each measured component from intrinsic systems are shown in Fig. 5(b), in which they are plotted against the velocity offset. There are no apparent trends. Misawa et al. (2007) found that the class A+B N V NALs have lower C_f values than for C IV and Si IV NALs. However, upon visual inspection of our sample plotted in Fig. 5(b), no such relation is apparent. The coverage fractions of the N V lines appear uniformly distributed between 0 and 1, as do those of the C IV and Si IV NALs. One trend apparent in our data that is not present in the Misawa et al. (2007) data is that the EWs of relatively low-velocity intrinsic NALs appear to be systematically larger than those of high-velocity intrinsic NALs.

In Fig. 7, we plot the evolution of EW and coverage fraction for components within the intrinsic (class A+B) systems, and the total column density of the class A+B systems with respect to redshift. Upon inspection, there does not appear to be any evolution of these parameters with redshift. The region centred around $z \approx 2.3$ appears to have larger EWs and column densities than the other regions, but there is simply a higher number of systems in that region, with a distribution similar to the distribution outside that region. Additionally, the Si IV and N V systems tend to have higher EWs than C IV does. When only the intrinsic C IV systems are compared, there is no discernible difference between those systems whose host quasar resides at $z \approx 2.3$ and those that are located elsewhere. Over the redshift range of our sample, there is no evidence for a change in the properties of intrinsic systems.

In our sample, we found that 8–11 per cent of all C IV systems could be intrinsic. Those numbers are 6–8 per cent for Si IV systems, and 33–38 per cent for N V systems. Summing over all ions, we found that 9–12 per cent of all systems are intrinsic. In comparison, Misawa et al. (2007) found that 11–19, 14–18, and 75 per cent of C IV, Si IV, and N V systems were intrinsic, respectively, while Ganguly et al. (2013) found that 10–19 per cent of all mid- to high-ionization NALs were intrinsic. We note that with our larger sample, the fraction of intrinsic systems is consistently lower for each ion than what was found in the sample of Misawa et al. (2007). One possible explanation for why our sample had consistently lower fractions of intrinsic NALs across all ion types is that we were able to find weaker systems than previous studies. Class C C IV systems

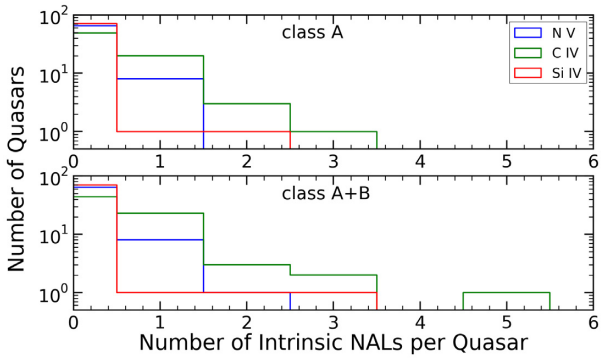

Figure 8. The distribution of the number of intrinsic NAL systems per quasar. The top panel shows the distribution of only reliably intrinsic NAL systems (class A). The bottom panel shows the distribution of reliable and potential intrinsic NAL systems (class A+B). The solid blue line is the distribution of N V systems, the green dashed line is the distribution of C IV, and the dotted–dashed red line is the distribution of Si IV systems.

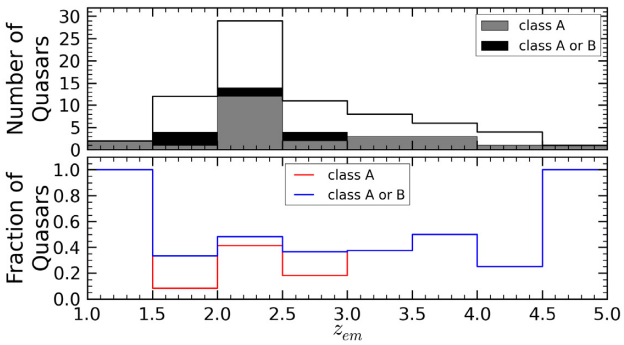

Figure 9. The distribution of quasars showing intrinsic NALs based on redshift. In the top panel, the unshaded bins represent the distribution of all quasars, the grey-shaded bins represent those quasars that contain at least one class A system, while the black-shaded regions are those quasars with at least one class A or B system. In the bottom panel, the fraction of quasars with intrinsic systems is plotted, using the same bins. The red line is the fraction of quasars with a class A system, while the blue line is the fraction of quasars with a class A or B system. See Section 4.4 of the text for further discussion.

have an average rest-frame EW that is half of the average value of class A or class B systems, while the average rest-frame EW of class C systems is a third of that for class B systems, and a fifth of the average rest-frame EW for class A systems. Since it is more difficult to demonstrate conclusively that weaker systems are intrinsic and since our sample has a larger fraction of weak systems compared to other studies, the total fraction of confirmed intrinsic systems in our sample is lower compared to other studies. Interestingly, N V class C systems have a larger rest-frame EW than do either class A or class B N V systems. However, it must once again be noted that all of these fractions of systems that are intrinsic are actually lower limits to the true fractions.

4.4 Fraction of quasars showing intrinsic NALs

In this survey, we found 35 reliably intrinsic systems (31 NALs, 3 mini-BALs, and 1 BAL), plus 11 potentially intrinsic NAL systems within the spectra of 73 quasars. We found 24 quasars with only one intrinsic system, four quasars with two intrinsic systems within their spectra, and one quasar with three intrinsic systems, for a total of 29 quasars with at least one class A system. Including the potentially intrinsic systems, there are then 22 quasars containing only one intrinsic system, 8 quasars with two intrinsic systems within their spectra, one quasar with three intrinsic systems, and one quasar has five intrinsic systems, with 32 quasars with at least one intrinsic NAL. Bootstrapping statistical trials were performed to determine if this distribution implied preferred sightlines to the quasars within which NALs appear, such as a given geometry increasing the likelihood of finding an intrinsic NAL, or if the distribution of intrinsic systems was consistent with random chance. In these trials, 42 systems were randomly placed within 73 quasars to determine the random distribution, i.e. how many quasars there were with 1 system, how many with 2 systems, etc. This trial was repeated 100 000 times, and the results were totalled. The average distribution of systems in these statistical trials was consistent with the distribution within our sample. This holds true even if the four mini-BALs and the BAL are included with the other intrinsic absorbers. Thus, we can conclude that it is unlikely that there are preferred sightlines to quasars within which intrinsic absorbers are formed in our sample.

In Fig. 8, we plot the distribution of the number of intrinsic systems per quasar, with reliably intrinsic (class A) systems in the top panel, and all reliable and potentially intrinsic (class A+B) systems in the bottom panel. Out of the 73 quasars, 24 (≈33 per cent) have at least one class A C IV system, while 29 (≈40 per cent) have at least one class A or B system. The number of quasars with at least one intrinsic N V system of class A are 8 of 73 (≈11 per cent), while at least 9 of 73 (≈12 per cent) quasars have a class A or B system. For Si IV, 2 of 73 (≈3 per cent) quasars have a class A system, while 3 of 73 (≈4 per cent) quasars have either a class A or class B system. Although at first glance, it would appear that the C IV absorbers have a global covering factor[4] higher than N V or Si IV absorbers, these are simply lower limits since some of the systems with $C_f = 1$ could still be intrinsic. Also, due to contamination by the Ly α forest, we are not able to search for absorption lines throughout the entire spectra, leaving us with a reduced velocity range in which to search for intrinsic systems, particularly for N V systems. The total number of quasars with a class A system in at least one of the three transitions is 27 (≈37 per cent), while for class A or B systems, this number is 29 (≈40 per cent). These fractions are similar to those found in Misawa et al. (2007) (43 and 54 per cent for class A and A or B systems, respectively), but are much higher than those found in variability studies, such as Narayanan et al. (2004) or Wise et al. (2004), who found intrinsic systems in 25 and 27 per cent of quasars, respectively.

In Fig. 9, we plot the number of quasars containing intrinsic systems against redshift. The unshaded region represents all quasars in our sample. In the top panel, the shaded region represents the quasars that contain at least one class A system, while in the bottom panel, it instead represents those quasars with at least one class A or B system. We are unable to determine any evolution with respect to redshift in the frequency of intrinsic systems occurrence within quasar spectra. This is consistent with the results of Ganguly et al. (2001) and Ganguly et al. (2013).

[4]The global covering factor is a different value from the coverage fraction. As described in Section 3.2, the coverage fraction refers to an individual system, and describes the flux ratio of the two members of a doublet line, and is indicative of partial coverage of the background source(s) covered along our sightline. The global covering factor is the fraction of sky occulted by the absorbers present around the quasar.

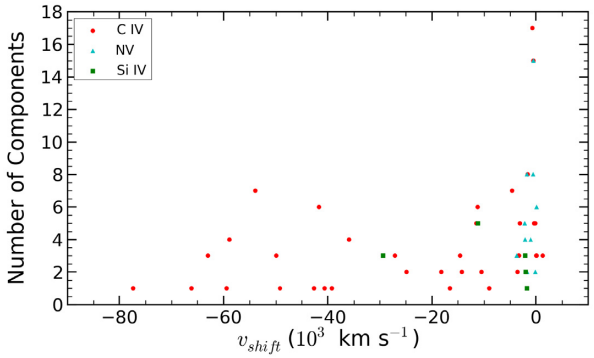

Figure 10. Number of components per intrinsic absorption system plotted against that system's velocity offset. KS tests between associated and non-associated intrinsic C IV systems show a trend towards a larger number of components at decreasing velocity offset, though KS tests between associated and non-associated intrinsic NALs of all ions (C IV, N V, and Si IV) are inconclusive. This could be caused by a number of effects. See Section 4.5 for more details.

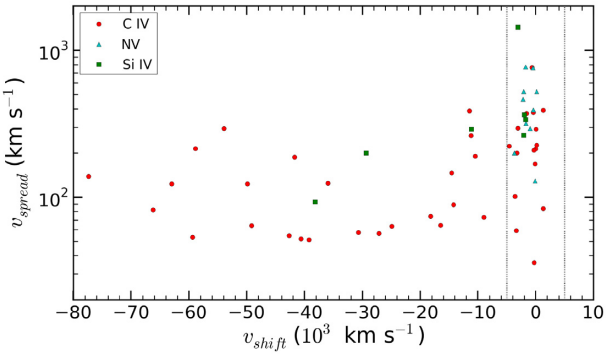

Figure 11. Velocity spread of components per intrinsic absorption system plotted against that system's velocity offset. Any point between the black, vertical dotted lines is in the associated region. KS tests between associated and non-associated intrinsic C IV NALs and between associated and non-associated intrinsic NALs of all ion types indicate that there is a definite trend towards higher velocity spread of components at decreasing velocity offset.

4.5 Component structure of systems

Absorption systems are made up of components, which determine the shape and width of the system, and even help determine if a system is intrinsic (Barlow & Sargent 1997). In Fig. 10, we plot the number of components against the velocity offset. In order to determine if there is a difference in the distribution of the number of components in associated and non-associated systems, we divided the intrinsic C IV systems into those two groups and performed a KS test. The KS test showed a statistically significant difference in the two distributions. This trend is likely due to nearly half of the non-associated systems only having a single component, while none of the associated systems have just one component, resulting in an increasing number of components as velocity decreases. The average number of components per system in the associated region was 6, while outside the associated region, the average was less than 3. This trend remains statistically significant even if two C IV outlier systems with 15 and 17 components at low velocity offset are removed from the sample. We also determined whether or not velocity spread evolved with increasing velocity offset, which can be used as a proxy for distance from the quasar (see Fig. 11). As velocity offset decreases, the velocity spread of the system increases. Again, dividing the intrinsic C IV systems between associated and non-associated systems, a KS test shows that there is < 1 per cent chance that these two samples come from the same parent population. This could indicate that the number density of the clouds forming the components is greater closer to the quasar, or that more parcels of material are being launched by the wind. As they move out, some of the parcels could disperse until the column density along the line of sight is low enough that the parcel is no longer a distinct unit, and the component it forms in the quasar spectra no longer being present. Other parcels of gas may combine, merging the two components into a single component. Additionally, some of the components may be launched at slightly different angles away from the quasar. This would result in the different components of the system to gradually move out of the cylinder of sight[5] as they propagate away from the quasar. Additionally, if the higher velocity offsets truly do equate with larger distances from the host quasar, then these absorbers could have taken a relatively longer time to travel to those distances. That time could allow various effects, like those described above, to vary the velocity offset of the components of a system. This could mean that once close components are now far enough away in velocity space to be considered separate systems. Another possibility is that parcels of gas responsible for different kinematic components form *in situ* at some distance away from the quasar because of thermal instabilities. Thus, they have the velocity corresponding to the ambient gas out of which they formed.

4.6 Relation between quasar properties and system properties

We examine the effects of the quasar properties on the number of intrinsic systems, their velocity offset distribution, and other system properties. Fig. 12 shows the properties of intrinsic systems (C_f, v_{shift}, EW_{rest}) plotted against their quasar properties. Although there do not appear to be any trends within the coverage fraction plots, in each of the velocity offset plots and the plot of EW_{rest} versus $\mathcal{R}$, there are areas that are noticeably devoid of points. In the v_{shift} versus L_ν(4400 Å) plot, there are no points at large velocity offsets in those quasars with low optical luminosity. This could indicate that quasars with low optical luminosities are incapable of accelerating intrinsic systems to as large of velocities as those with larger optical luminosities, and is consistent with previous surveys (i.e. Laor & Brandt 2002). Similarly, in the v_{shift} versus L_ν(5 GHz) plot, there is an absence of points with large velocity offset, but among quasars with high radio luminosity. This translates to the plot of v_{shift} versus $\mathcal{R}$, as the top right corner of the figure is devoid of points as well. Finally, in the EW_{rest} versus $\mathcal{R}$ plot, there is only one point with an EW greater than 0.4 Å in radio-loud quasars ($\mathcal{R} > 30$). This is consistent both previous surveys (e.g. Ganguly et al. 2001) and with what is observed in BAL quasars (e.g. Becker et al. 2000), and suggests an important underlying connection to either black hole spin, the role of magnetic fields, or both.

[5]Quasars are far enough away from an observer that the light arriving at the telescope is essentially parallel. However, the quasar has a finite projected area, and emits that parallel light from the entire projected area of the quasar. Because the quasar's central engine is disc-like in nature, the cross-section of the parallel light is a circle. Tracing the paths of the light emitted from the quasar through the quasar's host environment results in a 'cylinder of sight', rather than a line of sight.

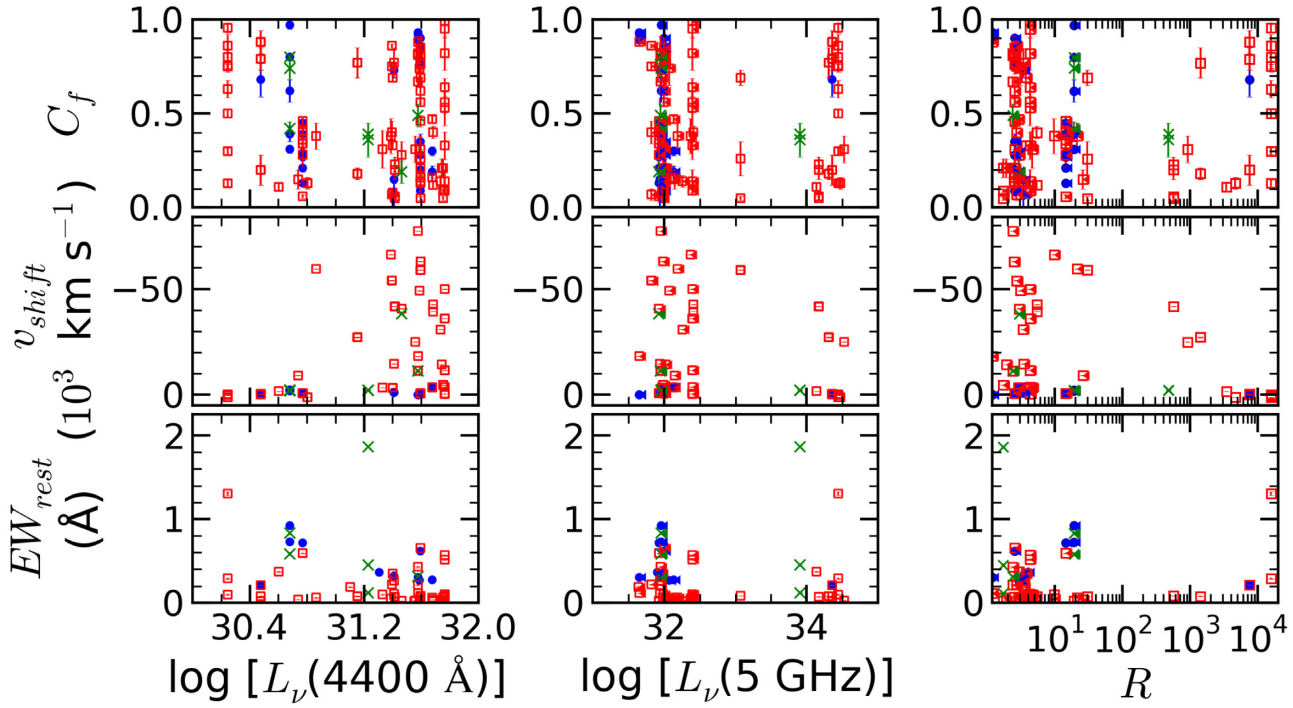

Figure 12. Coverage fractions (C_f, top), the velocity offset (v_{shift}, middle), and the rest equivalent width (EW_{rest}, bottom) plotted against quasar properties: L_ν(4400 Å), L_ν(5 GHz), and $\mathcal{R}$. Only intrinsic NALs (class A+B), whose coverage fractions are physical (i.e. $0 < C_f \leq 1$) and evaluated with high reliability [i.e. $\sigma(C_f) < 0.1$], are plotted. The filled blue circles denote N V NALs, the open red squares represent C IV NALs, while the green x's represent Si IV NALs.

Table 4. Radio properties of sample quasars.

Ion (1)	Class (2)	Radio loud (3)	Radio quiet (4)	Unknown (5)
N^a	–	19	53	1
All ions^b	A	6 (32%)	23 (43%)	0 (0%)
	B	3 (16%)	5 (9%)	0 (0%)
	C	17 (89%)	53 (100%)	1 (100%)
	A+B	7 (37%)	25 (47%)	0 (0%)
C IV^b	A	5 (26%)	19 (36%)	0 (0%)
	B	2 (11%)	5 (9%)	0 (0%)
	C	17 (89%)	52 (98%)	1 (100%)
	A+B	6 (32%)	23 (43%)	0 (0%)
N V^b	A	1 (5%)	7 (13%)	0 (0%)
	B	0 (0%)	1 (2%)	0 (0%)
	C	3 (16%)	10 (19%)	1 (100%)
	A+B	1 (5%)	8 (15%)	0 (0%)
Si IV^b	A	1 (5%)	2 (4%)	0 (0%)
	B	1 (5%)	0 (0%)	0 (0%)
	C	4 (21%)	24 (45%)	0 (0%)
	A+B	1 (5%)	2 (4%)	0 (0%)

Note. [a]The total number of quasars with the given radio property. [b]The number of quasars, either radio loud or radio quiet, containing at least one of the given class of system. The number in parenthesis is the fraction of quasars of the given radio property with at least one such system.

As Table 4 illustrates, the radio properties of a quasar do not affect the probability that it hosts an intrinsic system in its spectrum. The fractions of radio-loud and radio-quiet quasars hosting intrinsic systems are very similar. 21 per cent of class A systems are found in radio-loud quasars, while 79 per cent are found in radio-quiet quasars (cf. consistent with the fractions of radio-loud and radio-quiet quasars in our entire sample, which are 28 and 72 per cent, respectively). Even with respect to the ion with which a system was found, the numbers are very similar. There is no discernible difference between the coverage fractions of intrinsic systems in radio-loud quasars and those in radio-quiet quasars. Optical luminosity also does not have an effect on intrinsic systems. KS tests were performed on the distribution of optical luminosity as a function of radio-loudness and reliability class. They showed no discernible difference from the distribution of all quasars.

The velocity distribution of intrinsic systems for different ions in the two types of quasars, radio loud and radio quiet, is plotted in Fig. 13. It is analogous to Fig. 4. The two distributions are very similar. However, intrinsic systems in radio-quiet quasars can be found out to higher offset velocities than those in radio-loud quasars in our sample. In contrast, Ganguly et al. (2013) find much more similar velocity distributions for intrinsic NALs in radio-loud and radio-quiet quasars.

4.7 Distance estimates using excited-state lines

A possible distance indicator comes from the excited-state lines of ions present in our sample. There are two relatively low ionization lines with ground-state and excited-state wavelengths covered in this survey. They are Si II λ1260/Si II* λ1264 and C II λ1335/C II* λ1336. The excited-state lines have oscillator strengths similar to those of the related ground-state lines, which allows the ratio of the column densities of the two lines to be used as an electron density diagnostic. Using the prescription used in Arav et al. (2018), and applying

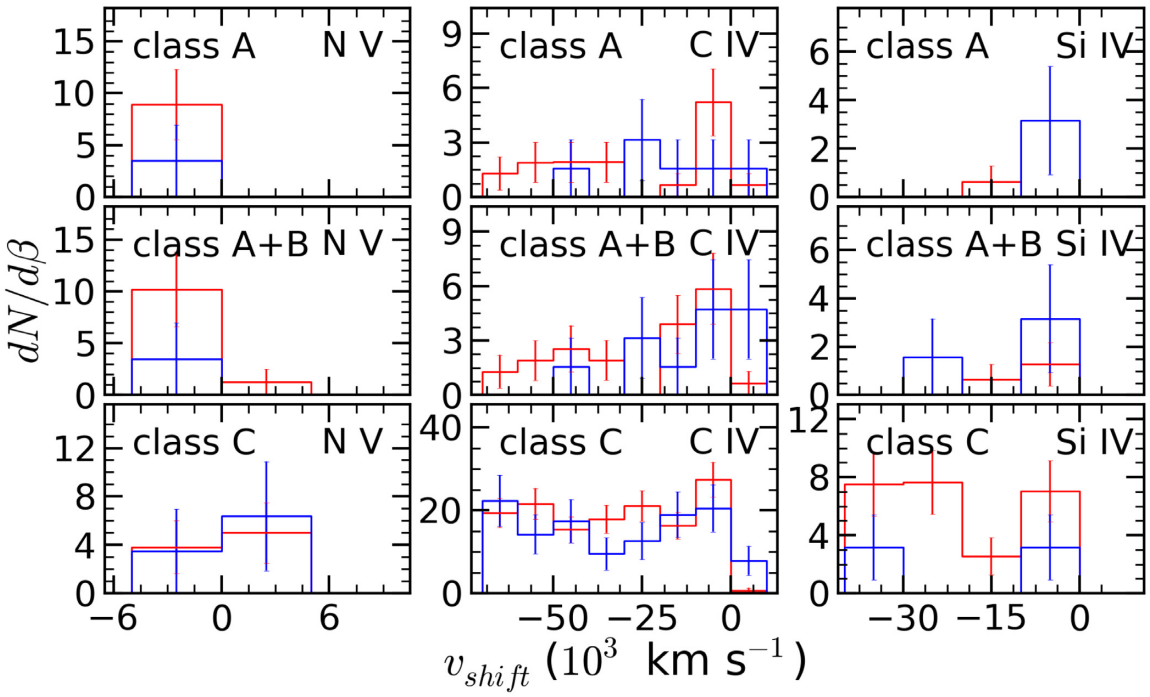

Figure 13. Velocity offset distribution is shown for each ion, and separated by class. Analogous to Fig. 4, but the histograms for radio-loud quasars (blue) and radio-quiet quasars (red) are plotted separately.

it to Si II* and C II*, we find that Si II has a critical density of $n_e \sim 2000$ cm^{-3}, while C II has a critical density of $n_e \sim 100$ cm^{-3}. If the ground state of either ion is found, but the excited state is not, a lower limit is placed on the distance to the quasar. In the case of Si II, the lower limit of the distance to the quasar is 200 pc. In the case of C II, the lower limit is much more stringent. If the ground state is present, but the excited state is not, the lower limit on the distance to the quasar is 1000 pc. Any systems whose distance can be constrained in this way would be far from the quasar accretion disc. Such gas parcels are either very long-lived to travel from the quasar's immediate surroundings to that distance, or they must arise in a different manner, they may be material from the host galaxy or an unusually small intervening gas cloud.

There are only four systems in our sample that both have C II and/or Si II covered, and either of those ions are detected. Only three of those systems have a statistically significant detection. Of those three systems, two are believed to be unusually small damped Ly$-\alpha$ systems, and are discussed further in Section 7.4. This shows that it is possible for intrinsic systems to exist at large distances from the quasar.

5 FAMILIES OF NALS ACCORDING TO IONIZATION STATE

Misawa et al. (2007) found that all intrinsic NAL systems in their sample from Keck/HIRES observations of $z \sim 2$ quasars could be grouped into either 'strong C IV' systems or 'strong N V' systems. An intrinsic strong C IV system contains both strong C IV and strong Ly α lines, the Ly α line is saturated and black, and the EW of the Ly α line is at least twice that of the N V line. Conversely, a strong N V system is one in which the EW of Ly α is less than twice the EW of N V. In systems containing strong N V lines, Ly α is often saturated, but not black,[6] which is very unlike intervening absorbers. A system can still be considered to be a strong N V system, even if the EW of the C IV doublet is larger than that of the N V.

Our sample reaches lower EW limits than the Misawa et al. (2007) survey. In that survey, intrinsic absorbers were classified into two families: 'strong C IV' and 'strong N V'. The two families arose from a consideration of the EW(Ly α)/EW(N V 1239) ratio. However, our current sample includes systems that would qualify as 'strong C IV' in spite of having a low-EW C IV absorption feature. Hence, we revise our terminology to refer to these families as 'C IV dominant' and 'N V' dominant, respectively, so as to avoid confusion.

In addition, our sensitivity and wavelength coverage permits further subclassification according to the behaviour of the Ly α absorption, and the detection of other species with a range of ionization potentials spanning nearly 0.5 dex (13–48 eV). In the former case, we consider whether the saturated Ly α feature contains only components with partial covering (i.e. non-black saturation), or if there is a mix of both black and non-black saturated components. In the latter case, we consider whether accompanying absorbing species have low-ionization potentials (<30 eV; e.g. O I λ1302, Si II $\lambda\lambda$1190, 1193, 1260, 1527, Al II λ1671, C II λ1335) or intermediate ionization potentials (30–48 eV; e.g. Si III λ1207, Si IV $\lambda\lambda$1394, 1403, C III λ977). Table 5 gives a summary of the low-, intermediate-, and high-ionization lines detected for each class

[6]Despite being a singlet, Ly α can be shown to be saturated but not black in N V systems in multiple ways. The profiles of Ly α in such systems are flat-bottomed, implying saturation. Additionally, the profiles of Ly α also sometimes match that of N V, with the components slightly broadened, such as in the case of the system in Q1158-1843 at $z_{abs} = 2.4425$, $v_{shift} = -479$. Finally, it has been shown that it is essentially impossible to get Ly α profiles with ratios to N V without partial coverage of Ly α (Wu et al. 2010).

Table 5. Ionization states of Class A and Class B NALs.

QSO (1)	z_{abs} (2)	Low-ion.[a] 13–24 eV (3)	Interm.-ion.[b] 33–48 eV (4)	C IV 65 eV (5)	N V 98 eV (6)	O VI 138 eV (7)	Ionization class[c] (8)
			Class A systems				
Q0011+0055	2.2858	N	Y	–	Y	–	1, HI
Q0055–269	3.0388	N	N	Y	–	–	1, H
	3.0859	N	Y	Y	–	N	1, HI
Q0109–3518	1.7514	N	–	Y	N	–	1, H
Q0122–380	1.7925	N	N	Y	Y	–	1, H
	1.8157	N	Y	Y	N	–	1, HI
Q0130–4021	2.9733	N	N	Y	Y	Y	2, H
	2.978	N	N	Y	Y	Y	2, H
Q0151–4326	2.7136	N	N	–	Y	–	1, H
Q0329–255	2.2041	N	N	Y	N	–	1, H
Q0329–385	1.8156	N	–	Y	–	–	1, H
Q0421–2624	1.5171	–	–	Y	–	–	H
	2.1568	Y	Y	Y	N	–	1, HIL
	2.1574	Y	Y	Y	N	–	1, HIL
Q0425–5214	2.2389	N	–	Y	Y	–	1, H
Q0549–213	2.0711	N	N	Y	N	–	2, H
	2.2418	N	–	Y	N	–	2, H
	2.2438	N	–	Y	Y	–	2, H
Q0952+179	1.258	N	N	Y	–	–	H
Q1114–0822	3.3907	N	–	Y	–	–	1, H
Q1114–220	2.2963	Y	Y	Y	Y	–	HIL
Q1122–1648	2.353	N	–	Y	N	–	1, H
Q1157+014	1.969	N	Y	–	Y	–	2, HI
	1.9797	N	Y	–	Y	–	2, HI
Q1158–1843	2.4425	N	N	Y	Y	Y	2, H
	2.4426	N	N	Y	Y	Y	2, H
Q1202–0725	3.8137	N	N	Y	N	N	1, H
	4.0484	N	Y	Y	–	–	1, HI
	4.6265	N	N	Y	N	–	1, H
Q1209+0919	2.518	N	–	Y	–	–	1, H
Q1341–1020	2.1165	N	N	Y	Y	–	2, H
Q1347–2457	2.3702	N	N	Y	N	–	1, H
Q1444+014	2.1988	N	N	Y	Y	–	2, H
	2.2003	N	N	Y	Y	–	2, H
Q1621–0042	3.2411	N	N	Y	–	–	1, H
Q2000–330	3.3924	N	Y	Y	N	N	1, HI
Q2059–360	2.9712	N	–	Y	N	Y	1, H
Q2116–358	2.3064	N	–	Y	Y	–	2, H
Q2132–433	2.3828	N	N	Y	Y	–	1, H
Q2215–0045	1.4755	Y	Y	Y	–	–	HIL
Q2225–2258	1.4106	N	N	Y	–	–	1, H
Q2314–409	2.4629	N	N	Y	N	Y	1, H
			Class B systems				
Q0002–422	2.5394	N	N	Y	N	–	1, H
Q0011+0055	2.2868	N	Y	–	Y	–	1, HI
	2.2905	N	Y	–	Y	–	2, HI
	2.2908	N	Y	–	Y	–	2, HI
Q0136–231	1.8773	Y	Y	Y	Y	–	1, HIL
Q0151–4326	2.1699	N	–	Y	–	–	1, H
Q0425–5214	2.0959	N	Y	Y	N	–	1, HI
	2.1385	N	Y	Y	N	–	1, HI
Q0549–213	2.2437	N	–	Y	Y	–	1, H
Q0810+2554	1.3525	N	Y	Y	–	–	HI
	1.5011	N	N	–	Y	–	H
Q1114–220	2.282	N	–	Y	N	–	H
	2.2836	–	–	Y	N	–	H
Q1157+014	1.7192	N	Y	Y	–	–	HI

Table 5 – *continued*

QSO	z_{abs}	Low-ion.[a] 13–24 eV	Interm.-ion.[b] 33–48 eV	C IV 65 eV	N V 98 eV	O VI 138 eV	Ionization class[c]
(1)	(2)	(3)	(4)	(5)	(6)	(7)	(8)
Q1202–0725	4.4808	N	Y	Y	N	–	1, HI
	4.6876	N	Y	Y	Y	–	1, HI

Notes. A 'Y' indicates that one or more lines of a given type are detected, a 'N' indicates that no lines from that category were detected, while ellipses mean that either the spectrum did not cover those transitions, that the transitions were severely blended with the Ly α forest, or there were data defects.
[a]Low-ionization lines (from ions with ionization potentials between 13 and 24 eV): O I λ1302, Si II $\lambda\lambda$1190, 1193, 1260, 1527, Al II λ1671, C II λ1335.
[b]Intermediate-ionization lines (from ions with ionization potentials between 33 and 48 eV): Si III λ1207, Si IV $\lambda\lambda$1394, 1403, C III λ977.
[c]1 = C IV dominant system, 2 = N V dominant system. H, I, and L mean that the system contains high-, intermediate-, and low-ionization lines, respectively. A system without a 1 or 2 does not have coverage of Ly α and/or N V, and so the system has no definitive determination of which type of system it is.

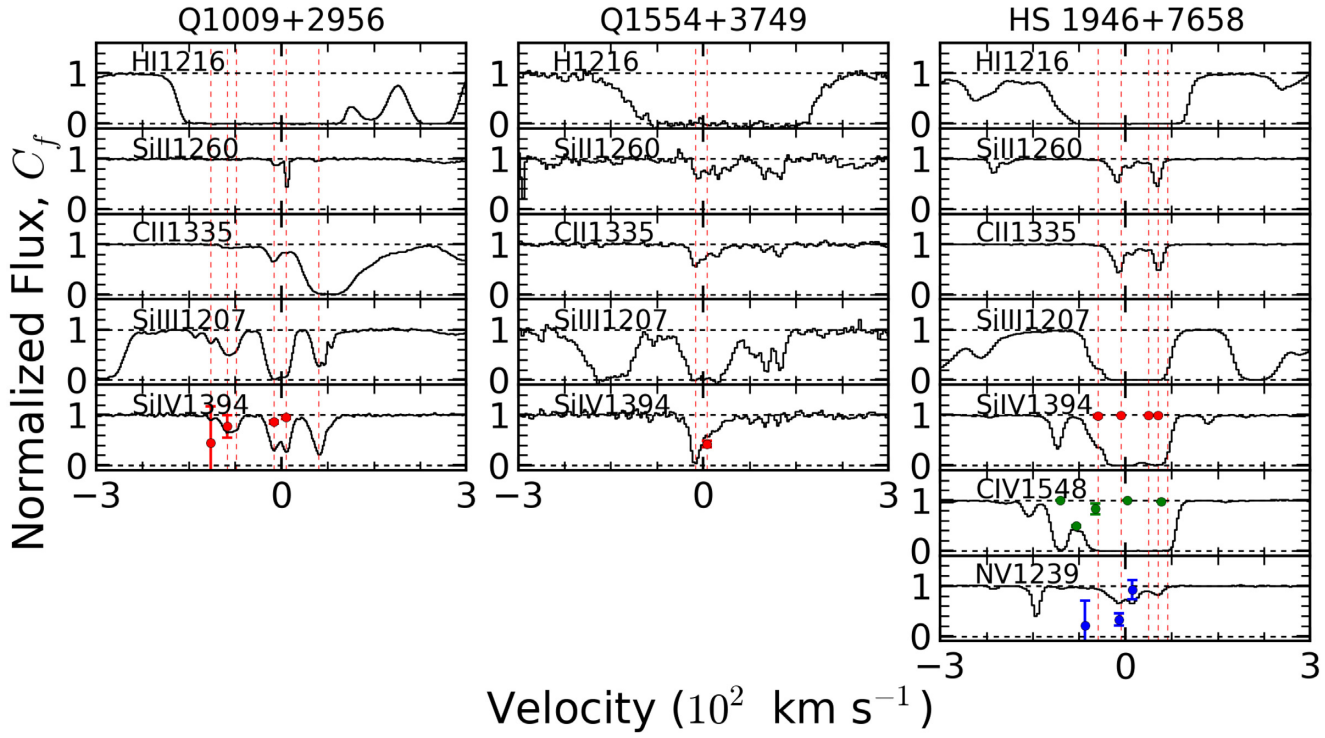

Figure 14. Velocity aligned absorption profiles of three of the C IV dominant systems with low-ionization lines. All scales on the horizontal axis are the same. The red vertical dashed lines represent components within the system. The green points represent physical coverage fractions ($0 < C_f \leq 1$) for C IV. Coverage fractions for N V (blue) and Si IV (red) are also shown for some systems. All systems are from the Misawa et al. (2007) sample. The system from Q1009+2956 has $z_{abs} = 2.2536$, $v_{shift} = -33\,851$ km s^{-1}. The system from Q1554+3749 has $z_{abs} = 2.3777$, $v_{shift} = -24\,354$ km s^{-1}. The system from HS 1946+7658 has $z_{abs} = 3.0497$, $v_{shift} = -96$ km s^{-1}.

A and B system, or indicates if they were not detected or if the spectrum did not have the necessary wavelength coverage. We do not claim that these families are physically distinct, but rather form a continuous sequence with respect to ionization parameter. We discuss these families below:

(i) **Low-ionization systems:** Intrinsic C IV dominant systems containing low-ionization lines such as Si II $\lambda\lambda$1190, 1193, 1260, 1527, Al II λ1671, and/or C II λ1335. The Ly α lines are saturated and black, and their EWs are at least twice those of the N V lines. Only 5 examples of this type of system were found in our sample, though the Misawa et al. (2007) sample contained an additional 13 systems of this type. The systems with the strongest low-ionization lines from either sample were all found within the Misawa et al. (2007) sample. We present three examples of this type of system from the Misawa et al. (2007) sample in Fig. 14. These types of systems are found at velocity offsets ranging between +5000 and −55 000 km s^{-1}.

(ii) **C IV dominant with no low-ionization lines:** These systems primarily consist of C IV, Ly α, and occasionally Si IV, and are often fairly weak absorbers. Ly α lines are saturated and black. Of the 24 C IV dominant systems in the Misawa et al. (2007) sample, 11 of them belong to this subclass. In comparison, 27 of 35 C IV dominant systems in our sample are C IV dominant systems without low-ionization lines. See Fig. 15 for examples of this type of system.

(iii) **C IV dominant with partial coverage in Ly α:** C IV dominant systems, as defined in Misawa et al. (2007), have saturated, black Ly α lines. No C IV dominant intrinsic systems displayed partial coverage in Ly α in that sample. However, three C IV dominant systems in our sample do show partial coverage in Ly α. In those systems, the Ly α line appears saturated but non-black,

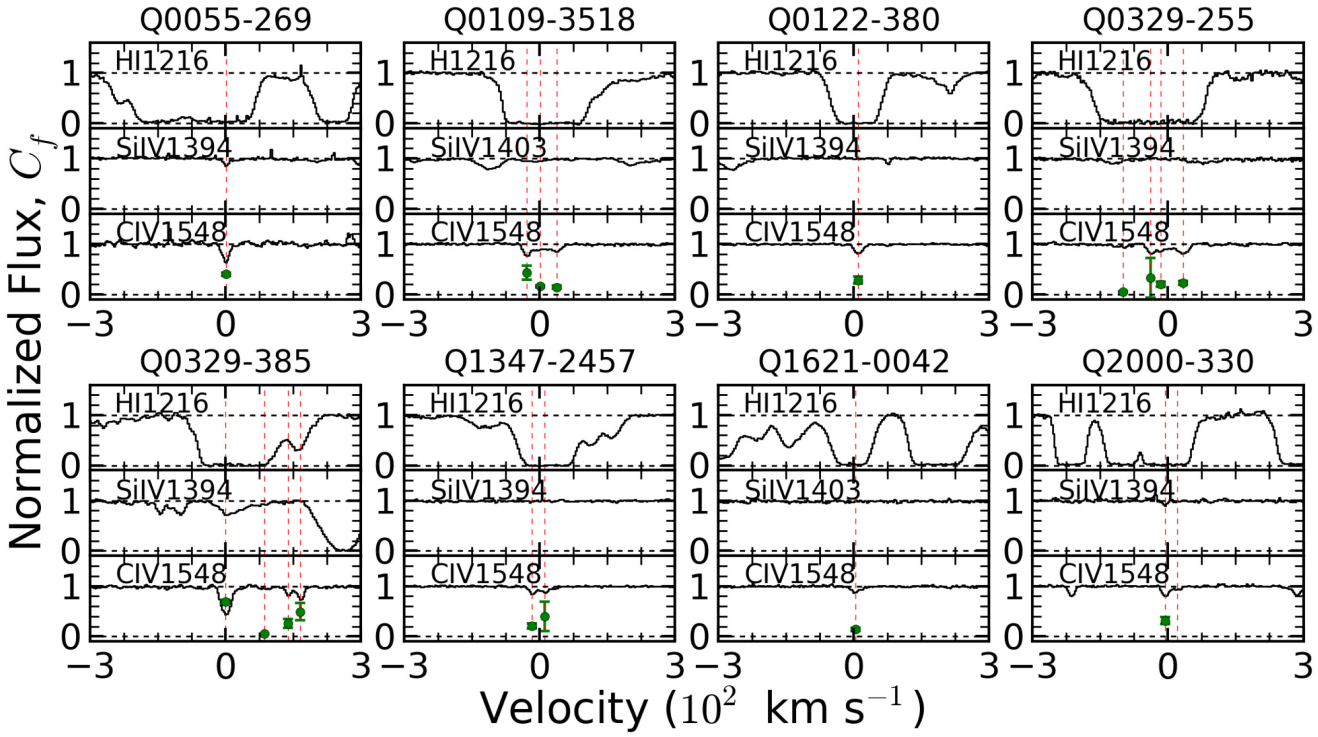

Figure 15. Same as Fig. 14, but for eight of the C IV dominant systems, showing Ly α, Si IV, and C IV. Si IV is only rarely detected, whereas low-ionization lines such as Si II or C II are never seen in these systems. All systems are from this sample. The system from Q0055–269 has $z_{abs} = 3.0859$, $v_{shift} = -39\,216$ km s^{-1}. The system from Q0109−3518 has $z_{abs} = 1.7514$, $v_{shift} = -62\,990$ km s^{-1}. The system from Q0122–380 has $z_{abs} = 1.7925$, $v_{shift} = -40\,613$ km s^{-1}. The system from Q0329–255 has $z_{abs} = 2.2041$, $v_{shift} = -41\,680$ km s^{-1}. The system from Q0329–385 has $z_{abs} = 1.8156$, $v_{shift} = -58\,879$ km s^{-1}. The system from Q1347−2457 has $z_{abs} = 2.3702$, $v_{shift} = -14\,227$ km s^{-1}. The system from Q1621−0042 has $z_{abs} = 3.2411$, $v_{shift} = -30\,714$ km s^{-1}. The system from Q2000–330 has $z_{abs} = 3.3924$, $v_{shift} = -24\,873$ km s^{-1}.

similar to those of the N V dominant systems found in Misawa et al. (2007). One possible interpretation is that these systems are at an intermediate ionization state between C IV dominant and N V dominant systems. Fig. 16 displays some of the relevant transitions for the three C IV dominant systems with partial coverage in Ly α in our sample.

(iv) **Mixed Ly α systems:** This class of intrinsic absorbers displays saturated Ly α with both black and non-black components within the same line. This type of absorber was found in both N V dominant and C IV dominant systems. There were three such systems in the Misawa et al. (2007) sample and three in the present sample. See Fig. 17 for spectra of the relevant transitions for the three systems in our sample.

(v) **Classic N V systems:** As described in Misawa et al. (2007), a N V dominant system is one in which the EW of Ly α is less than twice the EW of N V. In N V dominant systems, Ly α is often saturated, but not black, which distinguishes them from intervening absorbers. A system is still considered to be a N V dominant system, even if the EW of the C IV doublet is larger than that of the N V. Three such systems exist within our sample, while five are present in Misawa et al. (2007). See Fig. 18 for examples of N V systems, from both this sample and that of Misawa et al. (2007).

(vi) **Mini-BALs:** Absorption systems with widths between 500 and 2000 km s^{-1}. In both samples, the mini-BALs often have absorption in both N V and Si IV, implying an intermediate ionization parameter. N V generally has a larger coverage fraction than Si IV, though the two lines have similar component structure, which suggests that they are either in the same phase or are in some way kinematically related. Three mini-BALs were found in our sample, and two were found in Misawa et al. (2007). See Fig. 19 for examples of mini-BALs, from both this sample and that of Misawa et al. (2007).

In addition to these families, we also remind the reader of two additional families from the literature, which we will also consider in our discussions:

(i) **O VI systems:** O VI dominant systems have been suggested in Misawa et al. (2007) and confirmed in Tripp et al. (2008) and Ganguly et al. (2013), who discussed the existence of an associated O VI absorber class. O VI systems have a higher ionization parameter than those discussed above. These types of systems were also found to often include N V, C IV, and/or Si IV. Many absorbers in this O VI group exhibit full coverage, though it is estimated that ∼60 per cent are intrinsic to the quasar. Only 14–21 per cent of the absorbers showed evidence of partial coverage.

(ii) **Ne VIII systems:** At even higher ionization parameters, Ne VIII dominant systems can form (Muzahid et al. 2013). These systems were largely found in the associated region of the host quasar, and were detected in ∼40 per cent of quasars observed. These types of systems typically have a multiphase structure, with one phase containing Ne VIII, and occasionally Na IX and Mg X, while a second phase contains lower ionization ions such as N IV, O IV, and O V. Muzahid et al. (2013) reported 12 Ne VIII systems appearing in the spectra of 20 quasars. Of these, only three of the quasar spectra showed a Ne VIII absorption system with partial

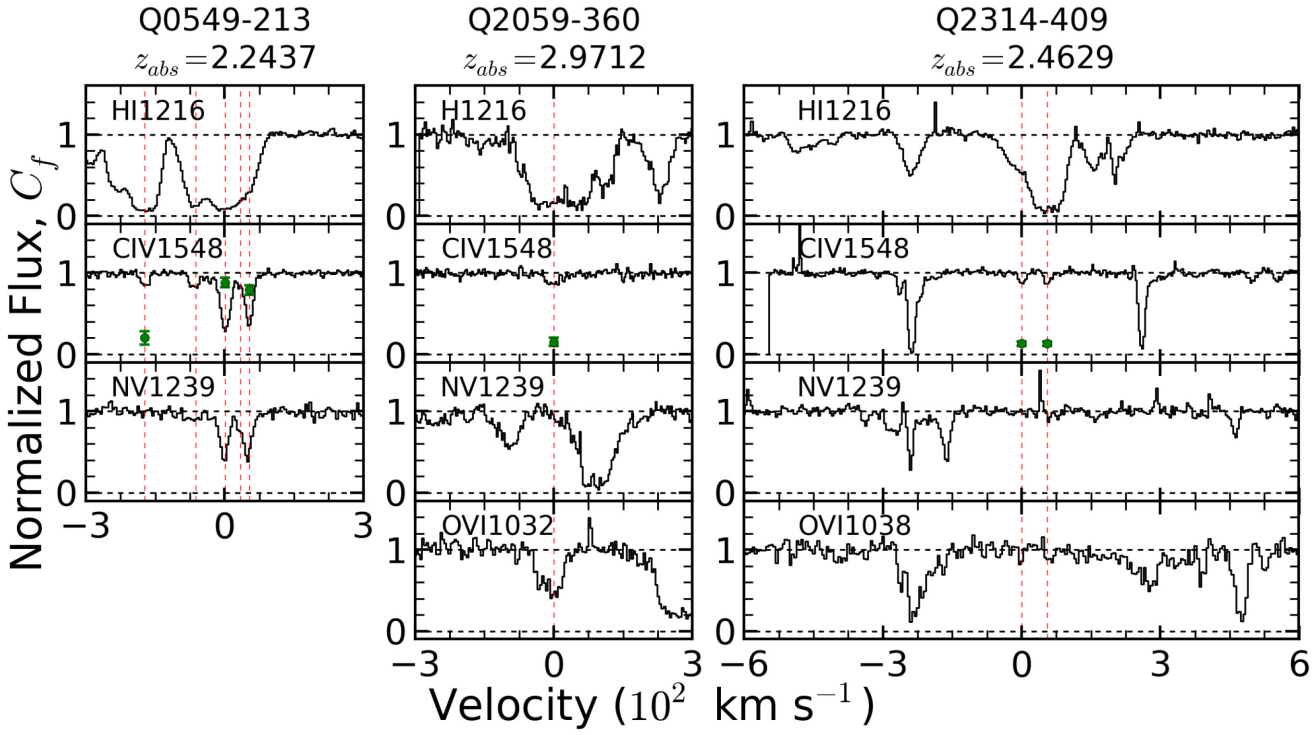

Figure 16. Same as Fig. 14, but for the three C IV dominant systems with non-black Ly α, showing Ly α, C IV, N V, and O VI (when present). All systems are from this sample. The $v_{\rm shift}$ for the systems, from left to right, are -120, -8987, and $+1294$ km s^{-1}.

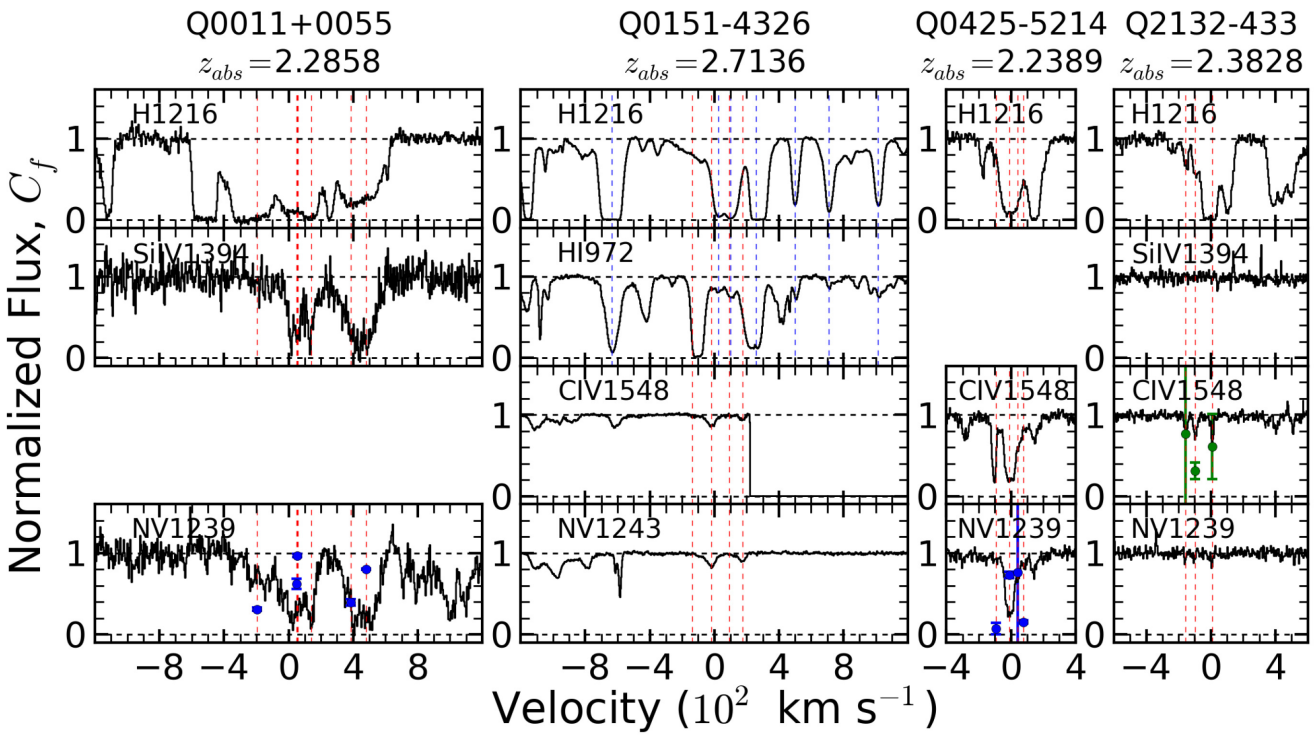

Figure 17. Same as Fig. 14, but for the four systems with both black and non-black Ly α, showing Ly α, Ly δ or Si IV (when present), C IV (when present), and N V. The blue vertical dashed lines in Ly α represent components without metals. The $v_{\rm shift}$ for the systems, from left to right, are -2110, -2125, -1026, and -3281 km s^{-1}. All systems are from this sample.

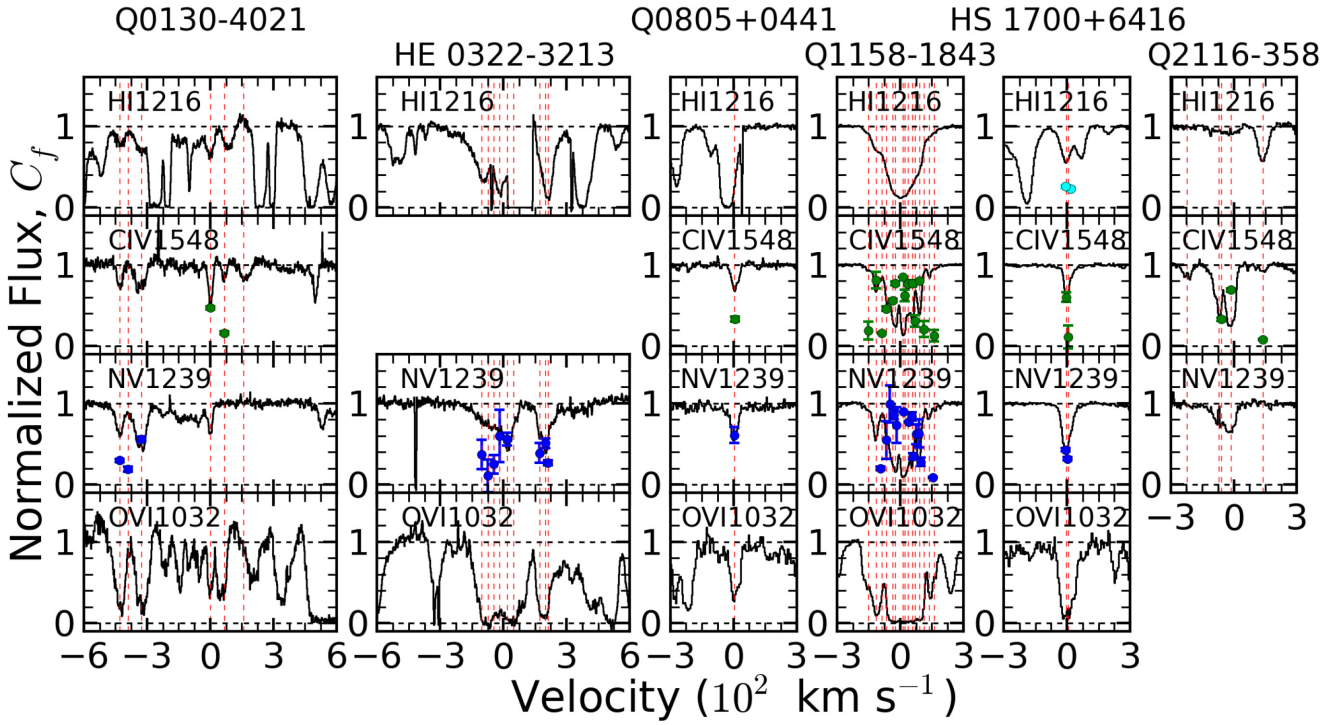

Figure 18. Same as Fig. 14, but for five N V dominant systems, showing Ly α, C IV, N V, and O VI (when present). The systems labelled HE 0322−3213 $z_{\rm abs}$ = 3.2781, Q0805+0441 $z_{\rm abs}$ = 2.8589, and HS 1700+6416 $z_{\rm abs}$ = 2.7125 are all from the Misawa et al. (2007) sample. For HS 1700+6416 in that sample, Ly α and Ly β were fitted to give a coverage fraction for H I. That coverage fraction is shown in light blue in the Ly α panel. The redshifts and velocity offsets are as follows: the system from Q0130−4021 has $z_{\rm abs}$ = 2.9780, $v_{\rm shift}$ = −3374. The system from HE 0322−3213 has $z_{\rm abs}$ = 3.2781, $v_{\rm shift}$ = −1671. The system from Q0805+0441 has $z_{\rm abs}$ = 2.8589, $v_{\rm shift}$ = −1636. The system from Q1158−1843 has $z_{\rm abs}$ = 2.4425, $v_{\rm shift}$ = −479. The system from HS 1700+6416 has $z_{\rm abs}$ = 2.7125, $v_{\rm shift}$ = −767. The system from Q2116–358 has $z_{\rm abs}$ = 2.3064, $v_{\rm shift}$ = −3123.

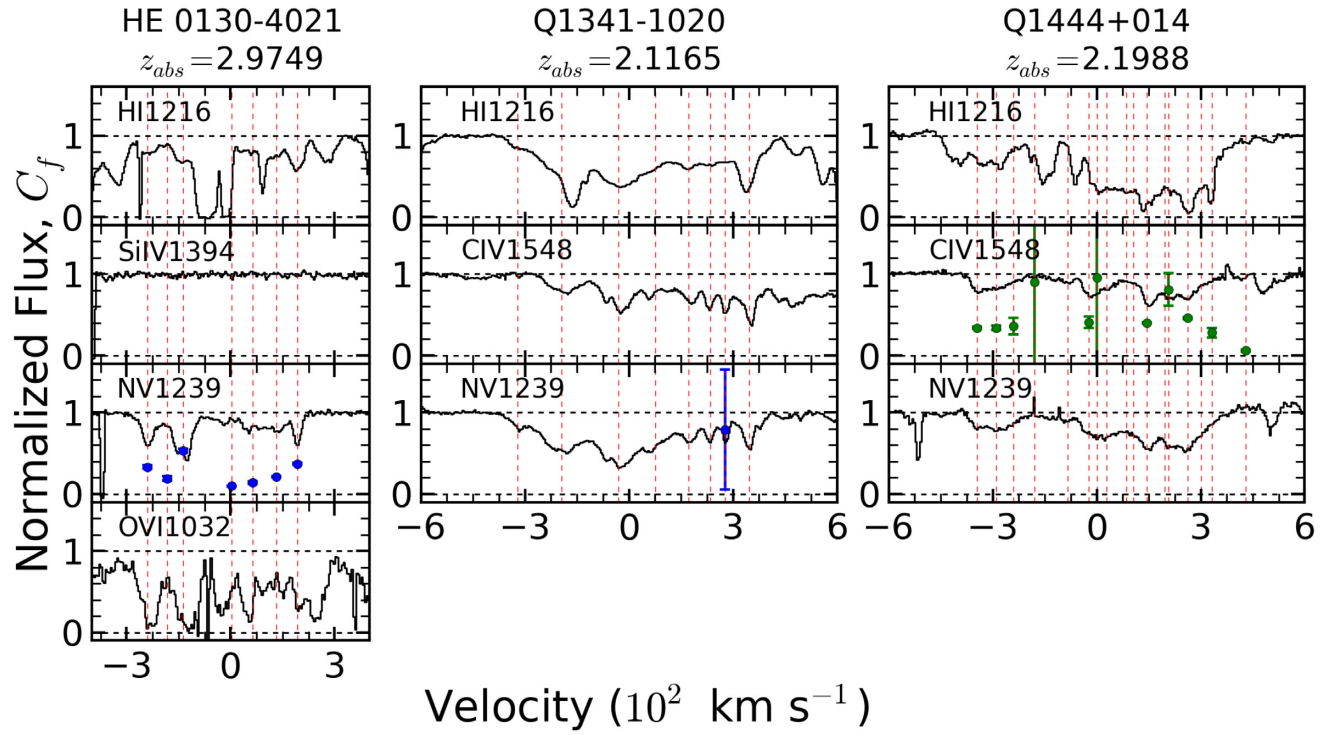

Figure 19. Same as Fig. 14, but for two mini-BALs from this sample and one (HE 0130−4021, $z_{\rm abs}$ = 2.9749) from Misawa et al. (2007). All the mini-BALs in both samples would be N V dominant systems, if they were NALs. The figure displays Ly α, C IV when present (Si IV when it is not), N V, and O VI (when present). The $v_{\rm shift}$ for the systems, from left to right, are −4130, −1776, and −674 km s^{-1}.

coverage. We can therefore expect ∼15 per cent of quasars to have partially covered Ne VIII systems.

6 PARTIAL COVERAGE OF THE BELR AND THE CONTINUUM SOURCE

Thus far in this paper, we have considered the coverage fraction of a system with respect to the background radiation. However, that radiation has two sources; the BELR and the continuum source, which should be considered separately. Each of these regions has a different size, and thus a different coverage fraction associated with it. We define

$$W = \frac{F_{\rm BELR}}{F_{\rm c}} - 1 \quad (1)$$

as the ratio of the BELR to the continuum source flux at the wavelength of a NAL. The underlying, *effective* continuum flux for an absorption line that falls on the broad emission line, $F_{\rm BELR}$, is a combination of the flux from the BELR and the continuum. Therefore, the contribution from the continuum at the absorption line can be removed by using W. With these definitions, we can write the normalized flux as

$$R = 1 - \frac{[C_{\rm c} + (1+W)C_{\rm BELR}](1-{\rm e}^{-\tau})}{2+W}, \quad (2)$$

where $C_{\rm c}$ and $C_{\rm BELR}$ are the continuum and BELR coverage fractions, respectively. Using the same optical depth scaling argument as in equation (5) of Ganguly et al. (1999) (see also Gabel et al. 2003; Scott et al. 2004; Misawa et al. 2007; Gabel et al. 2005; Gabel, Arav & Kim 2006), this reduces to

$$C_{\rm f} = \frac{C_{\rm c} + (1+W)C_{\rm BELR}}{2+W}. \quad (3)$$

Because the continuum source and BELR coverage fractions cannot be determined independently, the best that we can do is put constraints on the combination of the two values. Fig. 20 shows one example of the range of possibilities of coverage fractions for each of the components in a system. For the given W and the components with physically meaningful coverage fractions less than one, a range of parameters for the continuum coverage fraction and the BELR coverage fraction are generated. Those components in the top right corner of the figure put constraints on both coverage fractions as neither $C_{\rm c}$ nor $C_{\rm BELR}$ can be zero, and one, but not both, can be equal to one. Similarly, those components in the bottom left corner have a $C_{\rm c}$ and a $C_{\rm BELR}$ such that neither source can be fully covered. Any component that runs the entire length of the x-axis leaves $C_{\rm BELR}$ unconstrained, while those that run the entire length of the y-axis (not shown in Fig. 20) leave $C_{\rm c}$ unconstrained.

In order to further constrain these coverage fractions for the quasars in our sample, we measured the fraction of the total flux absorbed at the minimum normalized flux in the profile of each ion, for each intrinsic system [the fractional depth, $D = 1 - \min(R)$, where R is the normalized flux]. If the fractional depth of the line exceeds the fraction of the flux contributed by the BELR or continuum source, then even if the absorber creating the line were to remove all photons from the given background source, additional photons from the other background source must still be absorbed. Therefore:

(i) The fractional depth is greater than the fraction of the total flux contributed by the BELR if $D > W/(W+1)$. Such a system requires that the continuum be at least partially covered (and possibly fully covered).

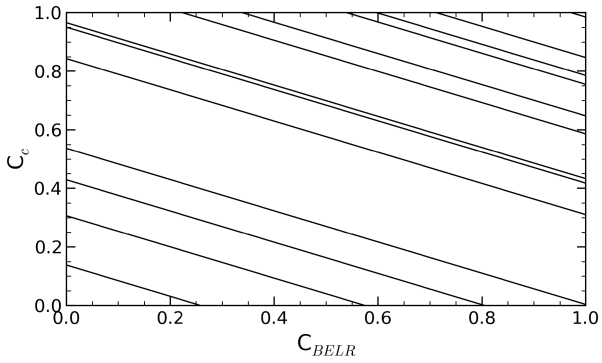

Figure 20. A figure showing the coverage fraction of the continuum source, $C_{\rm c}$, versus the coverage fraction of the BELR, $C_{\rm BELR}$, for the Q1158–1843 NAL at $z = 2.4426$. The systems has $w = 0.533$ and total coverage fractions for the various components of: 0.99, 0.90, 0.86, 0.84, 0.77, 0.73, 0.63, 0.62, 0.55, 0.35, 0.28, 0.20, and 0.09. Each line represents the range of possibilities for each component within the system. Components in the upper right ($0 < C_{\rm c} \leq 1$ and $0 < C_{\rm BELR} \leq 1$, extending from the top horizontal axis to the one on the right vertical one) would be plotted in the top region of Figs 21–23. Those in the central region, spanning the entire x-axis ($0 < C_{\rm c} < 1$ and $0 \leq C_{\rm BELR} \leq 1$, extending from the left vertical axis to the right one), belong in the left region. Those in the bottom left ($0 \leq C_{\rm c} < 1$ and $0 \leq C_{\rm BELR} < 1$, left vertical axis to bottom horizontal axis) would be plotted in the bottom region. Not shown are those from the right region, which are unconstrained on the y-axis ($0 \leq C_{\rm c} \leq 1$ and $0 < C_{\rm BELR} < 1$, top horizontal axis to bottom axis).

(ii) The fractional depth is greater than the fraction of the total flux contributed by the continuum source if $D > 1/(W+1)$. The system requires that the BELR be at least partially covered by the absorber.

(iii) The fractional depth is greater than the fraction of the total flux contributed by either the continuum source or the BELR if $D > W/(W+1)$ *and* $D > 1/(W+1)$. The system requires that both the continuum source and the BELR be at least partially covered. Assuming $C_{\rm f} < 1$, one but not both of the background sources can be fully covered.

Because each NAL in a system will be on a different emission line, or possibly covering only continuum emission, the value of W will be different for each transition within a system. All data can be seen in Table 6, which provides the quasar name, the absorption redshift, and the velocity offset of each absorber. There are also four columns showing the value of W, the minimum D for which the continuum source must be at least partially covered, the minimum D for which the BELR must be at least partially covered, and the actual measured D for each of five absorption lines or doublets (O VI, Ly α, N V, Si IV, and C IV). Figs 21–23 show the fractional depth D versus W for the Ly α, N V, and C IV transitions within each intrinsic NAL, provided that the wavelength coverage allows it. The transitions are plotted whether they are present or not. The criterion requiring that the continuum be at least partially absorbed, $D > W/(W+1)$, is represented by the blue line in Figs 21–23. The requirement that at least some of the BELR flux is absorbed, $D > 1/(W+1)$, is represented by the red line in those figures. These constraints divide the parameter space into four distinct regions. In order to reside in the upper region, a line must have both $0 < C_{\rm c} \leq 1$ and $0 < C_{\rm BELR} \leq 1$. Within the left region, the continuum source must be at least partially covered, but it cannot be fully covered. If the continuum source was fully covered, the point for the system would be on or above the red line in Figs 21–23. Within the right region, the BELR must be at least partially covered, but it cannot

Table 6. Ratio of BELR and continuum emission in assorted ions.

			O VI				Ly α				N V			
QSO	z_{abs}	v_{shift}	W	Min depth (continuum)	Min depth (emission)	D	W	Min depth (continuum)	Min depth (emission)	D	W	Min depth (continuum)	Min depth (emission)	D
(1)	(2)	(3)	(4)	(5)	(6)	(7)	(8)	(9)	(10)	(11)	(12)	(13)	(14)	(15)
BAL														
Q1157+014	1.9690	−3086	–	–	–	–	4.649	82.3%	17.7%	68.0%	0.878	46.8%	53.2%	100.0%
Mini-BAL														
Q0130–4021	2.9780	−3374	0.208	17.2%	82.8%	76.9%	1.169	53.9%	46.1%	34.1%	1.318	56.9%	43.1%	38.5%
Q1341–1020	2.1165	−1776	3.706	78.8%	21.2%	100.0%	1.437	59.0%	41.0%	63.0%	1.057	51.4%	48.6%	67.9%
Q1444+014	2.1988	−674	–	–	–	–	1.326	57.0%	43.0%	100.0%	0.748	42.8%	57.2%	60.0%
N V dominant														
Q1158–1843	2.4425	−479	3.942	79.8%	20.2%	98.4%	2.923	74.5%	25.5%	87.5%	0.533	34.8%	65.2%	90.6%
Q2116–358	2.3064	−3123	–	–	–	–	1.021	50.5%	49.5%	85.0%	0.813	44.8%	55.2%	72.1%
Mix														
Q0011+0055	2.2858	−2201	–	–	–	–	5.227	83.9%	16.1%	97.4%	0.000	0.0%	100.0%	93.4%
Q0151–4326	2.7136	−2125	0.013	1.3%	98.7%	91.3%	1.401	58.4%	41.6%	98.6%	1.647	62.2%	37.8%	24.4%
Q0329–385	1.8156	−58 879	–	–	–	–	2.737	73.2%	26.8%	100.0%	2.501	71.4%	28.6%	–
Q0425–5214	2.2389	−1026	–	–	–	–	2.072	67.4%	32.6%	91.8%	1.439	59.0%	41.0%	75.8%
Q1122–1648	2.3530	−4616	4.039	80.2%	19.8%	–	0.701	41.2%	58.8%	100.0%	1.326	57.0%	43.0%	0.0%
Q2132–433	2.3828	−3281	26.210	96.3%	3.7%	76.5%	0.089	8.2%	91.8%	91.5%	0.463	31.6%	68.4%	22.6%
C IV dominant w/non-black Ly α														
Q0549–213	2.2418	−296	–	–	–	–	5.696	85.1%	14.9%	92.4%	0.995	49.9%	50.1%	18.9%
Q0549–213	2.2437	−120	–	–	–	–	5.728	85.1%	14.9%	93.3%	0.968	49.2%	50.8%	64.0%
Q2059–360	2.9712	−8987	0.233	18.9%	81.1%	70.7%	0.915	47.8%	52.2%	98.6%	1.277	56.1%	43.9%	0.0%
C IV dominant														
Q0002–422	2.5394	−18 116	0.878	46.8%	53.2%	44.1%	0.249	19.9%	80.1%	100.0%	0.732	42.3%	57.7%	–
Q0055–269	3.0388	−42 630	0.413	29.2%	70.8%	–	0.205	17.0%	83.0%	100.0%	0.239	19.3%	80.7%	0.0%
Q0055–269	3.0859	−39 216	0.976	49.4%	50.6%	0.0%	0.350	25.9%	74.1%	100.0%	0.041	3.9%	96.1%	0.0%
Q0109–3518	1.7514	−62 990	–	–	–	–	3.511	77.8%	22.2%	100.0%	2.459	71.1%	28.9%	0.0%
Q0122–380	1.7925	−40 613	–	–	–	–	2.369	70.3%	29.7%	100.0%	1.430	58.8%	41.2%	–
Q0151–4326	2.1699	−49 168	1.988	66.5%	33.5%	0.0%	0.165	14.2%	85.8%	100.0%	0.076	7.1%	92.9%	0.0%
Q0329–255	2.2041	−41 680	–	–	–	–	0.096	8.8%	91.2%	100.0%	0.055	5.2%	94.8%	0.0%
Q0425–5214	2.0959	−14 561	–	–	–	–	0.119	10.6%	89.4%	100.0%	0.595	37.3%	62.7%	0.0%
Q0425–5214	2.1385	−10 469	–	–	–	–	0.352	26.0%	74.0%	100.0%	0.829	45.3%	54.7%	100.0%
Q0549–213	2.0711	−16 507	–	–	–	–	0.180	15.3%	84.7%	100.0%	0.051	4.9%	95.1%	0.0%
Q1114–0822	3.3907	−66 198	–	–	–	–	1.263	55.8%	44.2%	100.0%	3.225	76.3%	23.7%	–
Q1202–0725	3.8137	−49 916	0	100.0%	0.0%	X	0.034	96.7%	3.3%	100.0%	0.136	88.0%	12.0%	37.3%
Q1202–0725	4.0484	−35 929	0.095	8.7%	91.3%	–	0.039	3.8%	96.2%	100.0%	0.000	0.0%	100.0%	–
Q1202–0725	4.4808	−11 443	0.495	33.1%	66.9%	100.0%	0.192	16.1%	83.9%	100.0%	0.495	33.1%	66.9%	–
Q1202–0725	4.6265	−3577	–	–	–	–	0.189	15.9%	84.1%	100.0%	4.948	83.2%	16.8%	0.0%
Q1202–0725	4.6876	−227	0.006	0.6%	99.4%	–	0.291	22.5%	77.5%	100.0%	3.647	78.5%	21.5%	0.0%

Table 6 – *continued*

			O VI				Ly α				N V			
QSO	z_{abs}	v_{shift}	W	Min depth (continuum)	Min depth (emission)	D	W	Min depth (continuum)	Min depth (emission)	D	W	Min depth (continuum)	Min depth (emission)	D
(1)	(2)	(3)	(4)	(5)	(6)	(7)	(8)	(9)	(10)	(11)	(12)	(13)	(14)	(15)
Q1209+0919	2.5180	−59 421	0.000	0.0%	100.0%	–	0.163	14.0%	86.0%	100.0%	?????	–	–	100.0%
Q1347–2457	2.3702	−14 227	1.403	58.4%	41.6%	–	0.066	6.2%	93.8%	100.0%	0.361	26.5%	73.5%	–
Q1621–0042	3.2411	−30 714	1.558	60.9%	39.1%	–	0.000	0.0%	100.0%	100.0%	0.066	6.2%	93.8%	–
Q2000–330	3.3924	−24 873	1.171	53.9%	46.1%	0.0%	0.355	26.2%	73.8%	100.0%	0.237	19.2%	80.8%	0.0%
C IV dominant w/low-ionization lines														
Q0136–231	1.8773	−1632	–	–	–	–	7.498	88.2%	11.8%	100.0%	4.280	81.1%	18.9%	16.1%
Q0421–2624	2.1568	−11 206	–	–	–	–	0.275	21.6%	78.4%	100.0%	0.245	19.7%	80.3%	0.0%
Q2225–2258	1.4106	−53 926	–	–	–	–	–	–	–	–	–	–	–	–
Unknown type														
Q0421–2624	1.5171	−77 360	–	–	–	–	–	–	–	–	–	–	–	–
Q0810+2554	1.3525	−18 221	–	–	–	–	–	–	–	–	–	–	–	–
Q0810+2554	1.5011	132	–	–	–	–	–	–	–	–	2.213	68.9%	31.1%	100.0%
Q0952+179	1.2580	−27 090	–	–	–	–	–	–	–	–	–	–	–	–
Q1114–220	2.2820	0	–	–	–	–	0.178	15.1%	84.9%	–	0.690	40.8%	59.2%	–
Q1114–220	2.2963	1304	–	–	–	–	1.906	65.6%	34.4%	–	2.345	70.1%	29.9%	–
Q1157+014	1.7192	−29 358	–	–	–	–	–	–	–	–	–	–	–	–
Q2215–0045	1.4755	61	–	–	–	–	–	–	–	–	0.214	17.6%	82.4%	–
BAL														
Q1157+014	1.9690	−3086	0.190	16.0%	84.0%	73.4%	–	–	–	–	–	–	–	–
Mini-BAL														
Q0130–4021	2.9780	−3374	0.104	9.4%	90.6%	0.0%	0.438	30.5%	69.5%	51.6%	–	–	–	–
Q1341–1020	2.1165	−1776	0.363	26.6%	73.4%	0.0%	0.617	38.2%	61.8%	49.1%	–	–	–	–
Q1444+014	2.1988	−674	0.394	28.3%	71.7%	0.0%	3.666	78.6%	21.4%	34.6%	–	–	–	–
N V dominant														
Q1158–1843	2.4425	−479	0.544	35.2%	64.8%	0.0%	1.006	50.1%	49.9%	85.7%	–	–	–	–
Q2116–358	2.3064	−3123	0.689	40.8%	59.2%	97.6%	0.351	26.0%	74.0%	63.9%	–	–	–	–
Mix														
Q0011+0055	2.2858	−2201	0.394	28.3%	71.7%	90.6%	–	–	–	–	–	–	–	–
Q0151–4326	2.7136	−2125	0.018	1.8%	98.2%	0.0%	0.039	3.8%	96.2%	12.9%	–	–	–	–
Q0329–385	1.8156	−58 879	0.000	0.0%	100.0%	–	0.113	10.2%	89.8%	56.9%	–	–	–	–
Q0425–5214	2.2389	−1026	–	–	–	–	0.794	44.3%	55.7%	79.7%	–	–	–	–
Q1122–1648	2.3530	−4616	0.052	4.9%	95.1%	0.0%	0.132	11.7%	88.3%	16.5%	–	–	–	–
Q2132–433	2.3828	−3281	0.066	6.2%	93.8%	0.0%	0.258	20.5%	79.5%	37.0%	–	–	–	–

Table 6 – *continued*

QSO	z_{abs}	v_{shift}	O VI W	O VI Min depth (continuum)	O VI Min depth (emission)	O VI D	Ly α W	Ly α Min depth (continuum)	Ly α Min depth (emission)	Ly α D	N V W	N V Min depth (continuum)	N V Min depth (emission)	N V D
(1)	(2)	(3)	(4)	(5)	(6)	(7)	(8)	(9)	(10)	(11)	(12)	(13)	(14)	(15)
Non-black Ly α														
Q0549–213	2.2418	−296	–	–	–	–	1.791	64.2%	35.8%	17.6%	–	–	–	–
Q0549–213	2.2437	−120	–	–	–	–	1.906	65.6%	34.4%	74.1%	–	–	–	–
Q2059–360	2.9712	−8987	–	–	–	–	0.020	2.0%	98.0%	15.1%	–	–	–	–
C IV dominant														
Q0002–422	2.5394	−18 116	0.539	35.0%	65.0%	0.0%	0.120	10.7%	89.3%	12.9%	–	–	–	–
Q0055–269	3.0388	−42 630	2.266	69.4%	30.6%	0.0%	0.057	5.4%	94.6%	16.5%	–	–	–	–
Q0055–269	3.0859	−39 216	1.564	61.0%	39.0%	15.1%	0.088	8.1%	91.9%	44.9%	–	–	–	–
Q0109–3518	1.7514	−62 990	0.155	13.4%	86.6%	40.1%	0.294	22.7%	77.3%	24.3%	–	–	–	–
Q0122–380	1.7925	−40 613	0.275	21.6%	78.4%	0.0%	0.241	19.4%	80.6%	20.0%	–	–	–	–
Q0151–4326	2.1699	−49 168	0.863	46.3%	53.7%	0.0%	0.200	16.7%	83.3%	36.2%	–	–	–	–
Q0329–255	2.2041	−41 680	2.008	66.8%	33.2%	–	0.114	10.2%	89.8%	21.0%	–	–	–	–
Q0425–5214	2.0959	−14 561	0.081	7.5%	92.5%	–	0.340	25.4%	74.6%	83.6%	–	–	–	–
Q0425–5214	2.1385	−10 469	0.071	6.6%	93.4%	64.0%	0.333	25.0%	75.0%	55.9%	–	–	–	–
Q0549–213	2.0711	−16 507	0.233	18.9%	81.1%	0.0%	0.040	3.8%	96.2%	45.8%	–	–	–	–
Q1114–0822	3.3907	−66 198	0.131	11.6%	88.4%	–	1.887	65.4%	34.6%	32.5%	–	–	–	–
Q1202–0725	3.8137	−49 916	0.464	68.3%	31.7%	X	0.252	79.9%	20.1%	6.8%	–	–	–	–
Q1202–0725	4.0484	−35 929	3.874	79.5%	20.5%	63.8%	0.851	46.0%	54.0%	40.2%	–	–	–	–
Q1202–0725	4.4808	−11 443	0.999	50.0%	50.0%	–	0.037	3.6%	96.4%	70.0%	–	–	–	–
Q1202–0725	4.6265	−3577	0.793	44.2%	55.8%	0.0%	0.547	35.4%	64.6%	29.8%	–	–	–	–
Q1202–0725	4.6876	−227	0.605	37.7%	62.3%	43.2%	0.151	13.1%	86.9%	94.9%	–	–	–	–
Q1209+0919	2.5180	−59 421	0.059	5.6%	94.4%	–	0.334	25.0%	75.0%	3.1%	–	–	–	–
Q1347–2457	2.3702	−14 227	0.573	36.4%	63.6%	0.0%	0.009	0.9%	99.1%	16.5%	–	–	–	–
Q1621–0042	3.2411	−30 714	0.294	22.7%	77.3%	0.0%	0.438	30.5%	69.5%	14.6%	–	–	–	–
Q2000–330	3.3924	−24 873	0.005	0.5%	99.5%	–	0.005	0.5%	99.5%	19.5%	–	–	–	–
C IV w/low-ionization lines														
Q0136–231	1.8773	−1632	0.079	7.3%	92.7%	41.8%	0.819	45.0%	55.0%	61.8%	–	–	–	–
Q0421–2624	2.1568	−11 206	0.276	21.6%	78.4%	73.9%	0.045	4.3%	95.7%	70.9%	–	–	–	–
Q2225–2258	1.4106	−53 926	3.163	76.0%	24.0%	81.8%	0.356	26.3%	73.7%	98.2%	–	–	–	–

Table 6 – *continued*

			O VI				Ly α				N V			
QSO	z_{abs}	v_{shift}	W	Min depth (continuum)	Min depth (emission)	D	W	Min depth (continuum)	Min depth (emission)	D	W	Min depth (continuum)	Min depth (emission)	D
(1)	(2)	(3)	(4)	(5)	(6)	(7)	(8)	(9)	(10)	(11)	(12)	(13)	(14)	(15)
Unknown type														
Q0421–2624	1.5171	−77 360	3.107	75.7%	24.3%	–	0.120	10.7%	89.3%	72.5%	–	–	–	–
Q0810+2554	1.3525	−18 221	2.280	69.5%	30.5%	22.7%	0.180	15.3%	84.7%	85.9%	–	–	–	–
Q0810+2554	1.5011	132	1.162	53.7%	46.3%	38.5%	–	–	–	–	–	–	–	–
Q0952+179	1.2580	−27 090	9.044	90.0%	10.0%	0.0%	1.925	65.8%	34.2%	64.7%	–	–	–	–
Q1114–220	2.2820	0	–	–	–	–	0.919	47.9%	52.1%	76.0%	–	–	–	–
Q1114–220	2.2963	1304	1.203	54.6%	45.4%	–	0.892	47.1%	52.9%	97.4%	–	–	–	–
Q1157+014	1.7192	−29 358	0.113	10.2%	89.8%	50.2%	0.485	32.7%	67.3%	89.4%	–	–	–	–
Q2215–0045	1.4755	61	1.953	66.1%	33.9%	32.4%	0.104	9.4%	90.6%	34.0 %	–	–	–	–

Note. W, the minimum depth of the line that is required for the continuum to be at least partially covered, the minimum depth of the line that is required for the broad emission-line region to be at least partially covered, and the actual depth of the line, which corresponds to the fraction of light removed from the spectra by the absorption line for each of the intrinsic systems in five different ions, arranged by increasing wavelength (O VI, Ly α, N V, Si IV, and C IV). See Section 6 for more information.

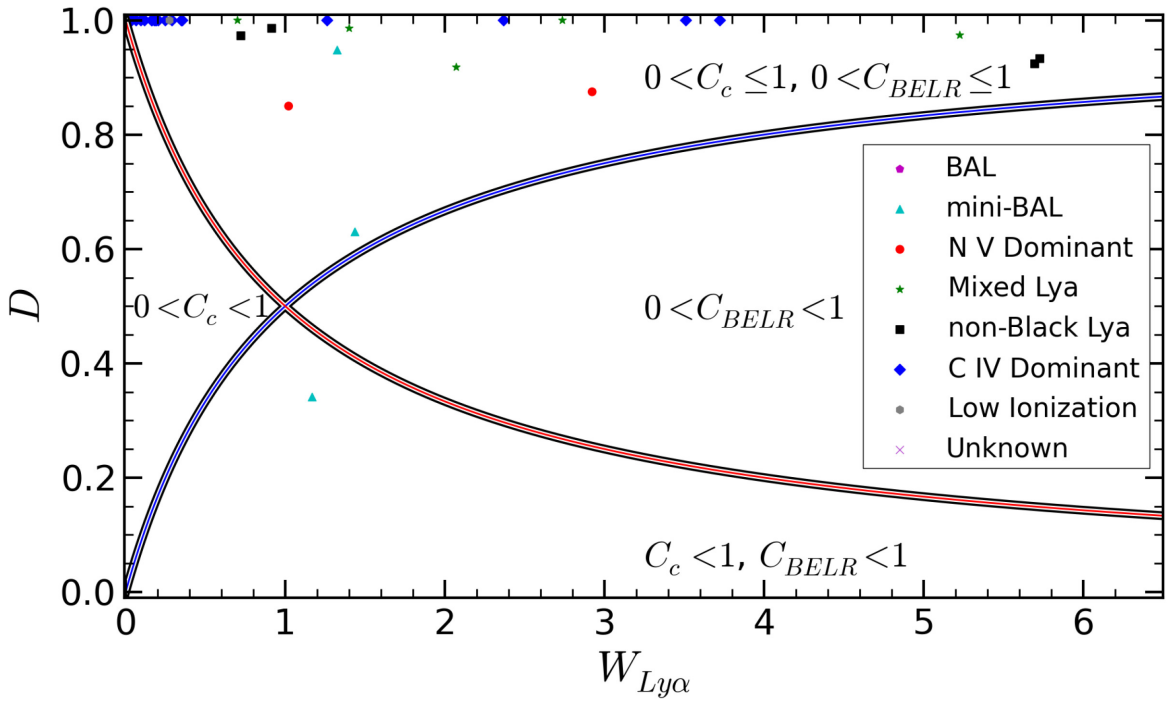

Figure 21. A figure showing fractional depth, D, versus W (defined in Section 6) for the Ly α line for each system at the location of the Ly α absorption line, with different symbols used to represent the different types of systems as described in Section 5. The blue line, $D = 1/(1 + W)$, represents the line above which the continuum emission has to be at least partially covered (i.e. $C_c > 0$), while a point above the red line, $D = W/(1 + W)$, represents those systems which require that the BELR to be at least partially covered (i.e. $C_{\rm BELR} > 0$). The black lines delineate the regions described in Section 6. BALs are marked with a magenta pentagram, mini-BALs with a cyan triangle, N V dominant systems with a red circle, mixed Ly α systems with a green star, C IV dominant systems with partial coverage in Ly α are black squares, C IV dominant systems are blue diamonds, C IV dominant systems with low-ionization lines are grey hexagons, and systems whose type is not definitively known are purple x's.

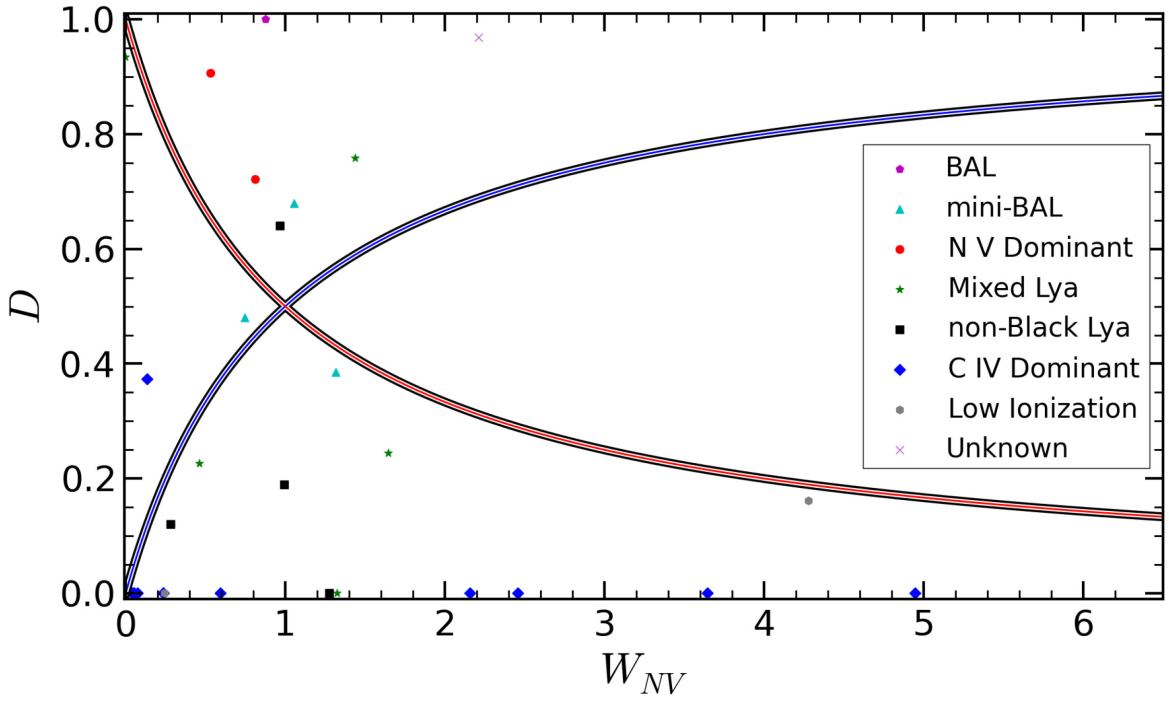

Figure 22. Same as Fig. 21, except that W is measured at the N V λ1239 absorption line in each system.

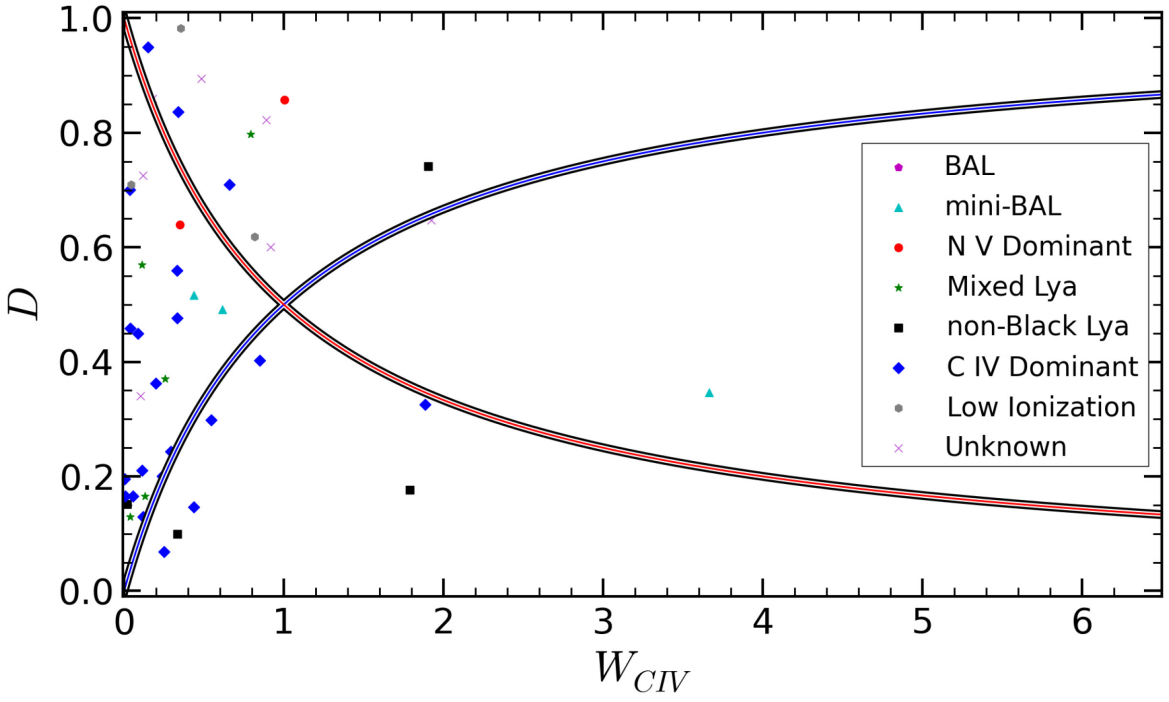

Figure 23. Same as Fig. 21, except that W is measured at the C IV λ1548 absorption line in each system.

be fully covered. Similarly, if the BELR was fully covered, it would be on or above the blue line in Figs 21–23. In the bottom region, one or both of the continuum source and the BELR can be partially covered, but neither can be fully covered.

It is important to note that although the fractional depth and the coverage fraction are not the same, the fractional depth does make a suitable approximation for the coverage fraction for our purposes in our sample. Given that the systems are intrinsic, the fractional depth and the coverage fractions for those systems that have both values measured were similar. Using the definitions of D and R, $D = \max[C_f(1 - e^{-\tau})]$. Given a large enough optical depth, $C_f \approx D$. In practice, there were no systems whose coverage fraction would place them in the bottom region, but whose fractional depth would place them elsewhere. Similarly, apart from one Si IV system whose coverage fraction and W place it directly on the red line, there is no system whose fractional depth places it in the left region, but plotting coverage fraction against W would place it in any other region. There are a small number of systems whose fractional depth places them within the top or bottom region, but whose coverage fraction places them in the right or left region, but the measured coverage fractions simply change the constraints for C_c and C_{BELR}. Thus, fractional depth is a reasonable approximation of the coverage fraction for our purposes. We have a suitable substitute for coverage fraction for every ion covered, including Ly α, which is not a doublet line, O VI, which did not have its coverage fraction measured, and for those doublet lines for which MINFIT was unable to calculate a coverage fraction, or the coverage fraction was unphysical.

Knowing the constraints on the C_c and C_{BELR}, we are able to place constraints on the transverse size of the absorbers of those systems falling in the top, left, and right regions. For those in the right and top regions where the BELR must be at least partially covered, the transverse size of the absorber is most likely of the order of the BELR size. Bentz et al. (2013) calculate a best fit for the relationship between the radius of the BELR of H β and the luminosity. Using this best fit and the optical luminosities of our quasars, we find that the quasars in our sample would have a BELR radius between 10^{-2} and 10^{-1} pc. Rest-frame time delays for C IV, N V, and Si IV are factors of a few smaller, due to stratification of the BELR. The radius of the BELR for those ions would be smaller than for H β, but still of the same order of magnitude. For those systems within the left region (based on our analysis, the continuum source must be partially, but not fully covered in this region), the absorber's transverse size is likely of the order of the size of the continuum source. In order to estimate the size of the continuum source, we use equation (2.12) of Shakura & Sunyaev (1973), which gives the temperature in terms of M_{BH} and the radius in the accretion disc. Inserting the expression for the temperature into the Planck function, we calculate the luminosity at a particular wavelength of interest as

$$L(r, \lambda) = \int_0^r 2\pi r B[T(r), \lambda] \mathrm{d}r \, . \quad (4)$$

We define the size of the continuum source by the radius, r_{cont}, at which 90 per cent of the luminosity of the disc originates at distances $r < r_{cont}$. We used $\lambda = 1450$ Å as it is near the relevant transitions, but away from any emission lines. We considered black hole masses ranging from 10^8 to 10^9 $M_\odot$, and found that the continuum source is $\approx$20 times smaller than the size of the BELR, or between $\approx 5 \times 10^{-4}$ and 5×10^{-3} pc.

From this analysis, an absorber has a maximum transverse size that is dependent on the background source(s) it covers. A system with a transverse size $\gtrsim 10^{-1}$ pc will most likely cover both the continuum and the BELR, and thus cannot be distinguished from intervening absorbers through partial covering. High-velocity systems with $v_{shift} < -5000$ km s^{-1} would have their absorption lines redshifted off of the emission lines, and so would not absorb flux from the BELR. If a high-velocity system had a transverse size greater than $\gtrsim 5 \times 10^{-3}$ pc, it would likely fully cover the continuum

Table 7. Composition of the various absorbers.

Absorber type	Dense core	Tenuous atmosphere
N V dominant	Ly α, C IV, N V, O VI, $\log U \sim -1$	O VI and high-ionization lines, $\log U \gtrsim -0.5$
C IV dominant w/non-black Ly α	Ly α, C IV, N V, $\log U \sim -1.5$	O VI, high-ionizations lines, possibly N V, $\log U \gtrsim -0.5$
C IV dominant	Ly α, Si IV, possibly C IV, $\log U \sim -2.5$	Ly α, possibly C IV and/or N V, $\log U \sim -1.5$
C IV dominant w/low-ionization lines	Ly α, low-ionization lines, $\log U \lesssim -3$	Ly α, Si IV, C IV, $\log U \sim -2$

Table 7 lists the different absorber types, and possibilities for the composition and ionization parameter, $U = n_\gamma/n_{\rm H} = Q_{\rm H}/4\pi r^2 n_{\rm H}$, of the two regions within the absorber. See Section 7.1 for more information.

source. Both of these types of systems would result in full coverage, and so would not be identified as intrinsic by our analysis.

7 PROPOSED MODEL FOR THE ABSORBERS

Partial coverage and/or multiple phases are observed in all of the intrinsic absorption line systems. We propose a plausible, though not unique, model to offer insight into the structure of the absorber. If the absorbing clouds consist of a dense core surrounded by a less dense atmosphere, then the ionization states of the observed absorption systems can be reproduced by varying the ionization parameter. Such a system could have multiple cores contained within the atmosphere, representing the multiple components seen within the systems. In this scenario, the coverage fraction will be different for different ions, depending on whether the lines from that ion can be produced in the atmosphere, core, or both. For an ion that can only be produced in the core, the coverage fraction is determined by the total projected area of all the dense cores that fall within the cylinder of sight. For an ion that can only be produced in the atmosphere, the absorber could be considered to be 'patchy', and the coverage fraction is related to the total projected area within the cylinder of sight *not* covered by the dense cores. In the case of an ion that can be produced in both the atmosphere and the core, such as Ly α in relatively low ionization systems, the ion would be fully covered, unless the size of both the atmosphere and the core is less than the size of the background source(s).

7.1 Ionization structure of the absorbers

In this model, each of the different absorber classes can be reproduced simply by varying the ionizing parameter and/or density of one or both of the regions. Brief descriptions of the composition of both the atmosphere and core for each of the various types of absorbers can be found in Table 7. Starting with N V dominant systems at high ionization and decreasing the ionization parameter, we describe the conditions and ions expected to be in each of the regions.

7.1.1 N V dominant systems

These absorbers have a core that provides high-ionization UV lines like C IV, N V, and/or O VI. However, its ionization parameter is too high for any lower ionization lines other than H I to exist. Even with the low fraction of hydrogen still in the ground state, the abundance of hydrogen allows enough H I for Ly α to be saturated in this region. The atmosphere of a N V dominant absorber is even more highly ionized, resulting in an even lower fraction of hydrogen in the ground state. Ly α in the atmosphere is no longer saturated, and potentially undetectable. This results in Ly α not appearing black, as well as explaining how Ly α can have a higher coverage fraction than N V or C IV as observed in this class. Additionally, the ionization parameter in the atmosphere is too high for even C IV, N V, and, depending on the system, possibly even O VI. However, if there is a smooth transition from the core to the atmosphere, rather than two sharply defined regions, then the density and the ionization parameter would have a gradual change between the two regions. This would increase the region from which detectable column densities can occur for each ion, though a higher ionization line like O VI would have a larger increase than a relatively lower ionization line like N V or C IV. This could explain why higher ionization lines in N V dominant absorbers have larger coverage fractions than relatively lower ionization lines.

Evidence for both core/atmosphere absorbers and for clumpy absorbers comes from some of our N V systems. The coverage fraction and fractional depth of the N V absorption line indicate that two N V systems (Q2116–358, $z_{\rm abs} = 2.3064$ and Q1341–1020, $z_{\rm abs} = 2.1165$) are BELR-sized and cover both the continuum and the BELR almost fully. However, the coverage fraction and fractional depth of the C IV line require partial coverage of the continuum source, hence the C IV absorber size is comparable to that of the continuum source. Such a contradiction can only occur if portions of the region of the absorber covering the continuum source have a high enough column density to produce N V over this region, yet not enough of a column density to produce C IV. This implies that although the whole of the absorber is large enough to nearly fully cover the background sources, there are small dense cores within the absorber in which lower ionization lines are produced. Alternatively, parts of the absorber directly over the continuum source could have lower densities than the majority of the cloud, which would cause C IV to be ionized to C V in that region, but still have enough nitrogen in the form of N V to produce N V absorption.

7.1.2 C IV dominant systems with partial coverage in Ly α

This type of system can be explained in one of two different ways. The first way is to model the system in the same way as the N V dominant absorber, just with a slightly higher density (hence lower ionization parameter) in the core, creating more Ly α and C IV, and less N V absorption. Column densities and ionization parameters for this type of system can have a large enough range that N V can be either present or absent. When N V is present, it appears to come from the same region forming the C IV lines. However, the core would have a low enough column density and high enough ionization parameter that low-ionization lines such as Si II or C II still cannot be seen. The atmosphere would remain highly ionized, and produce only higher ionization lines like O VI. This would lead to a greater difference in density between the core and atmosphere of the absorber than is seen in N V dominant systems. This explanation could apply to systems such as Q0549–213, $z_{\rm abs} = 2.2437$ in Fig. 16, which appears to have Ly α, C IV, and N V all in the same phase.

Another possible way to create a C IV dominant system with Ly α partially covered using the core/atmosphere model is by having weak absorbers with an ionization parameter in the core that is

conducive to creating C IV, but only a small region within the absorber with a density that is high enough to allow a large enough C IV column density for a C IV absorption feature to be seen. The rest of the absorber is tenuous enough and/or with a low enough metallicity that no line other than Ly α has a high enough column density to be detected. Eventually, the density decreases to a low enough level that the ionization parameter becomes too high for Ly α to be strong, resulting in partial coverage for Ly α, but with a higher coverage fraction than that of C IV. High-ionization lines would be weak or not detected due to the low column density in the atmosphere of this relatively thin absorber. This explanation could apply to systems such as Q2314–409, $z_{\rm abs} = 2.4629$ in Fig. 16, which has only weak C IV, and no other NUV metal lines. The fact that there are multiple methods to explain the different systems within this class implies that although such systems are rare, they need not all have the same physical origin and properties.

7.1.3 C IV dominant systems without low-ionization lines

Within this type of absorption system, differences among the individual absorbers imply that there are multiple ways to create such a system, especially for systems within the associated region. The transitions exhibited by these high-velocity C IV dominant intrinsic systems in the NUV are Ly α, C IV, and occasionally Si IV. Additionally, C IV and Si IV (when present) are very weak, often having small fractional depths and coverage fractions. This would imply that the region that produces absorption is small, and this small core would be the only place with a high enough column density for metal absorption lines to exist. The atmosphere is thin enough and has a low enough density that only H I can create strong lines, owing to hydrogen's large abundance. Despite the higher ionization parameter in the atmosphere, N V would not appear in this region if the thickness of the atmosphere and the core are similar. Nitrogen and carbon have an abundance ratio of 1:5 for solar-type abundances, and N V λ1239 has a slightly lower oscillator strength than does C IV λ1548. The low density and low column density of C IV make it very unlikely that N V, or any other NUV metal line, would be detected in the atmosphere.

C IV dominant systems in the associated region cannot be classified as easily. Many have coverage fractions and fractional depths that place them in the top region of Fig. 23, giving them a transverse size of the order of the BELR size. Those systems are likely analogues to the N V dominant systems, but with slightly lower ionization parameters, or systems with cores similar to the C IV dominant systems with Ly α partially covered, but with the atmosphere of the absorber either slightly denser or thicker, hence capable of creating Ly α column densities large enough to allow Ly α to have full coverage. O VI might also be detected in this region. Other systems within the associated region have depths that place them in either the left region of Fig. 23, giving them a transverse size of the order of the size of the continuum source, or in the bottom region, where size constraints cannot be easily obtained. One possibility for the geometry of an absorber in the bottom region of Fig. 23 would be a weak absorber as described above, with the atmosphere of the absorber the size of the BELR, if not bigger, in order to have full coverage in Ly α. In this case, the core of the absorber could represent a cloud of gas whose transverse size is only large enough to cover a small fraction of the continuum source. In all likelihood, there would be many such cores within the atmosphere in order that alignment with one or more along the line of sight would be probable. Multiple cores would also explain multiple absorbing components in C IV along the same sightline. Another possibility is that the core could be an off-centre overdensity in the cloud, blocking only a portion of the BELR (and not the continuum source).

7.1.4 C IV dominant systems with low-ionization lines

The different subclasses of C IV dominant systems with full coverage in Ly α can arise from variations in the properties of the dense core. In the absorbers with no low-ionization transitions, the absorber has the right ionization parameter, is thin enough, and/or has a low enough metallicity that Ly α, C IV, and Si IV are the only lines to come from this area. From the atmosphere, only Ly α, and in some cases O VI, are present. The systems with low-ionization lines are thick enough along the line of sight, dense enough, have a higher metallicity, and/or have a low enough ionization parameter that low-ionization lines have a large enough column density to be detectable. As a lower ionization region within the same system as a higher ionization region implies an increase in density, rather than a decrease in flux, the low-ionization lines must be coming from a denser region in the absorber. In some cases, there is a noticeable velocity offset between the C IV and Si IV lines and the low-ionization lines, and differences in the absorption profile for the different lines, which arise in separate phases.

The best way to model such a two-phase structure would be to use our core/atmosphere model with a dense, thin absorber relatively close to the quasar. An overdense region would create the low-ionization lines, while the surrounding less dense region would produce C IV and relatively higher ionization lines. A thin absorber would not have enough column density in C IV for it to be present along the line of sight in the same region as the low-ionization lines. The overdense region would appear as a 'gap' or 'hole' in the C IV absorbing region. Ly α would have a high enough column density to be seen throughout both the atmosphere and the core, resulting in a coverage fraction of unity for Ly α.

For those cases where the low-ionization lines and C IV do not have radically different absorption profiles or different velocity offsets, we can use our core/atmosphere model as we have previously for N V dominant and C IV dominant systems, simply with a lower ionization parameter. The core would have a density high enough that low-ionization lines are present and gradually transition to a lower density atmosphere. During that gradual transition, or possibly even throughout the core, the ionization parameter will be intermediate between what is most conducive to producing C IV and the preferred ionization parameter for low-ionization lines, allowing both species to exist in the same region. The size of the core would determine the relative strengths between the low-ionization lines and C IV. For example, if the core is nearly the size of the cylinder of sight, the low-ionization lines would be much stronger than the C IV line. A small core would equate to weak low-ionization lines and potentially strong C IV absorption.

7.1.5 Mixed Ly α systems

These absorbers appear to be systems in which one or more components have geometries like that of either the C IV dominant systems with partial coverage in Ly α or the N V dominant systems, while others have components like those of the C IV dominant systems with full coverage in Ly α systems. One possible interpretation is that these systems act as a transition phase between C IV dominant and N V dominant lines and show varying ionization states within

the same system. Another interpretation is that there are density variations between two separate components, resulting in different ionization parameters for the two components. In certain regions, Ly α could have a high enough column density throughout the line of sight to the quasar to be detectable, resulting in full coverage of Ly α in some components. In other regions, the atmosphere could have a low enough density and column density to give partial coverage in Ly α in other components.

7.1.6 *Extension of the model to Ne VIII and O VI systems*

Using ground-based telescopes, such as those used in this survey, it is nearly impossible to detect Ne VIII. Only Ne VIII absorption systems with $z \gtrsim 4$ could be observed in this manner. However, due to the small number of systems found at such high redshifts, as well as contamination from the Ly α forest, no such systems were identified in this survey. In the spectra of Muzahid et al. (2013), where the Ne VIII lines *are* found, the N V $\lambda\lambda$1239, 1243 doublet lines are not often covered. In the few cases in which N V and Ly α were covered (PG 1338+416, $z_{\rm abs} = 1.215\,34$, PG 1206+459, $z_{\rm abs} = 1.028\,54$), N V is present with about the same strength as Ly α. Such an absorber, if it were in our sample, would be a N V dominant system. In the systems in which N V is not covered, most have FUV lines from ions such as O IV, O V, and N IV, indicating that N V would be detected if the wavelength coverage of the spectra allowed it. This would suggest that Ne VIII absorbers would often have a relatively low ionization phase containing N V, and imply that the N V dominant absorbers that we see in our sample could in fact be one phase of the same system as the Ne VIII absorbers.

O VI systems found in previous papers (i.e. Tripp et al. 2008; Ganguly et al. 2013) are possibly even less distinct. In our sample, we could not study many intrinsic O VI absorbers because the relevant rest-frame wavelength region was not often covered, and because when it was covered, contamination by the Ly α forest was severe. However, intrinsic O VI absorbers likely fit within our ionization-based scheme for absorption line properties. Whenever N V absorption occurs, O VI absorption is always present when the relevant wavelengths are covered. Thus it is likely that O VI absorption occurs within all N V dominant systems. Similarly, O VI absorption occurs in all but one of the Ne VIII systems found in Muzahid et al. (2013). Even some C IV dominant systems both in this paper and in Misawa et al. (2007) exhibit O VI absorption. For all ionization parameters for which O VI is detected and strong, higher and/or lower ionization states are also likely to be detected. As such, those systems defined elsewhere as O VI systems would therefore likely be incorporated into one of the other classes that we define here, and so we do not explicitly define an O VI dominant class.

7.2 Physical characteristics of the absorbers

When considering the properties of the absorbers, not only is the ionization state important, but also other physical characteristics such as shape, number density, and mass. The shape of each absorber will be different, but, as noted in Section 6, the transverse size of absorbers can sometimes be estimated. In our sample, N V dominant systems have $|v_{\rm shift}| < 5000$ km s^{-1}, which means that they are superposed on the Ly α and N V emission-line blend. From Fig. 22, it becomes apparent that most intrinsic N V-dominant systems found in our sample must at least partially cover the BELR, and so likely have transverse sizes of the order of the BELR size. C IV dominant systems in the associated region are distributed throughout Figs 22 and 23, and so these absorbers are likely to have a broad range of sizes. C IV dominant systems at high velocity were found to have transverse sizes of the order of the continuum source.

The number density of an absorber can be determined by utilizing the definition of flux, $F = L/4\pi r^2$, and ionization parameter, $U = n_\gamma/n_{\rm H} = Q_{\rm H}/4\pi r^2 n_{\rm H}$, where n_γ is the photon number density, $n_{\rm H}$ is the hydrogen number density, and $Q_{\rm H}$ is the rate of hydrogen ionizing photons. This leads to

$$\left(\frac{n_{\rm H}}{10^8\ {\rm cm^{-3}}}\right) = \left(\frac{\nu L_\nu(2500\ {\rm \AA})}{8\times10^{46}\ {\rm erg\ s^{-1}}}\right)\left(\frac{U}{10^{-1.9}}\right)^{-1}\left(\frac{r}{1\ {\rm pc}}\right)^{-2}, \quad (5)$$

where the luminosity $\nu L_\nu(2500\ {\rm \AA}) = 8\times10^{46}$ erg s^{-1} is an average value of the near-UV luminosity of our sample quasars, an ionization parameter of $\log U = -1.9$ is the optimal value for a C IV dominant system, based on fig. 11 of Hamann (1997), and a reasonable distance outside of the accretion disc wind launch radius is used. If we take the measured ionic column densities calculated by minfit, we can find the total column density for a given atom using fig. 11 of Hamann (1997). Assuming solar abundance patterns, we can estimate a total column density, $N_{\rm tot}$. We are then able to constrain the thickness of that absorber, Δr, by combining this total column density and the calculated number density:

$$\begin{aligned}\left(\frac{\Delta r}{10^{11}\ {\rm cm}}\right) &= \left(\frac{N_{\rm tot}}{10^{19}\ {\rm cm^{-2}}}\right)\left(\frac{n_{\rm H}}{10^8\ {\rm cm^{-3}}}\right)^{-1}\\ &= \left(\frac{N_{\rm tot}}{10^{19}\ {\rm cm^{-2}}}\right)\left(\frac{\nu L_\nu(2500\ {\rm \AA})}{8\times10^{46}\ {\rm erg\ s^{-1}}}\right)^{-1}\\ &\quad\times\left(\frac{U}{10^{-1.9}}\right)\left(\frac{r}{1\ {\rm pc}}\right)^{2}. \quad (6)\end{aligned}$$

As the distance from the quasar increases, the thickness of the absorber increases, and so does the radial filling factor $\Delta r/r$. The number density, however, decreases with the increasing distance. If we were to use values for an average C IV dominant system such as $N_{\rm tot} = 10^{18}$ cm^{-2} and $\log U = -1.9$, an average luminosity like $\nu L_\nu(2500\ {\rm \AA}) = 8\times10^{46}$ erg s^{-1}, and estimate a distance of 10^3 pc, then the density is $n_{\rm H} = 10^2$ cm^{-2}, while the thickness is $\Delta r = 10^{-2}$ pc. Such an absorber has a thickness roughly equal to the size of the BELR. If we instead use values for an average N V dominant system such as $N_{\rm tot} = 10^{19}$ cm^{-2} and $\log U = -0.5$, the same luminosity, and estimate a distance of 1 pc, we would find a thickness of $\Delta r = 10^{-1}$ au or about 10^{-6} pc, and a density of $n_{\rm H} = 10^6$ cm^{-3}. If such an absorber were to fully cover the background source(s), it would have a transverse size much larger than the thickness along the line of sight, and would have the shape of a flat disc or sheet of material (Hamann et al. 2013). This could represent a shock front in the wind propagating out from the quasar or a thin layer of a larger structure.

We are also able to make an order of magnitude calculation for the mass of an absorber using the column density and by calculating the volume of the absorber as $V \approx \Delta r R^2$, where R is the transverse size of the absorber, which we approximate here as the size of the BELR:

$$\begin{aligned}M &= m_{\rm H} n_{\rm H} V\\ &\sim m_{\rm H} N_{\rm tot} R^2\\ &\sim 10^{27}\ {\rm g}\left(\frac{R}{10^{-2}\ {\rm pc}}\right)^2\left(\frac{N_{\rm tot}}{10^{19}\ {\rm cm^{-2}}}\right). \quad (7)\end{aligned}$$

We estimate a conservative size of the BELR to be $R \sim 10^{-2}$ pc, as described in Section 6. Using a typical total column density of $\sim 10^{19}$ cm^{-2}, we get a mass of 10^{27} g or 10^{-6} M$_{\odot}$, which is comparable to the mass of the Earth. If we were to instead use the size of the continuum source as the transverse size of the absorber, the mass decreases by roughly two orders of magnitude, or less than the mass of the moon. We note that these estimates refer to the portion of the absorber that we detect via absorption lines. They are lower limits to the mass of the parcels of gas in which the lines form.

7.3 Using velocity offset as a proxy for distance

There are many factors that might cause differences between the properties of different intrinsic NALs. Some examples are ionization parameter, column density, metallicity, metal abundance, coverage fraction, geometry of the NAL, and distance of the absorber from the ionizing source(s). Distance is one of the simpler variables to explore. Although we cannot determine the distance of the absorber directly, we can use the velocity offset of the absorber as a proxy for distance. If gas clouds are ejected by the wind with a wide range of velocities, or if they are accelerated, then the ones with the largest velocities will quickly move away from the quasar, and thus have a lower ionization parameter than an identical cloud at a shorter distance from the quasar. Under that assumption, we can then put interesting constraints on the properties of the various subclasses.

Most of the differences between the different types of systems can be explained by a changing ionization parameter, as described in Section 7.1, which can vary based on the distance from the quasar and/or variations in the density of the absorber at a given distance. Starting close to the quasar, the simplest model would have:

(i) Ne VIII, Na IX, and Mg X absorbers are closest to the quasar, possibly representative of the shielding material/failed wind. This is supported by the observation that Ne VIII absorbers tend to be within 5000 km s^{-1} of the quasar (in the associated region), though some do have higher velocities (Muzahid et al. 2013).

(ii) O VI dominant systems are the next closest to the quasar. Those systems found in the associated region are the most likely to be intrinsic (Ganguly et al. 2013).

(iii) N V dominant systems are the next furthest out, though still likely in the quasar host environment. N V-dominated systems were found exclusively in the associated region in our sample. The fact that associated N V systems are not found at higher velocities, even when the Ly α forest is not present, places an interesting constraint on the ionization structure of the outflow (Fox et al. 2009; Culliton et al., in preparation).

(iv) Mixed Ly α and C IV dominant systems with non-black Ly α are at intermediate distances between N V and C IV dominant systems. These systems are mostly in the associated region, with only one such system in our sample at a higher velocity (Q2059–360, $z_{\rm abs} = 2.9712$, $v_{\rm shift} = 8987$ km s^{-1}). Such systems are also likely to reside close to the ionizing source.

(v) The zone of C IV dominant systems extends from the zone of N V dominant systems (possibly overlapping with it) to the edge of the galaxy and beyond. This is evidenced by the fact that C IV systems have radial velocities anywhere from $\sim$1000 km s^{-1} to the red of the quasar emission redshift to $\sim$80 000 km s^{-1} to the blue of the quasar. It is important to note that despite the wide range of velocity offsets, Fig. 3 shows a near constant number density of intrinsic absorbers at all velocities outside the associated region. This means that the filling factor must stay constant at all distances away from the quasar, implying that the density of these relatively small absorbers increases as distance from the quasar increases.

(vi) Lower ionization systems such as Mg II absorbers extend from the edge of the region dominated by the C IV dominant systems outwards.

Thus, if one cloud were placed at different distances from the quasar, with all else held constant, it could represent any of the different types of absorbers seen in this and other surveys. However, as noted in Section 7.1.6, there is likely a connection between the Ne VIII, O VI, and N V systems. The Ne VIII, O VI, and N V absorption seen in different observations could represent different phases of the gas within the same type of system, unifying those three types of absorbers, rather than being discrete absorption system types at different ionization parameters.

7.4 O I absorption and justification of our methods

It is noteworthy that in both our sample and that of Misawa et al. (2007), systems with O I present were determined to have partial coverage. The velocity offsets of these systems range between -1000 and -5500 km s^{-1}. The three examples of these systems from our sample can be seen in Fig. 24, which shows the spectra for relevant ions and the coverage fractions used to determine the class of the system. Most, if not all, of these systems are damped Ly α absorbers (DLAs). As such, they are unlikely to be intrinsic absorbers. However, this does not indicate an error in our analysis or methodology. Hacker et al. (2013) found at least 10 different intervening absorption systems with absorption line variability. Such short time-scale variability is indicative of small-scale structures of $\sim$10–100 au in size. Such an absorber would likely also exhibit partial coverage. This indicates that it is possible that not all of our absorption systems that exhibit partial coverage are in fact intrinsic. Partial coverage alone may not be enough to conclusively prove that a system is physically associated with the quasar.

8 IMPLICATIONS FOR MODELS OF QUASAR OUTFLOWS

In Section 7, we presented a model to describe the ionization structure of the NAL gas. Here, we consider two models of the origin of the NAL gas. In the first, a line-driving model, the absorbers are 'cold' filaments at middle to high latitudes above the fast, dense, equatorial wind. The wind closest to the SMBH is fully ionized by X-ray photons and loses its driving lines before it can be accelerated to its escape velocity, eventually falling back on to the inner disc or the central object. Winds at larger radii can occur anywhere the radiation from the disc is large enough to launch the gas above the disc. These winds are shielded from X-ray photons by the gas in the failed wind and are variable. The wind in the polar region is highly ionized and hot, while the region close to the equatorial plane is much denser and much less ionized. As the equatorial wind flows outward, instabilities can develop near the interface of the these two regions that result in dense filaments embedded in the hot phase. The models presented in Murray et al. (1995), Proga et al. (2000), and Proga & Kallman (2004) predict that such a wind would be launched at a radius of $r \sim 10^{16}$ cm, have radial velocities reaching as high as $v_r \sim 15\,000$ km s^{-1}, temperatures in the range 10^6 K $\lesssim T \lesssim 10^7$ K, number densities of $n_{\rm H} \sim 10^4$ cm^{-3}, and a widely varying ionization parameter of $-10 \lesssim \log U \lesssim 6$. The inner and outer boundaries of the simulation are 3×10^{-3} pc $\leq r \leq 3 \times 10^{-2}$ pc ($M_{\rm BH} = 10^7$ M$_{\odot}$).

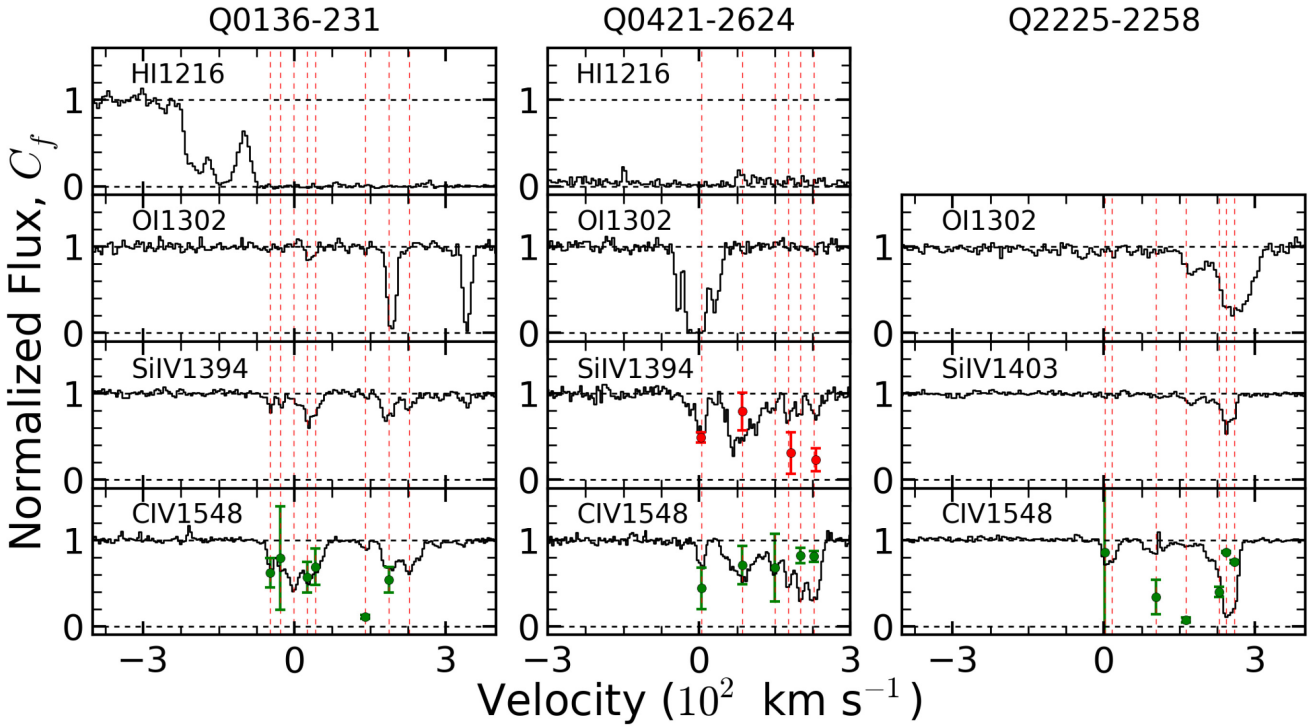

Figure 24. Velocity aligned absorption profiles of the three O I systems, showing Ly α (when present), O I, Si IV, and C IV. Red vertical dashed lines represent components within the system. Green points represent physical coverage fractions ($0 < C_f \leq 1$). If a second ion had physical coverage fractions for its components, it is plotted in blue.

The second model describes how the gas from the host galaxy is swept up as the wind propagates away from the central engine, creating intrinsic NALs. The models of Kurosawa & Proga (2009) predict that this wind is accelerated from the central engine at distances on the order of 1 pc, with radial velocities up to 3×10^3 km s^{-1}, temperatures of $T \lesssim 10^5$ K, number densities of $n_{\rm H} \gtrsim 10^4$ cm^{-3}, and an ionization parameter of $-4 \lesssim \log U \lesssim 0$. The inner and outer boundaries of the simulation are 10^{-2} pc $\leq r \leq 7$ pc.

Observationally, it is difficult to differentiate between the two models without knowing the distances of the absorbers from the quasar. Both models have distinct regions that could allow the different types of absorbers to arise. Further complicating this scenario is the fact that a combination of these two models is possible, if not likely. Additionally, the low spatial resolution of the simulations hides the fine structure of the gas and may also suppress acceleration mechanisms that depend on small-scale density fluctuations and a variable continuum flux (see e.g. Waters & Proga 2016). Although the models above do allow for identification of the types of regions where intrinsic absorbers postulated about here could arise, unfortunately, the resolution of the simulations is not yet high enough to allow for the fine detail required for the types of absorbers seen in our sample. Until simulations are able to produce the types of absorbers found in this sample and in others, the work of trying to simulate intrinsic NALs will not be finished.

9 SUMMARY

Using spectra of 73 quasars from the VLT/UVES archive, we constructed a large, relatively unbiased sample of intrinsic NALs with redshifts between 1.4 and 5. We identified 410 NAL systems, in which 374 C IV doublets, 25 N V doublets, and 56 Si IV doublets were found. Using a partial coverage analysis, we found 33 reliably intrinsic NALs, as well as 11 NALs that are potentially intrinsic. Additionally, we found four mini-BALs and one BAL. We described their properties, demographics, and relation of their properties to those of the quasars hosting them. Our findings and conclusions are as follows:

(i) The majority of intrinsic and intervening NAL systems have low rest-frame EWs, with very few systems having rest-frame EWs greater than 1.5 Å.

(ii) At a minimum, doublets that have been demonstrated to be reliably intrinsic systems through partial coverage make up 19 per cent of all associated doublets. If potentially intrinsic systems are included (with weak evidence for partial coverage), this fraction becomes 23 per cent.

(iii) At $|v_{\rm shift}| > 5000$ km s^{-1}, at least 5 per cent of all NALs are reliably intrinsic, and another 5 per cent are potentially intrinsic.

(iv) Among all systems, 9 per cent of all NALs are reliably intrinsic, while an additional 4 per cent were potentially intrinsic, as demonstrated through partial coverage. There can be additional intrinsic NALs with full coverage that could not be classified as such in our survey, so these numbers are lower limits.

(v) Of the 73 quasars in our sample, 29 have at least one reliably intrinsic system, while 32 have at least one reliably or potentially intrinsic system.

(vi) The distributions of the properties of intrinsic systems and the fraction of quasars containing an intrinsic absorption system are similar between radio-loud and radio-quiet quasars in this $1.4 < z < 5$ sample.

(vii) The 'C IV dominant' and 'N V dominant' families found in Misawa et al. (2007) are found in our survey as well. However, in this larger sample, we can see that these categories combine to form a continuous range of intrinsic NALs, from systems with a

low-ionization phase to the high-ionization Ne VIII systems, with each smoothly transitioning from one to the next.

(viii) We argue that the absorbers themselves can be represented as a dense core surrounded by a more tenuous atmosphere. Although the core of the absorber provides the majority of the absorption line, the atmosphere can contribute to produce different phases of gas, with higher ionization states, and/or to Ly α absorption.

(ix) Using velocity offset as a proxy for distance, one possible explanation for the varying ionization states of intrinsic absorbers is an increase in the distance from the host quasar. As distance increases, the ionization parameter decreases, leading to lower ionization states further from the quasar. Variations in the density of the absorber, either due to differences in wind properties, or due to evolution of outflowing material, can also be a contributing factor to the range of intrinsic NAL properties.

(x) Although current simulations can make intriguing predictions about the physical location of the absorbers that we have observed, the resolution of these simulations is not yet high enough to accurately re-create those absorbers.

Repeated observations of the NALs in this sample are extremely valuable as they would allow us to confirm the intrinsic nature of these NALs and get more direct constraints on their distances by using absorption line variability to constrain the density of the gas. Full wavelength coverage would allow us to access more transitions from a given system and thus detect any multiphase structure present in the NAL. Additionally, transitions from different ions of the same elements would allow us to infer the conditions in the absorbers without making assumptions about relative elemental abundances. Such constraints would greatly aid in the creation of quasar outflow models. Further progress can also be made through photoionization modelling and variability studies of the intrinsic systems found in this and other surveys. Improvements in the spatial resolution of the simulations could elucidate the multiphase structure of the absorbing gas and open the door to new observational tests.

ACKNOWLEDGEMENTS

We thank the anonymous referee for helpful comments and suggestions. This work was supported by NSF grant AST-0807993. TM acknowledges support from JSPS KAKENHI Grant Number 15K05020. We also acknowledge the ESO archive facility for providing data using a variety of programs as compiled in Table 1 of Narayanan et al. (2007).

REFERENCES

Anderson S. F., Weymann R. J., Foltz C. B., Chaffee F. H., Jr, 1987, AJ, 94, 278
Arav N., Li Z.-Y., Begelman M. C., 1994, ApJ, 432, 62
Arav N., Borguet B., Chamberlain C., Edmonds D., Danforth C., 2013, MNRAS, 436, 3286
Arav N., Liu G., Xu X., Stidham J., Benn C., Chamberlain C., 2018, ApJ, 857, 60
Balbus S. A., Hawley J. F., 1991, ApJ, 376, 214
Barlow T. A., Sargent W. L. W., 1997, AJ, 113, 136
Barlow T. A., Hamann F., Sargent W. L. W., 1997, in Arav N., Shlosman I., Weymann R. J., eds, ASP Conf. Ser. Vol. 128, Mass Ejection from Active Galactic Nuclei. Astron. Soc. Pac., San Francisco, p. 13
Barthel P. D., Tytler D. R., Vestergaard M., 1997, in Arav N., Shlosman I., Weymann R. J., eds, ASP Conf. Ser. Vol. 128, Mass Ejection from Active Galactic Nuclei. Astron. Soc. Pac., San Francisco, p. 48
Baskin A., Laor A., 2012, MNRAS, 426, 1144
Becker R. H., White R. L., Gregg M. D., Brotherton M. S., Laurent-Muehleisen S. A., Arav N., 2000, ApJ, 538, 72
Begelman M., de Kool M., Sikora M., 1991, ApJ, 382, 416
Bentz M. C. et al., 2013, ApJ, 767, 149
Blandford R. D., Payne D. G., 1982, MNRAS, 199, 883
Borguet B. C. J., Arav N., Edmonds D., Chamberlain C., Benn C., 2013, ApJ, 762, 49
Chamberlain C., Arav N., 2015, MNRAS, 454, 675
Chandrasekhar S., 1960, Proc. Natl. Acad. Sci., 46, 253
Chen Z.-F., Qin Y.-P., 2013, ApJ, 777, 56
Chen Z.-F., Gu Q.-S., Chen Y.-M., Cao Y., 2015, MNRAS, 450, 3904
Churchill C. W., Vogt S. S., 2001, AJ, 122, 679
Ciotti L., Ostriker J. P., 2007, ApJ, 665, 1038
Cirasuolo M., Celotti A., Magliocchetti M., Danese L., 2003, MNRAS, 346, 447
de Kool M., Begelman M. C., 1995, ApJ, 455, 448
Di Matteo T., Springel V., Hernquist L., 2005, Nature, 433, 604
Emmering R. T., Blandford R. D., Shlosman I., 1992, ApJ, 385, 460
Everett J. E., 2005, ApJ, 631, 689
Faucher-Giguère C.-A., 2012, in Chartas G., Hamann F., Leighly K. M., eds, ASP Conf. Ser. Vol. 460, AGN Winds in Charleston. Astron. Soc. Pac., San Francisco, p. 240
Faucher-Giguère C.-A., Quataert E., 2012, MNRAS, 425, 605
Foltz C. B., Weymann R. J., Peterson B. M., Sun L., Malkan M. A., Chaffee F. H., Jr, 1986, ApJ, 307, 504
Foltz C. B., Chaffee F. H., Hewett P. C., Weymann R. J., Anderson S. F., MacAlpine G. M., 1989, AJ, 98, 1959
Fox A. J., Prochaska J. X., Ledoux C., Petitjean P., Wolfe A. M., Srianand R., 2009, A&A, 503, 731
Gabel J. R. et al., 2003, ApJ, 583, 178
Gabel J. R. et al., 2005, ApJ, 631, 741
Gabel J. R., Arav N., Kim T.-S., 2006, ApJ, 646, 742
Ganguly R. et al., 2013, MNRAS, 435, 1233
Ganguly R., Brotherton M. S., 2008, ApJ, 672, 102
Ganguly R., Eracleous M., Charlton J. C., Churchill C. W., 1999, AJ, 117, 2594
Ganguly R., Bond N. A., Charlton J. C., Eracleous M., Brandt W. N., Churchill C. W., 2001, ApJ, 549, 133
Ganguly R., Masiero J., Charlton J. C., Sembach K. R., 2003, ApJ, 598, 922
Ganguly R., Sembach K. R., Tripp T. M., Savage B. D., 2005, ApJS, 157, 251
Ganguly R., Sembach K. R., Tripp T. M., Savage B. D., Wakker B. P., 2006, ApJ, 645, 868
Gebhardt K., Thomas J., 2009, ApJ, 700, 1690
Granato G. L., De Zotti G., Silva L., Bressan A., Danese L., 2004, ApJ, 600, 580
Hacker T. L., Brunner R. J., Lundgren B. F., York D. G., 2013, MNRAS, 434, 163
Hamann F., 1997, ApJS, 109, 279
Hamann F., Barlow T. A., Junkkarinen V., Burbidge E. M., 1997a, ApJ, 478, 80
Hamann F., Barlow T. A., Junkkarinen V., 1997b, ApJ, 478, 87
Hamann F., Chartas G., McGraw S., Rodriguez Hidalgo P., Shields J., Capellupo D., Charlton J., Eracleous M., 2013, MNRAS, 435, 133
Hewett P. C., Foltz C. B., 2003, AJ, 125, 1784
Hogg D. W., 1999, preprint (arXiv:e-print)
Ivezić Ž. et al., 2002, AJ, 124, 2364
Jones T., Misawa T., Mshar A., Charlton J. C., Ferland G. J., Stancil P. C., 2007, Bull. Am. Astron. Soc., 39, 823
Kellermann K. I., Sramek R., Schmidt M., Shaffer D. B., Green R., 1989, AJ, 98, 1195
Kellermann K. I., Sramek R. A., Schmidt M., Green R. F., Shaffer D. B., 1994, AJ, 108, 1163
Kobayashi N., Terada H., Goto M., Tokunaga A., 2002, ApJ, 569, 676
Konigl A., Kartje J. F., 1994, ApJ, 434, 446
Kormendy J., Richstone D., 1995, ARA&A, 33, 581
Kurosawa R., Proga D., 2009, ApJ, 693, 1929

Laor A., Brandt W. N., 2002, ApJ, 569, 641
Leighly K. M., Terndrup D. M., Baron E., Lucy A. B., Dietrich M., Gallagher S. C., 2014, ApJ, 788, 123
Misawa T., Yamada T., Takada-Hidai M., Wang Y., Kashikawa N., Iye M., Tanaka I., 2003, AJ, 125, 1336
Misawa T., Charlton J. C., Eracleous M., Ganguly R., Tytler D., Kirkman D., Suzuki N., Lubin D., 2007, ApJS, 171, 1
Misawa T., Charlton J. C., Eracleous M., 2014, ApJ, 792, 77
Murray N., Chiang J., 1998, ApJ, 494, 125
Murray N., Chiang J., Grossman S. A., Voit G. M., 1995, ApJ, 451, 498
Muzahid S., Srianand R., Arav N., Savage B. D., Narayanan A., 2013, MNRAS, 431, 2885
Narayanan D., Hamann F., Barlow T., Burbidge E. M., Cohen R. D., Junkkarinen V., Lyons R., 2004, ApJ, 601, 715
Narayanan A., Misawa T., Charlton J. C., Kim T.-S., 2007, ApJ, 660, 1093
Nestor D., Hamann F., Rodriguez Hidalgo P., 2008, MNRAS, 386, 2055
O'Meara J. M., Tytler D., Kirkman D., Suzuki N., Prochaska J. X., Lubin D., Wolfe A. M., 2001, ApJ, 552, 718
Onken C. A., Peterson B. M., 2002, ApJ, 572, 746
Ostriker J. P., Choi E., Ciotti L., Novak G. S., Proga D., 2010, ApJ, 722, 642
Petitjean P., Srianand R., 1999, A&A, 345, 73
Proga D., 2003, ApJ, 585, 406
Proga D., Kallman T. R., 2004, ApJ, 616, 688
Proga D., Stone J. M., Kallman T. R., 2000, ApJ, 543, 686
Reichard T. A. et al., 2003a, AJ, 125, 1711
Reichard T. A. et al., 2003b, AJ, 126, 2594
Richards G. T., 2001, ApJS, 133, 53
Richards G. T., York D. G., Yanny B., Kollgaard R. I., Laurent-Muehleisen S. A., Vanden Berk D. E., 1999, ApJ, 513, 576
Rodríguez Hidalgo P., 2009, PhD thesis, Univ. Florida
Roth N., Kasen D., Hopkins P. F., Quataert E., 2012, ApJ, 759, 36
Sargent W. L. W., Boksenberg A., Steidel C. C., 1988, ApJS, 68, 539
Savage B. D., Sembach K. R., 1991, ApJ, 379, 245
Scannapieco E., Oh S. P., 2004, ApJ, 608, 62
Scott J. E. et al., 2004, ApJS, 152, 1
Shakura N. I., Sunyaev R. A., 1973, A&A, 24, 337
Silk J., Rees M. J., 1998, A&A, 331, L1
Springel V., Di Matteo T., Hernquist L., 2005, ApJ, 620, L79
Srianand R., Petitjean P., 2000, A&A, 357, 414
Tolea A., Krolik J. H., Tsvetanov Z., 2002, ApJ, 578, L31
Tripp T. M., Sembach K. R., Bowen D. V., Savage B. D., Jenkins E. B., Lehner N., Richter P., 2008, ApJS, 177, 39
Velikov E. P., 1959, J. Exp. Theor. Phys., 36, 1398
Vestergaard M., 2003, ApJ, 599, 116
Wampler E. J., Bergeron J., Petitjean P., 1993, A&A, 273, 15
Wampler E. J., Chugai N. N., Petitjean P., 1995, ApJ, 443, 586
Waters T., Proga D., 2016, MNRAS, 460, L79
Weymann R. J., Williams R. E., Peterson B. M., Turnshek D. A., 1979, ApJ, 234, 33
Weymann R. J., Morris S. L., Foltz C. B., Hewett P. C., 1991, ApJ, 373, 23
Wild V. et al., 2008, MNRAS, 388, 227
Wise J. H., Eracleous M., Charlton J. C., Ganguly R., 2004, ApJ, 613, 129
Wu J., Charlton J. C., Misawa T., Eracleous M., Ganguly R., 2010, ApJ, 722, 997
Young P., Sargent W. L. W., Boksenberg A., 1982, ApJS, 48, 455
Yuan Q., Green R. F., Brotherton M., Tripp T. M., Kaiser M. E., Kriss G. A., 2002, ApJ, 575, 687

APPENDIX A: INTRINSIC NALS AND THEIR COMPONENTS

See Table A1. There we present each system, the emission redshift of the quasar, the ion that the system was detected in, the system's reliability class, its absorber type, any subsamples the system belongs to, the EW and error of the system, the absorption redshift of each component, the measured column density for each component, the Doppler b parameter for each component, and the coverage fraction for each component, as well as their associated errors. Absorber Type denotes where along the ionization continuum from Section 5 that the current absorber resides. BAL is a BAL. mBAL is a mini-BAL. NVD is a N V dominant system. MIX is a mixed Ly α system. CLP is a C IV dominant system with Ly α partially covered. CIV is a C IV dominant system. CLI is a C IV dominant system with low-ionization lines. UNK is a system of an unknown type, usually due to Ly α not being covered for the given system. Subsample denotes the properties of the given system or those of its host quasar, namely whether it is associated absorption line (AAL) or not, whether the host quasar is radio loud (L) or radio quiet (Q), whether the system is part of the homogeneous sample or not, and whether or not high-ionization lines (H), intermediate-ionization lines (I), or low-ionization lines (L) are present in the system. If the EW of the ion is too blended to get an accurate measurement, it is left blank.

Table A1. Intrinsic NALs and their components.

QSO (1)	z_{Em} (2)	Ion[a] (3)	Reliability Class[b] (4)	Absorber Type[c] (5)	Subsample[d] (6)	Rest EW (7)	σ_{EW} (8)	z_{Abs} (9)	log N_{ion} (10)	$\sigma_{\log N_{ion}}$ (11)	b (12)	σ_b (13)	c_f (14)	σ_{c_f} (15)
					Class A Systems									
Q0011+0055	2.31	N V	A	MIX	AAL, Q, homogeneous, HI	0.9214	0.0190	2.283 667	15.69	0.52	49.98	14.69	0.31	0.02
								2.286 415	14.33	0.30	19.52	1.93	− 29.5	19.69
								2.286 374	15.08	0.09	25.83	2.18	0.97	0.02
								2.286 340	15.10	0.09	97.64	6.72	0.62	0.06
								2.287 322	13.81	0.37	18.72	2.97	1.0	
Q0055–269	3.66	C IV	A	CIV	non-AAL, Q, homogeneous, H	0.0182	0.0014	3.038 847	13.88	0.17	12.30	1.32	0.12	0.02
Q0055–269	3.66	CIV	A	CIV	non-AAL, Q, homogeneous, HI	0.0370	0.0009	3.085 908	13.62	0.07	8.69	0.36	0.4	0.03
Q0109–3518	2.405	CIV	A	CIV	non-AAL, Q, homogeneous, H	0.0644	0.0009	1.751 753	13.65	0.12	9.81	0.94	0.14	0.03
								1.751 134	13.11	0.18	7.69	0.56	0.43	0.14
								1.751 415	13.90	0.10	26.73	3.13	0.16	0.02
Q0122–380	2.2	CIV	A	CIV	non-AAL, Q, homogeneous, H			1.792 591	13.46	0.17	10.56	0.75	0.28	0.07
Q0122–380	2.2	Si IV	A	CIV	non-AAL, Q, non-homogeneous, HI	0.0118	0.0007	1.815 727	13.53	0.03	12.94	0.21	1.0	
								1.816 022	9.62	9.99	8.04	0.61	1.0	
Q0130–4021	3.023	CIV	A	mBAL	AAL, Q, homogeneous, H	0.0599	0.0021	2.978 014	13.99	0.06	9.37	0.41	0.47	0.02
								2.978 888	14.54	1.97	6.62	4.96	0.16	0.02
								2.980 089	10.07	9.99	18.29	3.27	1.0	
Q0130–4021	3.023	NV	A	mBAL	AAL, Q, homogeneous, H	0.2725	0.0038	2.973 659	14.29	0.04	24.74	0.91	0.56	0.03
								2.972 828	14.64	0.12	78.13	9.13	0.19	0.03
								2.972 281	14.18	0.09	13.00	0.92	0.3	0.02
Q0151–4326	2.74	NV	A	MIX	AAL, Q, homogeneous, H	0.2660	0.0012	2.715 749	12.98	0.48	33.38	0.79	1.0	
								2.714 754	10.03	9.99	49.00	4.11	1.0	
								2.713 347	11.98	3.65	49.84	0.80	1.0	
								2.711 893	10.18	9.99	52.00	1.15	1.0	
Q0329–255	2.685	CIV	A	CIV	non-AAL, L, homogeneous, H	0.0701	0.0016	2.203 037	14.25	0.26	14.48	2.67	0.05	0.01
								2.203 690	13.00	0.64	7.82	1.93	0.33	0.39
								2.203 925	13.75	0.18	21.62	3.78	0.2	0.05
								2.204 451	13.72	0.11	14.96	1.06	0.23	0.04
								2.208 382	13.91	0.30	17.16	4.11	0.06	0.02
								2.209 386	9.66	9.99	96.22	19.88	1.0	
Q0329–385	2.435	CIV	A	MIX	non-AAL, Q, homogeneous, H	0.0823	0.0015	1.815 605	13.69	0.04	11.96	0.28	0.69	0.04
								1.816 413	15.99	9.99	5.50	37.20	0.05	0.01
								1.816 903	13.38	0.24	7.37	0.91	0.26	0.09
								1.817 158	13.25	0.20	8.48	0.65	0.49	0.17

Table A1 – *continued*

QSO (1)	z_{Em} (2)	Ion[a] (3)	Reliability Class[b] (4)	Absorber Type[c] (5)	Subsample[d] (6)	Rest EW (7)	σ_{EW} (8)	z_{Abs} (9)	log N_{ion} (10)	$\sigma_{\log N_{ion}}$ (11)	b (12)	σ_b (13)	c_f (14)	σ_{c_f} (15)
Q0421–2624	2.277	CIV	A	CLI	non-AAL, Q, homogeneous, H	0.2107	0.0086	1.517 100	14.31	0.06	19.20	0.87	0.67	0.02
Q0421–2624	2.277	CIV	A	CLI	non-AAL, Q, homogeneous, HIL	0.4289	0.0075	2.156 848	13.40	0.36	8.27	1.41	0.44	0.24
								2.159 190	13.78	0.07	12.65	0.82	0.81	0.06
								2.158 913	13.55	0.10	7.58	0.84	0.82	0.09
								2.157 698	13.82	0.18	33.60	2.28	0.71	0.22
								2.158 379	13.30	0.34	9.16	1.41	0.68	0.39
								2.158 666	12.90	0.59	9.85	1.40	1.0	
Q0421–2624	2.277	SiIV	A	CLI	non-AAL, Q, homogeneous, HIL	0.3121	0.0113	2.156 830	13.45	0.16	8.71	1.04	0.49	0.06
								2.157 498	11.39	9.99	3.55	1.87	1.0	
								2.157 696	13.50	0.17	33.05	2.89	0.79	0.22
								2.158 716	13.61	0.45	46.21	13.92	0.31	0.24
								2.159 239	13.27	0.59	6.47	3.26	0.23	0.13
Q0425–5214	2.25	NV	A	MIX	AAL, Q, homogeneous, H	0.3200	0.0082	2.237 902	15.20	9.99	38.55	99.99	0.07	0.07
								2.238 809	14.49	0.05	22.66	1.21	0.73	0.04
								2.239 351	13.01	3.41	9.51	4.20	0.76	5.43
								2.239 717	15.07	0.20	80.27	25.88	0.15	0.02
Q0549–213	2.245	CIV	A	CLP	AAL, L, homogeneous, H	0.0163	0.0017	2.241 838	13.58	0.31	8.50	1.51	0.2	0.08
								2.243 024	11.15	9.99	23.59	3.97	1.0	
								2.244 274	13.55	0.07	7.87	0.57	0.79	0.06
								2.243 714	13.64	0.05	11.31	0.40	0.88	0.06
								2.244 074	9.86	9.99	10.16	4.43	1.0	
Q0549–213	2.245	CIV	A	CLP	non-AAL, L, homogeneous, H	0.0779	0.0068	2.071 126	13.99	0.22	23.02	3.22	0.38	0.11
Q0549–213	2.245	NV	A	CLP	AAL, L, homogeneous, H	0.2089	0.0041	2.243 684	11.08	9.99	13.48	1.06	1.0	
								2.244 231	13.87	0.11	11.60	0.73	0.68	0.09
Q0952+179	1.472	CIV	A	UNK	non-AAL, L, homogeneous, H	0.0777	0.0032	1.256 322	14.31	2.77	4.67	5.07	0.18	0.03
								1.258 072	13.62	0.08	10.90	0.53	0.77	0.08
								1.261 827	13.36	0.88	11.39	2.67	0.74	1.07
Q1114–0822	4.495	CIV	A	CIV	non-AAL, Q, homogeneous, H	0.0487	0.0028	3.390 842	13.61	0.17	12.36	1.01	0.38	0.09
Q1114–220	2.282	CIV	A	UNK	AAL, L, homogeneous, HIL	1.3042	0.0198	2.296 540	17.79	0.55	13.59	1.24	0.63	0.05
								2.297 442	14.48	0.08	53.48	3.97	0.86	0.06
								2.295 300	15.42	0.15	42.84	2.90	0.75	0.01
Q1122–1648	2.405	CIV	A	MIX	AAL, Q, homogeneous, H	0.0631	0.0004	2.352 187	12.81	0.28	11.17	0.44	0.35	0.21
								2.352 523	13.12	0.13	10.84	0.96	0.21	0.05
								2.352 760	11.60	2.20	9.53	0.87	1.0	

Table A1 – *continued*

QSO (1)	$z_{\rm Em}$ (2)	Ion[a] (3)	Reliability Class[b] (4)	Absorber Type[c] (5)	Subsample[d] (6)	Rest EW (7)	$\sigma_{\rm EW}$ (8)	$z_{\rm Abs}$ (9)	log $N_{\rm ion}$ (10)	$\sigma_{\log N_{\rm ion}}$ (11)	b (12)	σ_b (13)	c_f (14)	σ_{c_f} (15)
								2.352 957	11.23	9.99	9.77	1.06	1.0	
								2.354 094	11.49	2.65	4.51	0.29	1.0	
								2.353 328	13.61	0.06	13.54	0.90	0.09	0.01
								2.353 709	13.73	0.13	23.70	4.41	0.05	0.01
Q1157+014	1.9997	SiIV	A	BAL	AAL, L, homogeneous, HI	0.4507	0.0059	1.979 463	13.29	0.20	11.04	1.33	0.36	0.09
								1.979 779	14.40	0.03	94.58	2.14	0.39	0.01
Q1158–1843	2.448	CIV	A	NVD	AAL, Q, homogeneous, H	0.6545	0.0009	2.440 754	13.29	0.29	18.48	1.56	0.19	0.11
								2.441 170	13.21	0.07	13.71	0.57	0.81	0.10
								2.441 495	13.83	0.04	12.29	1.77	0.16	0.01
								2.441 752	13.45	0.03	6.95	0.32	0.46	0.03
								2.444 054	12.38	0.88	9.23	0.74	1.0	
								2.442 074	13.95	0.05	22.61	2.48	0.56	0.02
								2.442 242	13.77	0.04	15.82	0.31	0.77	0.02
								2.443 779	13.04	0.25	7.22	1.30	0.21	0.10
								2.442 626	14.01	0.01	8.42	0.16	0.85	0.00
								2.442 763	13.34	0.06	5.20	0.55	0.62	0.07
								2.442 938	13.69	0.05	12.26	1.85	0.76	0.01
								2.443 156	13.48	0.04	6.76	0.37	0.77	0.04
								2.444 338	13.44	0.28	20.51	2.61	0.13	0.07
								2.443 315	13.50	0.10	8.59	4.09	0.31	0.07
								2.443 532	13.55	0.03	9.63	0.64	0.8	0.01
Q1158–1843	2.448	NV	A	NVD	AAL, Q, homogeneous, H	0.6165	0.0013	2.441 150	12.55	0.73	12.60	0.38	1.0	
								2.441 428	14.48	0.08	61.75	5.12	0.2	0.02
								2.441 749	13.27	0.17	6.89	1.10	0.55	0.23
								2.442 145	13.94	0.20	13.24	5.58	0.86	0.06
								2.441 931	13.38	0.35	12.26	3.23	0.99	0.23
								2.442 308	13.83	0.07	7.97	1.02	0.73	0.22
								2.442 661	14.43	0.01	13.31	0.27	0.9	0.00
								2.442 960	13.95	0.03	10.06	0.70	0.77	0.01
								2.443 128	13.58	0.09	5.16	0.52	0.84	0.05
								2.443 201	14.28	1.36	2.88	1.50	0.35	0.04
								2.443 369	13.67	0.23	12.23	6.66	0.62	0.12
								2.443 526	13.84	0.08	7.02	0.82	0.63	0.17
								2.443 612	13.97	0.19	12.88	3.64	0.28	0.05

Table A1 – *continued*

QSO (1)	z_{Em} (2)	Ion[a] (3)	Reliability Class[b] (4)	Absorber Type[c] (5)	Subsample[d] (6)	Rest EW (7)	σ_{EW} (8)	z_{Abs} (9)	log N_{ion} (10)	$\sigma_{\log N_{ion}}$ (11)	b (12)	σ_b (13)	c_f (14)	σ_{c_f} (15)
								2.444 040	12.10	6.61	9.04	0.99	1.0	
								2.444 264	14.24	0.13	25.39	3.94	0.09	0.01
Q1202–0725	4.694	CIV	A	CIV	AAL, Q, homogeneous, H	0.0644	0.0032	4.625 917	13.55	0.19	6.63	0.90	0.33	0.07
								4.626 510	13.39	0.46	21.31	2.86	0.56	0.51
Q1202–0725	4.694	CIV	A	CIV	non-AAL, Q, homogeneous, H	0.0832	0.0032	3.813 164	10.22	9.99	12.20	3.00	1.0	
								3.813 946	10.51	9.99	35.19	6.51	1.0	
								3.813 808	13.77	0.48	6.82	2.73	0.14	0.06
Q1202–0725	4.694	CIV	A	CIV	non-AAL, Q, homogeneous, HI	0.1019	0.0033	4.045 405	12.62	9.99	0.09	99.99	1.0	
								4.049 340	15.38	7.52	2.94	5.28	0.09	0.02
								4.048 035	13.27	0.72	19.05	4.87	0.48	0.70
								4.048 658	13.63	0.11	14.85	1.22	0.53	0.09
Q1209+0919	3.3	CIV	A	CIV	non-AAL, Q, homogeneous, H	0.0615	0.0066	2.517 988	13.97	0.22	13.30	2.02	0.38	0.07
Q1341–1020	2.135	NV	A	mBAL	AAL, Q, homogeneous, H	0.3623	0.0107	2.113 167	10.07	9.99	28.07	7.11	1.0	
								2.114 476	10.69	9.99	76.27	5.01	1.0	
								2.116 188	10.84	9.99	76.05	4.91	1.0	
								2.120 099	13.54	0.53	28.39	2.29	1.0	
								2.117 290	10.55	9.99	50.15	8.78	1.0	
								2.118 287	10.77	9.99	43.24	7.56	1.0	
								2.118 935	13.28	1.01	16.31	3.11	1.0	
								2.119 384	13.51	0.50	15.35	2.20	0.79	0.74
Q1347–2457	2.534	CIV	A	CIV	non-AAL, Q, homogeneous, H	0.0328	0.0007	2.370 007	13.29	0.15	7.30	0.61	0.21	0.05
								2.370 327	13.19	0.36	21.20	1.45	0.4	0.29
Q1444+014	2.206	CIV	A	mBAL	AAL, Q, homogeneous, H			2.195 129	14.11	0.04	19.56	0.77	0.34	0.01
								2.195 716	13.94	0.06	22.63	2.35	0.34	0.03
								2.196 243	13.65	0.14	21.58	2.90	0.36	0.10
								2.196 887	13.02	2.80	51.70	14.24	0.9	5.62
								2.197 908	12.74	2.78	25.11	3.75	1.0	
								2.198 556	13.66	0.10	16.96	1.86	0.41	0.07
								2.198 802	12.51	3.03	10.52	4.04	0.96	6.44
								2.199 107	13.04	0.91	32.45	9.37	1.0	
								2.199 930	12.08	9.99	8.28	5.18	1.0	
								2.199 716	12.39	9.74	18.70	16.73	1.0	
								2.200 336	14.20	0.03	17.31	0.61	0.4	0.01
								2.200 899	12.51	9.99	0.46	92.36	1.0	

Table A1 – *continued*

QSO (1)	z_{Em} (2)	Ion[a] (3)	Reliability Class[b] (4)	Absorber Type[c] (5)	Subsample[d] (6)	Rest EW (7)	σ_{EW} (8)	z_{Abs} (9)	log N_{ion} (10)	$\sigma_{\log N_{ion}}$ (11)	b (12)	σ_b (13)	c_f (14)	σ_{c_f} (15)
								2.201 006	13.66	0.12	37.23	1.83	0.81	0.20
								2.201 602	14.22	0.07	7.98	0.39	0.46	0.01
								2.202 342	13.35	0.59	1.38	0.43	0.28	0.06
								2.202 019	12.80	2.00	38.04	3.48	1.0	
								2.203 389	14.39	0.43	41.77	37.01	0.06	0.01
Q1444+014	2.206	NV	A	mBAL	AAL, Q, homogeneous, H	0.7147	0.0048	2.195 650	14.45	0.07	60.15	2.10	0.28	0.03
								2.202 426	16.98	0.55	7.80	0.85	0.13	0.01
								2.199 383	15.13	0.03	85.73	2.38	0.27	0.00
								2.201 970	16.94	0.28	6.86	0.38	0.29	0.01
								2.201 561	15.42	0.28	8.45	0.91	0.45	0.01
								2.200 514	15.54	0.19	17.45	1.22	0.29	0.01
								2.201 132	16.32	0.60	8.51	1.15	0.39	0.01
								2.204 173	14.18	0.29	9.36	1.68	0.21	0.02
Q1621–0042	3.7	CIV	A	CIV	non-AAL, Q, homogeneous, H	0.0174	0.0012	3.241 152	13.69	0.17	12.06	1.07	0.14	0.03
Q2000–330	3.773	CIV	A	CIV	non-AAL, L, homogeneous, HI	0.0261	0.0009	3.392 317	13.36	0.14	9.17	0.63	0.31	0.07
								3.392 705	10.19	9.99	11.57	2.59	1.0	
Q2059–360	3.092	CIV	A	CLP	non-AAL, Q, homogeneous, H	0.0366	0.0035	2.971 196	13.90	0.27	15.45	2.80	0.15	0.05
Q2116–358	2.341	CIV	A	NVD	AAL, Q, homogeneous, H	0.3487	0.0031	2.303 954	12.35	8.36	29.17	4.26	1.0	
								2.305 737	14.67	0.07	32.70	1.97	0.33	0.02
								2.306 252	14.25	0.02	18.01	0.41	0.69	0.02
								2.305 630	12.96	0.43	10.47	0.90	1.0	
								2.307 924	14.45	1.27	11.29	7.62	0.08	0.01
Q2132–433	2.42	CIV	A	MIX	AAL, Q, homogeneous, H	0.0989	0.0055	2.381 035	13.05	1.18	12.91	2.41	0.77	1.85
								2.381 703	13.74	0.24	14.16	1.90	0.31	0.10
								2.382 891	13.18	0.40	6.37	1.04	0.61	0.40
Q2215–0045	1.475	CIV	A	UNK	AAL, Q, homogeneous, HIL	0.1877	0.0056	1.475 264	13.81	0.18	23.43	3.97	0.37	0.16
								1.475 694	13.64	0.54	51.08	11.21	0.66	0.68
								1.477 075	12.70	2.93	18.38	2.65	1.0	
Q2225–2258	1.891	CIV	A	CLI	non-AAL, Q, homogeneous, H	0.2186	0.0031	1.410 612	12.75	0.60	5.80	1.12	0.86	1.03
								1.410 731	12.78	0.76	10.10	1.66	1.0	
								1.411 431	13.51	0.32	21.78	1.80	0.34	0.20
								1.411 906	13.87	0.33	13.89	3.10	0.07	0.03
								1.412 438	13.90	0.10	26.17	1.60	0.4	0.06
								1.412 681	13.78	0.03	5.73	0.35	0.75	0.02

Table A1 – *continued*

QSO (1)	z_{Em} (2)	Ion[a] (3)	Reliability Class[b] (4)	Absorber Type[c] (5)	Subsample[d] (6)	Rest EW (7)	σ_{EW} (8)	z_{Abs} (9)	log N_{ion} (10)	$\sigma_{\log N_{ion}}$ (11)	b (12)	σ_b (13)	c_f (14)	σ_{c_f} (15)
								1.412 553	13.95	0.02	7.54	0.31	0.86	0.01
Q2314–409	2.448	CIV	A	CLP	AAL, L, non-homogeneous, H	0.0107	0.0016	2.462 903	13.82	0.40	6.28	1.69	0.13	0.03
								2.463 543	14.05	2.03	5.30	5.34	0.13	0.03
					Class B Systems									
Q0011+0055	2.31	NV	B	MIX	AAL, Q, homogeneous, HI	0.7268	0.0152	2.290 030	15.41	0.44	33.42	6.62	0.39	0.04
								2.291 049	15.51	0.09	52.79	2.67	0.8	0.01
Q0011+0055	2.31	SiIV	B	MIX	AAL, Q, homogeneous, HI	0.5822	0.0157	2.286 212	12.87	1.40	37.20	5.49	1.0	
								2.286 770	14.79	0.17	74.64	8.17	0.42	0.04
								2.287 232	15.75	0.50	3.50	0.61	0.74	0.06
Q0011+0055	2.31	SiIV	B	MIX	AAL, Q, homogeneous, HI	0.8326	0.0181	2.290 644	14.65	0.04	87.00	2.39	0.8	0.02
Q0136–231	1.893	CIV	B	CLI	AAL, L, homogeneous, HIL	0.3709	0.0047	1.876 844	13.21	0.18	5.78	0.63	0.62	0.17
								1.877 031	13.02	0.39	8.08	1.43	0.79	0.60
								1.877 286	13.46	0.09	15.99	1.20	1.0	
								1.877 547	13.30	0.17	6.79	1.29	0.57	0.18
								1.877 699	13.41	0.19	14.15	2.13	0.69	0.21
								1.878 644	13.90	0.43	6.21	1.70	0.11	0.02
								1.879 101	13.51	0.16	15.03	1.18	0.54	0.15
								1.879 485	12.76	1.06	24.32	1.71	1.0	
Q0151–4326	2.74	CIV	B	MIX	non-AAL, Q, homogeneous, H	0.0386	0.0006	2.169 942	13.20	0.07	10.18	0.19	0.74	0.09
Q0425–5214	2.25	CIV	B	MIX	non-AAL, Q, homogeneous, HI	0.1065	0.0067	2.138 580	13.63	0.16	8.17	0.89	0.67	0.12
								2.140 179	13.10	0.69	8.15	1.54	0.96	1.23
Q0425–5214	2.25	CIV	B	MIX	non-AAL, Q, homogeneous, HI	0.2639	0.0094	2.095 437	12.99	0.50	7.37	1.33	1.0	
								2.095 635	13.24	1.57	23.42	6.84	0.98	3.16
								2.096 290	13.96	0.09	18.25	1.14	0.77	0.08
Q0549–213	2.245	CIV	B	CLP	AAL, L, homogeneous, H	0.2089	0.0041	2.241 837	13.57	0.31	8.58	1.55	0.2	0.08
								2.243 024	11.15	9.99	23.59	3.97	1.0	
								2.244 274	13.55	0.07	7.86	0.57	0.79	0.06
								2.243 714	13.64	0.05	11.31	0.40	0.88	0.06
								2.244 074	9.84	9.99	10.16	4.43	1.0	
Q0810+2554	1.5	CIV	B	UNK	non-AAL, Q, homogeneous, HI	0.1148	0.0014	1.352 470	12.45	4.20	19.27	5.53	1.0	
								1.352 627	13.74	0.02	9.62	0.29	0.88	0.02
Q0810+2554	1.5	NV	B	UNK	AAL, Q, homogeneous, H	0.3019	0.0044	1.500 036	13.99	0.23	18.88	2.13	0.33	0.11
								1.500 988	13.90	0.12	21.44	2.00	0.98	0.16
								1.501 253	14.84	0.11	11.48	0.96	0.89	0.01

Table A1 – *continued*

QSO (1)	z_{Em} (2)	Ion[a] (3)	Reliability Class[b] (4)	Absorber Type[c] (5)	Subsample[d] (6)	Rest EW (7)	σ_{EW} (8)	z_{Abs} (9)	log N_{ion} (10)	$\sigma_{\log N_{ion}}$ (11)	b (12)	σ_b (13)	c_f (14)	σ_{c_f} (15)
								1.501 550	13.80	0.15	15.83	1.76	0.74	0.17
								1.503 393	15.25	0.05	22.34	0.63	0.92	0.01
								1.502 739	14.91	0.03	21.52	0.56	0.93	0.01
Q1114–220	2.282	CIV	B	UNK	AAL, L, homogeneous, H	0.2909	0.0085	2.281 983	15.35	1.33	15.82	5.66	0.5	0.02
								2.283 686	17.22	0.67	15.06	1.66	0.75	0.01
								2.285 148	13.79	0.11	8.56	0.62	0.8	0.08
Q1157+014	1.9997	SiIV	B	BAL	non-AAL, L, homogeneous, HI	0.1165	0.0040	1.719 208	13.27	0.14	18.32	1.34	0.7	0.16
								1.719 582	13.10	0.29	12.60	1.76	0.46	0.22
								1.720 549	10.32	9.99	8.62	7.79	1.0	
Q1202–0725	4.694	CIV	B	CIV	AAL, Q, homogeneous, HI	0.5148	0.0043	4.686 642	13.95	0.06	14.43	1.12	0.95	0.05
								4.686 946	13.69	0.17	26.33	1.67	1.0	
								4.689 355	13.62	0.51	23.03	8.33	0.26	0.24
								4.687 954	13.52	0.08	9.74	0.58	0.82	0.09
								4.688 558	13.95	0.02	12.98	0.39	0.99	0.02
Q1202–0725	4.694	CIV	B	CIV	non-AAL, Q, homogeneous, HI	0.5691	0.0057	4.483 308	13.89	0.15	56.38	3.06	0.79	0.23
								4.481 920	13.69	0.06	10.16	0.49	0.64	0.05
								4.480 502	14.12	0.07	42.15	2.49	0.56	0.06
								4.479 018	12.20	4.88	29.89	1.72	1.0	
								4.479 955	13.41	0.14	6.42	0.62	0.69	0.12

Notes. [a]Ion used to identify absorption system.
[b]Absorber reliability class (see Section 3.2).
[c]Absorber type – BAL: broad absorption line, mBAL: mini-BAL, NV: N V-dominant, MIX: mixed Ly α, CLP: CIV dominant w/Ly α partial coverage, CIV: C IV-dominant, CLI: C IV dominant w/low-ionization lines, UNK: unknown (see Section 5).
[d]Absorber subclasses – AAL: associated absorption line, non-AAL: absorption line outside associated region, L: radio loud, Q: radio quiet, homogeneous: EW puts the absorber within the homogeneous sample, non-homogeneous: absorber not within the homogeneous sample. Also listed are the types of transitions found within the system – H: high-ionization lines, I: intermediate ionization lines, and L: low-ionization lines (see Table 5).

This paper has been typeset from a TEX/LATEX file prepared by the author.